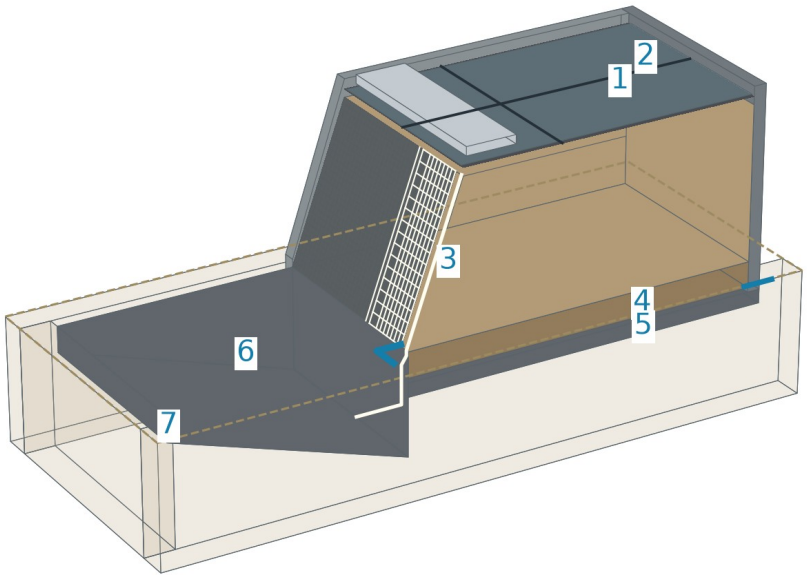
ConstruckSlope Plus 200
Complete chamber and deformation report

Consolidated illustrated assessment S6 8
13 October 2026
6 m inward bench x 4 m width x 3 m retained sand height



1 6 × 4 m bench 2 Concrete chamber 3 Plus 200 facing 4 Restricted soil
5 Independent base collector 6 Toe anchor 7 See-through natural ground level

Concrete chamber with an illustrative side opening, continuous see-through natural ground, independent lower collector and a forward toe anchor. Schematic apparatus, not a reinforcement drawing.

This report brings the complete chamber assessment and separate deformation studies together. It explains the apparatus, storm entry and drainage, saturation and suction, stress indicators, facing bulge, UV-cover response, grid extension, possible soil redistribution, conditional berm deformation and toe checks. The adopted-case findings retain the six-metre S6-1 hydraulic run. S6-7 adds five mechanical replays, pressure/friction sensitivities and explicit toe checks. Geometric deformation remains at its calculated scale; no new storm or coupled soil-displacement simulation is claimed. S6-8 adds gradual pressure-relief checks in sections 35D-F.

Main finding: the adopted pressure case meets the retained facing/toe screens, but a sustained at-rest pressure comparison fails the current toe contact check. A pressure-independent pass is not established. Actual soil displacement and berm settlement remain unresolved. The 17.87 mm conditional berm example retains its exact scale; it is not predicted final settlement.

S6 7 Technical corrections and sensitivity findings

This edition retains the corrected suction graph and every existing illustration, and adds mechanical pressure/friction checks and two graphs. Five replays use the same 53 hydraulic states. Toe equations, numerical diagnostics, reference roles and claim wording are corrected throughout. Fixed assumptions, the 4.70 m toe, storm, hydraulic fields and original deformation scales remain unchanged. [31,33]

The adopted case reproduces a 204.69 mm maximum bulge and the retained 1.133 toe sliding ratio. The at-rest pressure comparison gives 339.34 mm and cannot sustain the required toe contact under amplified reactions. The original pass is therefore model-specific. The agreed geometry is retained and the failed sensitivity is reported explicitly. Bench settlement, erosion performance and full-system validation remain unresolved.

Review item	Correction or clarification in this edition
Suction maximum	Retained analytical maximum: 61.58346% and 0.276920 kPa. The new no-suction replay confirms that suction enters the facing load and reduces its maximum bulge by 2.46 mm.
Rainfall and pond replay	Sections 9A, 9B and 15C publish fitted storm windows, hourly reconstruction and the distinction between supply-limited wetting and positive ponding.
Local fields and maxima	Section 12C states the saved-time sampling and unresolved hydraulic spatial convergence beside the local-field discussion.
Bench and toe interpretation	Sections 28A and 35A retain the unresolved movement compatibility. Section 35C records the upper-pressure contact failure; no physical collapse shape is inferred.
Reproducibility	Sections 8C, 17A, 35B and 35C add explicit pressure laws, new replay results and reproducible toe checks. Section 39A records the files.

All deformation illustrations retain their original calculated scale. Throughout retained graphs and captions, “peak” means the maximum among the reported saved states or checked scenario envelope, as applicable; it is not proof of a continuous-time maximum. Internal computational review is not external certification.

Guide to the consolidated report

Read the apparatus and water sections first, then the detailed movement views. All heights on face maps are measured above the original sand toe. Bulge values are perpendicular to the original 70 degree face, not horizontal distances. The bench extends 6 m inward; the retained face remains 3 m high and 4 m wide.

Topic	Views and information included
Chamber and loading	Concrete enclosure, see-through natural ground, exact slope-foot toe entry, 6 m screed, crossing joints and original 10 kPa strip
Water and soil response	Storm routing, pond replay, local saturation and suction, stress and wetting indicators, separate front and lower water accounts
Facing bulge	Whole chamber section, A-A close section, four cross-sectional states, full-face maps, profiles, timeline and stage values
UV cover	Layer cutaways, retained fragments, strain and curvature indicators, crack mechanisms and limits of crack-location information
Grid and moving soil	Fixed-end extension audit, toe-flexibility comparison, geometric volume balance and possible redistribution
Berm response	Full 6 m cross section at deformation x1, plan joint locations, exact joint crop and conditional bending profiles
Toe and final status	Foundation screen, verification, references, measurement plan and combined before-and-after overview

Three evidence categories are used: saved numerical results; conditional structural results requiring an imposed support-loss or restraint assumption; and unresolved physical mechanisms explained in words. Geometric deformation sections use the same horizontal and vertical scale and a displacement multiplier of one. Uniformly enlarging a local crop changes page magnification only. Data charts retain their explicitly labelled numerical axes; they are not pictures of an enlarged deformed body.

The earlier isolated reports supply the technical basis. Their former four-metre numbers and exaggerated deformation sketches are superseded here. Full-face maps and plan views remain for location information. No uncalculated cavity or crack aperture is drawn as a deformed shape. S6-8 adds sections 35D-F and Figure S3 after the toe comparisons, with supporting references 34-36. All earlier sections and illustrations remain.

Guide to the expanded hydraulic detail

Master report S6 7 retains the detailed hydraulic and soil interpretation added in S6 4 to the complete S6 3 report. All existing sections, figures, tables, references and true-scale deformation cross-sections are retained. New sections 12A to 16B sit beside the corresponding overview pages, so each topic can be read at summary and detailed levels.

Topic	Added detail
Local saturation	Fixed monitoring points, full time history, local wet fractions and upper versus lower storage
Suction and apparent cohesion	Equations, definitions, stage values and maps of gain and loss relative to the initial state
Pressure and lower wetting	Lower-zone close sections, pressure sign, discharge activation and the 25 cm review band
Across width and pond equivalence	Point comparisons, natural versus common-pond spatial entry and calibration meaning
Stress and reference wedge	Stress location, wedge dimensions and separation of wet pockets from mechanical failure

The detailed explanations are restored from the earlier chamber publication and isolated studies, with numerical examples taken from the retained six-metre S6-1 calculation. Superseded four-metre values and constant-flow trial results are not reused as current results. The added histories are post-processing of saved fields, not a new simulation.

The final visual summary remains at the end. Geometric deformation uses a multiplier of one. The conditional 17.87 mm bench example and fixed anchorage assumptions remain. New sections 17A and 35B-C extend the sensitivity evidence; the final conclusion now includes the upper-pressure toe failure.

Figure numbers 1 to 29 and hydraulic illustrations H1 to H7 remain unchanged. New sensitivity graphs are S1 and S2. Coordinates in the added detail use x inward from the original toe, y across the 4 m width and z above the bottom collector; the top of the restricted soil and slope foot are at z = 0.50 m.

1 Revised findings and status

Quantity	Retained six-metre result
Catchment rainfall	15,386.4 L over 24 m²
Joint intake by 120 h	2,006.53 L
Rear intake by 120 h / 240 h	0.00 / 190.43 L
Facing bulge: loaded before / peak / after	201.09 / 204.69 / 200.68 mm
Saved maximum response time	106 h from start of storm record window
Toe retained/selected	4.70 m forward; depth 2.00 → 0.50 m
Minimum toe sliding ratio	1.133 versus development criterion 1.10
Front collection: storm / later drainage	0.00 / 0.00 L
Actual bench settlement	Not established by the available solver

The adopted pressure proxy equilibrates a nonlinear grid membrane without solving soil plastic movement. A new sustained at-rest pressure comparison gives 339.34 mm bulge and fails the current toe contact screen (sections 17A and 35C). The adopted-case result is not robust to that pressure alternative. The earlier soil/contact solve did not converge; no actual settlement or physical failure is inferred. [24,33]

The reported screening margins retain the agreed development criteria. They are not interchangeable with a code-compliant field design or a universally acceptable factor of safety. Published sources support individual mechanisms and equations, not the proprietary assembly as a whole. [14–18]

2 What changes with the longer bench

Feature	Previous reference	This revision
Bench and catchment	4 × 4 m; 16 m²	6 × 4 m; 24 m² (+50%)
Top joint length	4 + 4 m	4 + 6 m (+25%)
Net 2 mm open-path area	0.015996 m²	0.019996 m²
Upper sand volume	54.551 m³	78.551 m³ (+24 m³)
150 mm screed volume	2.40 m³	3.60 m³ (+1.20 m³)
Screed self-weight per metre width	12 kN/m	18 kN/m (+6 kN/m)
Rear key position	4 m from crest	6 m from crest
Surcharge footprint	1 × 4 m, offset 0.15 m	Unchanged; total force 40 kN
Toe grid entry	Drawing showed a forward offset	Exactly at slope foot; L-turn inside toe

Joint intake rises from approximately 1,618.50 L in the prior 4 m case to 2,006.53 L, an increase of 24.0%. Rainfall volume increases 50%, while the routed leakage changes by a different amount.

The added soil is behind the existing face and is not automatically added to the unstable wedge. The updated model changes water storage, flow paths, screed-load influence and rear-key influence. It does not convert all of the additional 24 m³ into outward facing load. The additional dry sand weight is approximately 376.7 kN in total, or 94.2 kN per metre of chamber width. Its actual stress redistribution would require a continuum mechanical solution.

Joint locations remain 2 m inward from the crest and at the 2 m width centreline. The rear portion of the extended bench is therefore 4 m long. Moving the rear boundary does not prove that the last 2 m is undisturbed. The through-crack assumption is now explicit: partial control cuts have cracks extending to the sand, with an effective 2 mm hydraulic opening.

3 Chamber ground level and drainage

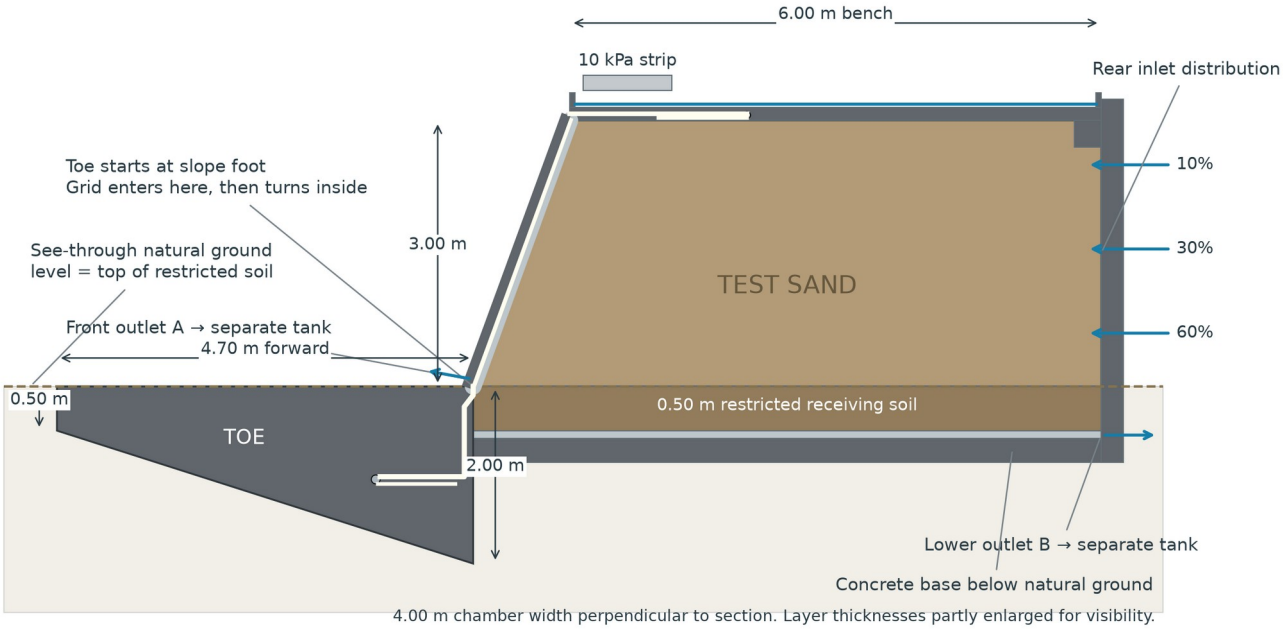


Figure 1. Revised section. Natural ground is the top of the 0.50 m restricted receiving layer. The chamber base and toe excavation lie below that level. No separate pedestal is drawn beneath the toe.

The chamber has two concrete sidewalls, a rear wall and a base slab. A separation layer and clearance isolate the facing from the sidewalls; no friction or arching benefit is credited. The base collector lies below the restricted receiving soil and drains independently. The external toe remains supported on compacted sand, not on the chamber base.

See-through ground is a drawing convention, not an additional hydraulic reservoir or a restraint in the model. The zero-head lower collector is below the restriction. Water must cross the restricted layer before reaching it. Outlet A carries only front-mat discharge; outlet B carries only the independent lower drainage. Route both away from the toe foundation.

The natural-ground datum is z = 0.50 m in the saved numerical coordinates; z = 0 is the top of the lower collector. Sand extends from z = 0.50 to 3.50 m. Wall/base reinforcement, excavation support and isolation details require a separate chamber construction design. [21,24]

4 Bench joints and rainfall routing

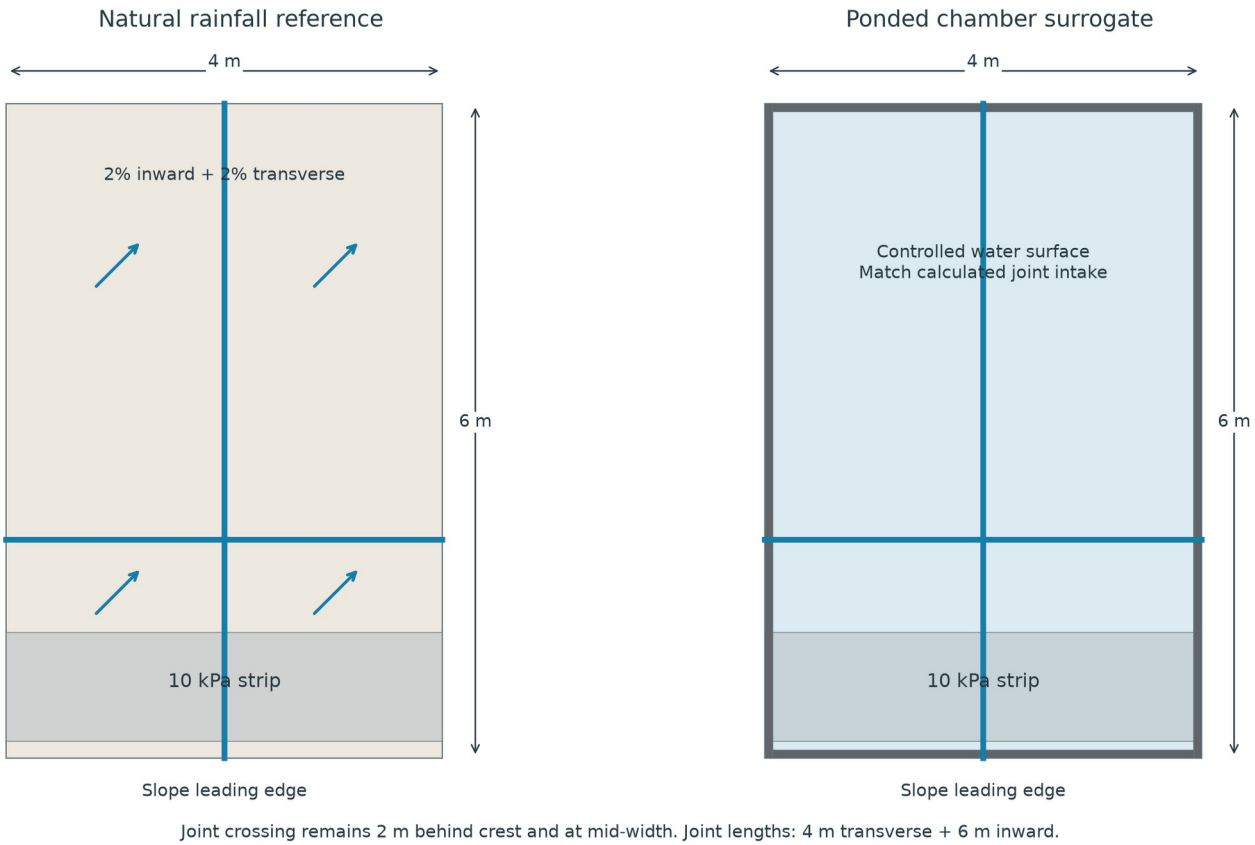


Figure 2. Extended joints and retained positions. Natural gradients route rain inward and transversely. Chamber ponding replaces the calculated soil entry, not the full rainfall catchment volume.

The effective opening is $0.002(6 + 4) - 0.002^2 = 0.019996$ m². The intersection is counted once. Cell routing uses both 2% grades and Manning n = 0.015. Intake is limited by weir entry, orifice entry and soil-contact conductance. The primary equivalent contact length is 0.10 mm; it is an unmeasured conductance parameter, not the screed thickness. [13,24]

The modelled natural joint split over the storm is 945.04 L through the transverse middle joint and 1,061.49 L through the inward joint. The split follows the adopted routing law; the historical 70/30 allocation is not imposed on top of that calculation.

Through-cracks permit the assumed water path. They do not establish a calibrated leakage coefficient, a constant real aperture throughout the test, or a mechanically free hinge. Changes in crack opening caused by bench movement are not fed back into this seepage run.

5 Fixed assumptions and checked behavior

Item	Treatment
Rear crest key	300 × 300 mm, fixed and of unlimited capacity
Bench grid loop	2 m route to rebar loop, approximately 1 m return tail; no failure or slip
Toe grid loop	Approximate 2 m embedded L-route, rebar loop and 1 m tail; no failure or slip
Transfer into concrete	Full transfer into connected screed/anchor body is assumed
Cover retention	Cracked cover remains attached to the Construck 3D mat
Under-toe water	Zero uplift is imposed; gross toe weight is available
Toe body	Rigid/intact body in the foundation screen; internal fracture not solved
Soil and water	Unsaturated flow and an assumed suction-strength relation are calculated
Facing and toe	Membrane equilibrium, nominal grid ratio, toe contact, sliding, bearing and elastic settlement are screened
Bench deformation	Only conditional beam comparisons; actual soil support change unresolved

Local load-transfer fixity does not fix the entire toe in space. The toe is checked against the calculated support reactions. Conversely, assuming a fixed top key does not establish the bending or shear behavior of the cracked screed between the face and the key.

These conditions are retained to isolate the proposed facing mechanism. They are assumptions for this exercise, not experimentally measured capacities. No Plus 400 C-channel details are introduced. No additional 30 cm perforated soil drains are included.

6 Exact toe entry and local load path

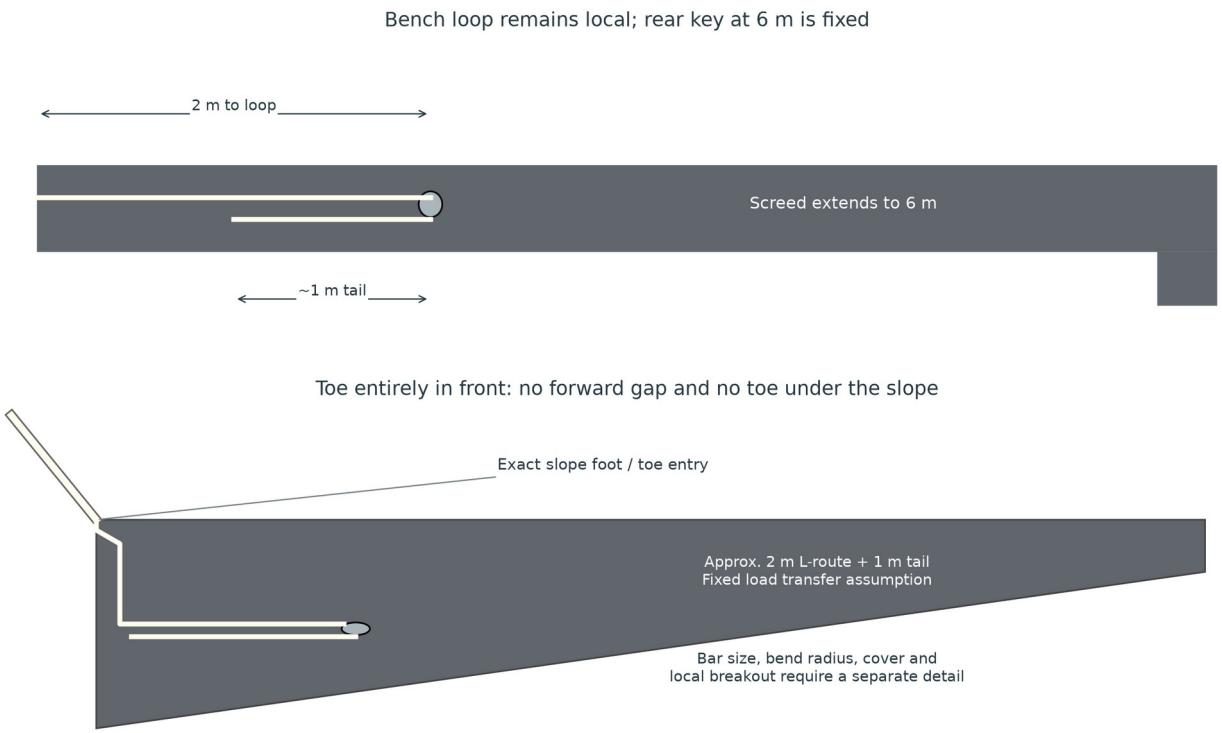


Figure 3. Revised local anchorage detail. The slope grid enters at the exact toe/slope boundary and turns within the forward trench. Layer and bar sizes are enlarged to explain the path.

The load path is grid tension → loop bearing on the transverse bar → local transfer into the screed → resistance of the anchor body. Both loop capacities remain fixed assumptions. Bar diameter, bend radius, cover, splitting resistance and tail development are not inferred from the illustrative dimensions.

The previous foundation calculation already placed the force at the slope-side edge. This revision sets its height exactly at toe top level, removing the previous 50 mm offset, and corrects the drawing. It does not introduce a fictitious forward lever arm. The toe continues entirely in front of the slope; no under-slope toe is used.

The drainage layer and 3D mat turn only slightly onto the leading bench edge; the 3D mat terminates above the bottom loop zone. The white grid continues into the toe. Centimetre-scale layer terminations and the loop itself are not resolved by the numerical mesh. The earlier 400-grade aperture test is not assigned to this Plus 200 connection. [22–24]

7 Soil facing and material inputs

Input	Value and qualification
Sand density / specific gravity	1600 kg/m³ / 2.67
Porosity	0.400749, density-derived
Effective friction / true cohesion	32° / 0 kPa; assumed sand properties
Sand elastic parameters	E = 25 MPa; ν = 0.30; not measured
Retention parameters	θr = 0.045; α = 14.5 m^{-1}; n = 2.68
Sand saturated conductivity	8.25×10^{-5} m/s
Initial pressure	Uniform −2.0 kPa suction; not hydrostatic equilibrium
Lower layer	0.50 m; Ksat = 8.25×10^{-7} m/s; same retention law
Screed	150 mm; 20 kN/m³; assumed E = 25 GPa
Cover	20 mm; E = 5 GPa; tensile 0.5 MPa; flexural 1.5 MPa
Grid	Nominal MD 200 / CMD 100 kN/m
Grid low-strain points	MD 34 kN/m at 1%; 48 kN/m at 2%
Front drain index cap	0.8 L/s/m × 4 m = 192 L/min

Hydraulic values are generic sand-class estimates, combined with density-derived porosity. The 32° strength is an adopted literature analog, not a sample test. The restricted soil changes conductivity only; it is not a calibrated cohesive geological stratum. [8,9,19]

The 200 kN/m index strength is compared with calculated internal grid tension (31.20 kN/m at the adopted peak). Index strengths and drainage data do not establish long-term capacities. Creep, installation damage, durability, filter clogging and assembled outlet losses are not calibrated here. CMD grid stiffness is approximated from the MD curve by the nominal strength ratio. [15–17,22]

8 Numerical method and equations

Water and suction

A three-dimensional prism mesh solves transient Richards flow using van Genuchten retention and Mualem conductivity. Storage change equals joint plus rear entry minus front, lower and other outflows. An implicit mixed storage treatment and adaptive time steps are used. The surface entry operator is checked by numerical differentiation. [5–7,11]

$Se = [1 + (\alpha|h|)^{n}]^{-m}$ for $h < 0$, with $m = 1 - 1/n$. Saturation $Sr = \theta/\text{porosity}$. The strength indicator is $c_{app} = Se \times \max(-u, 0) \times \tan(32°)$, where $u = 9.81h$ kPa. It enters the adopted pressure equations in section 8C. The relation is provisional for this sand; true cohesion remains zero. [10,12,20,32]

Facing and anchorage

Water pressure sampled 0.375 m horizontally behind the face enters an active/at-rest pressure proxy with gravity and strip-load influence. The larger screed footprint and moved rear key are included. A nonlinear grid net equilibrates this pressure and cover weight. The cover changes to a cracked state when an uncracked strain/curvature screen is exceeded. [24]

The crest grid endpoint is fixed. The primary toe support uses 5000 kN/m² translational stiffness; a rigid-toe limit is also calculated. These support treatments are not an iterative coupling to the separate foundation calculation. The latter screens the resulting reaction envelope.

Scope of coupling

Coupling is one way: water → pressure proxy → membrane reaction → toe screen. Soil plastic flow, changing pore volume, bench sag, evolving crack aperture and foundation-induced changes in membrane response are not solved together. Accordingly, the report does not certify a full coupled geotechnical simulation.

8A Hydraulic implementation and boundaries

These are the implemented choices for the retained primary calculation, not newly fitted material properties. They supplement sections 7 and 8 and the executable source retained under reference [24].

Item	Retained implementation
Spatial model	Full-width mesh: 5,355 nodes and 8,960 six-node prisms. Element conductivity uses the arithmetic mean of nodal relative conductivities; storage is lumped.
Storage term	Specific storage Ss = 0.0001 per metre. Integrated storage uses theta(h) + Ss h; theta(h) follows the adopted retention law.
Conductivity	Upper sand Ks = 8.25e-5 m/s; restricted soil Ks = 8.25e-7 m/s. Relative conductivity follows the retained Mualem law.
Joint conductance	g_j = A_j Ks / 0.0001 m. The short contact length is an equivalent resistance parameter, not the 150 mm physical screed thickness.
Rear and front conductance	g_r = A_r Ks / 0.01 m; g_f = A_f Ks / 0.01 m. A is the nodal tributary boundary area in m².
Lower outlet conductance	g_b = A_b (8.25e-7 m/s) / 0.01 m. The restricted layer itself is also resolved above the collector.
Drain activation	Front and lower boundaries discharge for positive pressure head h, using q = g max(h, 0). Exceeding the 192 L/min front limit stops the run; that limit was never reached.
Rear admission	Delayed outflow of the upstream reference cell is distributed 10%, 30%, 60% across upper, middle, lower rear zones, subject to the implemented head limit.

For the conductance formulas, g has units m²/s and q has units m³/s. The rear limiting head is 3.55 m minus the node elevation z. The initial h = -2/9.81 m is uniform pressure head, not hydrostatic total head; subsequent gravity redistribution is therefore expected even in the dry control.

The seepage-face form is consistent with an established pressure-activated drainage boundary [30]. It does not independently validate the selected contact resistance, filter losses, capillary transfer into the actual mat, or the zero-front-flow prediction. Hydraulic spatial convergence has not been established.

8B Facing pressure and support interpretation

Selected pressure and deformation model

The facing is a nonlinear membrane calculation driven by an adopted soil-pressure proxy. It is not a continuum solution for soil stress or plastic displacement. Pressure is sampled 0.375 m horizontally behind the face; moisture-dependent weight, the retained strip surcharge and active/at-rest limits are included. [24]

The mobilized proxy has the form p = p_a + (p_0 - p_a) exp[-max(w, w_history)/d_m]. Here p_a and p_0 are the adopted active and at-rest pressures, w is outward facing displacement and w_history retains its previous outward maximum. The displacement scale is d_m = max[(p_0 - p_a) H/E_eff, 0.0001 m].

The adopted stiffness is E_eff = 25,000 kPa [max(sigma_v_prime, 5 kPa)/100 kPa]^0.5, with H = 3 m. These relations are selected approximations. Fixed anchors do not independently validate this pressure-displacement law or its representation of the sand.

Treatment	Meaning and limit
Cover cracking	When the uncracked strain/curvature screen is exceeded, the whole modeled cover switches to 0.001 of its original bending stiffness. Retention by the 3D mat remains fixed.
Crack indicators	The retained tensile threshold is 0.010% and curvature threshold 0.030 per metre. Individual crack apertures and fragment motions are not solved.
Primary toe support	A translational spring of 5000 kN/m² per unit run provides the facing endpoint restraint. A rigid-end comparison is separately retained.
Foundation screen	The separate rigid-body contact and elastic foundation calculation screens reactions. Its movements are not fed back into the membrane solution.

Accordingly, the 7.17 mm foundation edge-compression envelope is not the toe movement imposed in the facing animation. Section 35A states the additional same-state comparison needed for a single compatible assembled deformation. The fixed crest, perfect loop transfer, cover retention and zero-under-toe-uplift assumptions remain intact.

8C Explicit pressure and suction calculations

This page makes the adopted load construction reproducible. The hydraulic fields, fixed end-transfer assumptions and 70 degree face are unchanged. The following equations are the implemented pressure approximation, not a calibrated continuum stress solution. [24,32,33]

Pressure limits and movement

Let u_plus = max(u, 0), s = max(-u, 0), and sigma_eff = max(sigma_v - u_plus, 0), all in kPa. With true cohesion c_prime = 0, c = c_prime + Se s tan(phi). The limits are p_a = max(K_a sigma_eff - 2 sqrt(K_a) c, 0) + u_plus and p_0 = max(K_n sigma_eff - 2 sqrt(K_n) c, 0) + u_plus. Suction therefore directly reduces both pressure limits.

For face angle beta = 70 degrees and phi = 32 degrees, K_0 = 1 - sin(phi) = 0.47008. Resolving the initial stress normal to the inclined face gives $K_n = K_0 \sin^2(\beta) + \cos^2(\beta) = 0.53207$. The implemented active coefficient is K_a = 0.17550. These coefficients describe different adopted limits; neither is a measured chamber pressure.

The planar trial maximizes $K_a = \sin(\beta) \times [(\cot(\alpha) - \cot(\beta))(\sin(\alpha) - \cos(\alpha)\tan(\phi)) / (\sin(\beta - \alpha) + \cos(\beta - \alpha)\tan(\phi))]$ over $\phi < \alpha < \beta$. The retained 1,500-point search gives alpha = 50.987 degrees. Figure 12 rounds this to 51.0 degrees. It is a coefficient-generating trial plane, not the 32 degree reference wedge or a solved slip surface.

The movement law and stiffness are given in section 8B. The cohesive subtraction, K_n extension and pressure sampled 0.375 m behind the face are adopted approximations. No claim is made that this combination is an exact active-pressure solution for an externally anchored flexible net.

New checks within the same chamber scope

S6-7 replays the adopted law, active-only limit, sustained at-rest limit, phi = 31.02 degrees, and zero suction-strength credit. Each uses the same 53 target hydraulic states, 24 × 16 net, nominal grid stiffness and primary toe spring, with loading at 0, 5 and 10 kPa. Alternative pressures are comparison cases; they do not replace the original storm, material set or fixed assumptions. [33]

Published suction-stress work supports the Se-weighted mechanism [32]. A wave-driven dune study also uses apparent cohesion as suction stress times tan(phi) [20]; its forcing differs from this chamber. Neither source calibrates this sand or validates the adopted facing-pressure law.

9 Hong Kong storm and inverse ponding

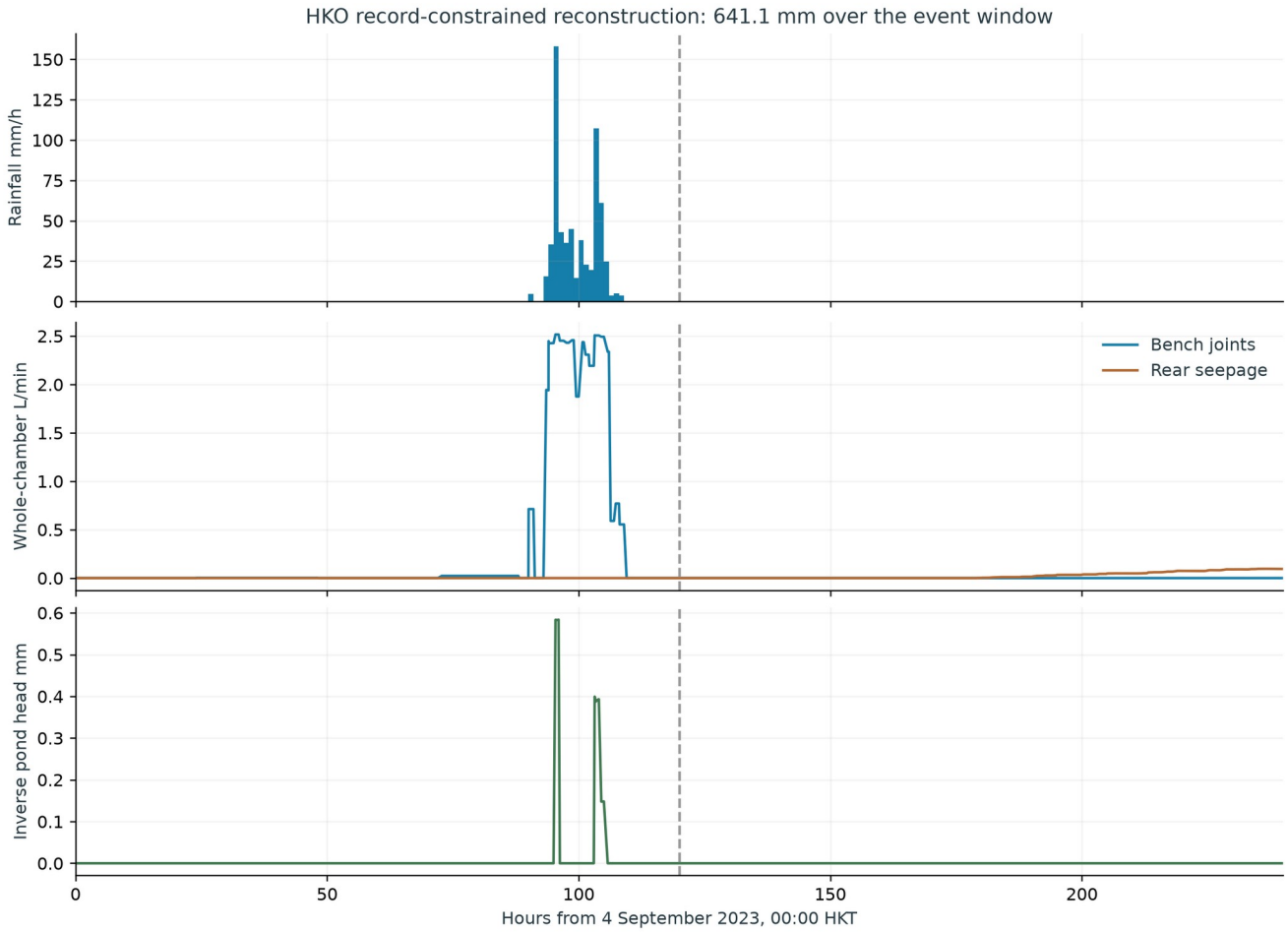


Figure 4. Reconstructed event, calculated joint/rear intake and inverse pond head. The 120 h storm window is followed by 120 h of drainage; the peak intensity is not held constant for five days.

The retained reconstruction uses HKO rainfall totals for 4–8 September 2023 and the published hourly chart. Total 641.1 mm over 24 m² gives 15,386.4 L. The reported 158.1 mm/h peak corresponds to 63.24 L/min of gross bench rainfall. This is a documented severe event, not a claimed world-maximum duration. It is not a complete raw observed hourly series. [1–4]

The primary model admits 2,006.53 L through the joints, with a peak 2.517 L/min. Maximum calculated common pond head is 0.584 mm. Zero-head intervals can still admit supply-limited water; deep standing water is not prescribed.

A single level pond matches the aggregate intake only. It cannot independently impose each natural joint segment's flux. Laboratory makeup, controlled removal, head and admitted volume must all be measured. If spatial matching is required, use calibrated separately supplied joint zones rather than claiming equivalence from total volume alone.

9A Storm fitting windows and residuals

The 120 hourly intervals run from 4 September 2023 00:00 to 9 September 2023 00:00 in Hong Kong time, HKT (UTC+8). Rainfall is reconstructed from the retained HKO event totals and hourly chart; it is not the complete raw observed station series. A further 120 h is used for drainage. [1-4,24]

Constraint	Reconstruction window in HKT	Target mm	Rebuilt mm
4 to 8 September	Entire 120 h event window	641.1	641.1
Daily totals	4 / 5 / 6 / 7 / 8 September	0 / 0.4 / 0 / 215.7 / 425.0	Same
1 h maximum	7 Sep 23:00 to 8 Sep 00:00	158.1	158.1
2 h maximum	7 Sep 23:00 to 8 Sep 01:00	201.0	201.0
3 h maximum	7 Sep 23:00 to 8 Sep 02:00	237.3	237.3
6 h maximum	7 Sep 23:00 to 8 Sep 05:00	334.9	334.9
12 h maximum	7 Sep 22:00 to 8 Sep 10:00	605.8	605.8
Specified 24 h total	7 Sep 16:00 to 8 Sep 16:00	638.5	638.5
Largest sliding 24 h in reconstruction	7 Sep 13:00 to 8 Sep 13:00	See note	638.9125

The listed fitted constraints have zero residual to the displayed precision. The reconstructed maximum sliding 24 h total is 0.4125 mm above the published 638.5 mm value, in a different window. Thus the specified published window is matched, but exact agreement with every possible moving-duration record is not claimed. This detail does not change the retained 641.1 mm event accumulation.

Gross catchment volume = 641.1 mm x 24 m² = 15,386.4 L. The 158.1 mm/h peak gives 63.24 L/min gross rainfall. Neither quantity is the joint intake: surface routing and the adopted joint-entry resistance reduce the retained total joint admission to 2,006.53 L.

This is a documented severe Hong Kong event, not a demonstrated worldwide longest or maximum storm. The multiday window includes low-rain and dry periods; the peak intensity is not applied continuously. Section 9B publishes the retained hourly reconstruction so that this distinction is reproducible.

9B Retained hourly rainfall reconstruction

Hourly depth in millimetres. Each row starts at the stated HKT hour and ends one hour later. All 120 retained inputs are shown, rounded to four decimal places. These are reconstructed values, not newly obtained raw observations. [1-4,24]

Hour HKT	4 Sep	5 Sep	6 Sep	7 Sep	8 Sep
00:00	0	0.0167	0	0.1375	42.9
01:00	0	0.0167	0	0.1375	36.3
02:00	0	0.0167	0	0.1375	45.0537
03:00	0	0.0167	0	0.1375	14.5659
04:00	0	0.0167	0	0.1375	37.9805
05:00	0	0.0167	0	0.1375	22.9789
06:00	0	0.0167	0	0.1375	19.5643
07:00	0	0.0167	0	0.1375	107.1253
08:00	0	0.0167	0	0.1375	61.0277
09:00	0	0.0167	0	0.1375	24.9301
10:00	0	0.0167	0	0.1375	3.866
11:00	0	0.0167	0	0.1375	5.0855
12:00	0	0.0167	0	0.1375	3.6221
13:00	0	0.0167	0	0.1375	0
14:00	0	0.0167	0	0.1375	0
15:00	0	0.0167	0	0.1375	0
16:00	0	0.0167	0	0	0
17:00	0	0.0167	0	0	0
18:00	0	0.0167	0	4.6973	0
19:00	0	0.0167	0	0	0
20:00	0	0.0167	0	0	0
21:00	0	0.0167	0	15.429	0
22:00	0	0.0167	0	35.2737	0
23:00	0	0.0167	0	158.1	0

10 Water budget and separate outlets

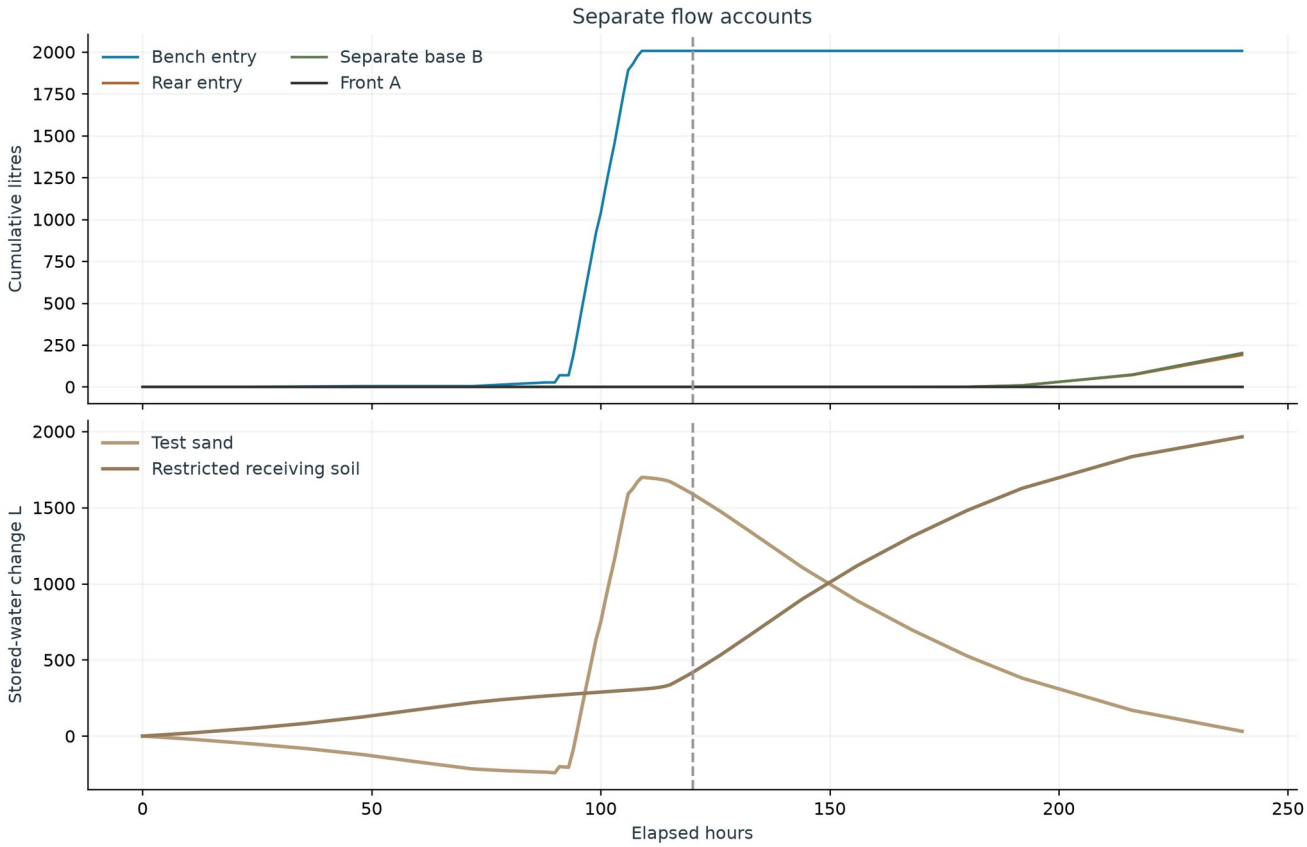


Figure 5. Conserved water accounts and storage. Lower collection is shown only to close the water balance; it is never included in front-drain performance.

Whole chamber	At 120 h	At 240 h
Bench intake	2,006.53 L	2,006.53 L
Rear intake	0.00 L	190.43 L
Front outlet A	0.00 L	0.00 L
Separate lower outlet B	0.00 L	201.58 L
Upper storage change	1,590.26 L	31.38 L
Lower storage change	416.27 L	1,964.01 L

Rear supply is the calculated restricted-layer discharge of an otherwise similar upstream reference cell. It is distributed 10%, 30% and 60% across upper, middle and lower rear zones. It is not forced to equal this chamber’s bottom outflow at the same instant. Upstream storage produces time lag. Supply can continue during the nominal post-storm period.

Maximum recorded soil mass-balance error is 0.00128 L. Good balance checks bookkeeping; it does not validate the local wetting pattern or the joint leakage parameters. Significant stored water may remain after the equal-duration drainage window.

11 Front drain collection attachment

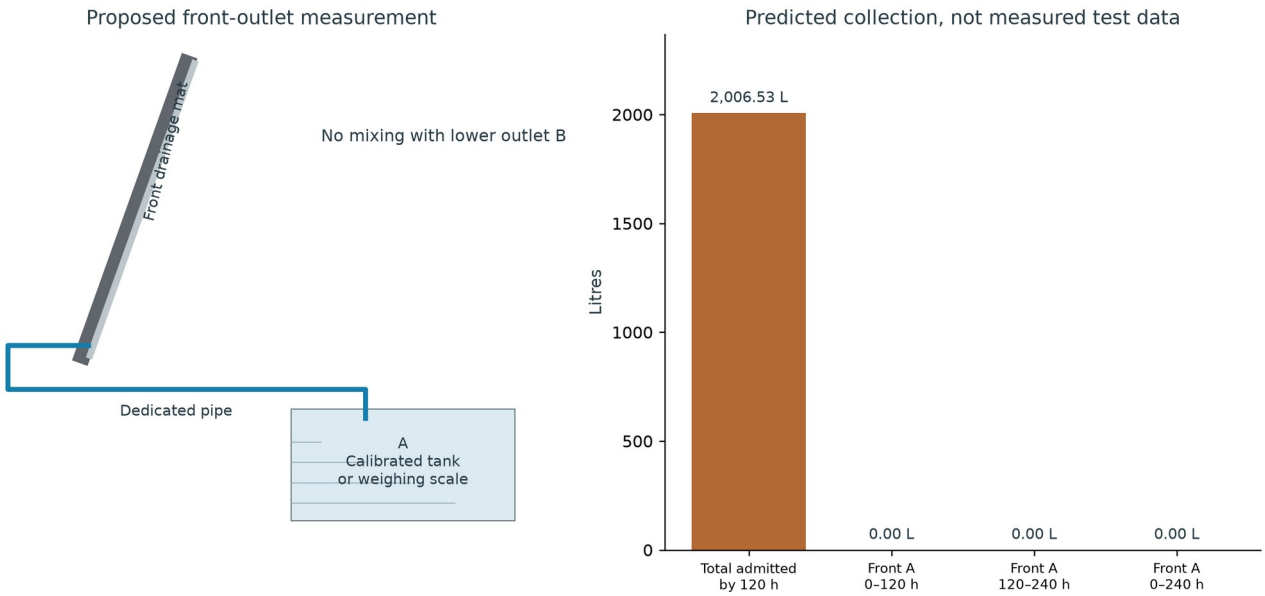


Figure 6. Dedicated front-mat pipe to a calibrated collector. All figures are predictions from this model, not observations from a completed chamber test.

Front drainage only	Predicted volume
Collected by storm end, 0–120 h	0.00 L
Additional collection, 120–240 h	0.00 L
Total front collection, 0–240 h	0.00 L
Total bench + rear entry by 120 h	2,006.53 L
Total bench + rear entry by 240 h	2,196.96 L

Use an independently tared weighing tank or calibrated volume tank downstream of the front outlet. Record cumulative reading at 120 h and again at 240 h; their difference is the post-storm collection. A tipping/flow device can provide the time series, with overflow captured and separately recorded. Keep collector head from backing up the pipe.

The front boundary releases water only where positive pressure reaches the face. A zero prediction means that boundary is inactive in this scenario; it does not mean a physical mat removes no water, that its capacity is proven, or that all inflow has left. The lower collector and stored water must account for the remainder. A different initial condition, leakage law or boundary may activate the front outlet.

12 Local saturation through time

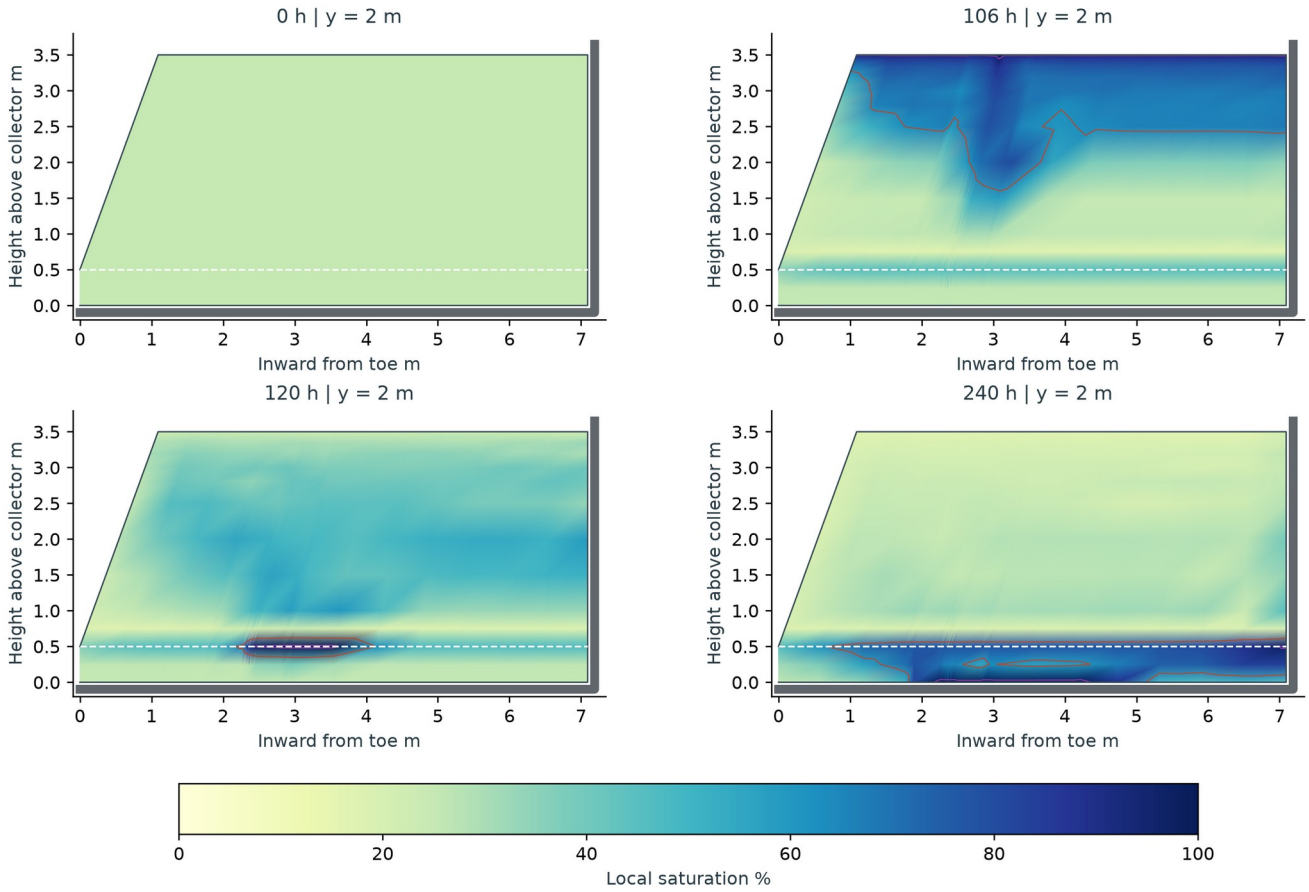


Figure 7. Centre section at loaded start, peak facing response (106 h), storm end and after drainage. Red contour: 62%; purple: 95%, wherever present. These are model fields, not measured saturation pockets.

Stage	Mean upper sand	Local range	Maximum u
0 h	25.13%	25.1–25.1%	-2.0000 kPa
106 h	30.18%	15.0–100.0%	-0.0190 kPa
120 h	30.18%	14.5–100.0%	0.0427 kPa
240 h	25.23%	14.0–96.5%	-0.2459 kPa

A local wet pocket and the volume-average saturation describe different things. Continued inflow does not imply uniform full saturation, and a drained face does not guarantee absence of internal saturation. Field detail depends strongly on retention, conductivity, joint pathways and lower boundary calibration. Spatial convergence is not established. [5–12]

12A Local saturation and fixed monitoring points

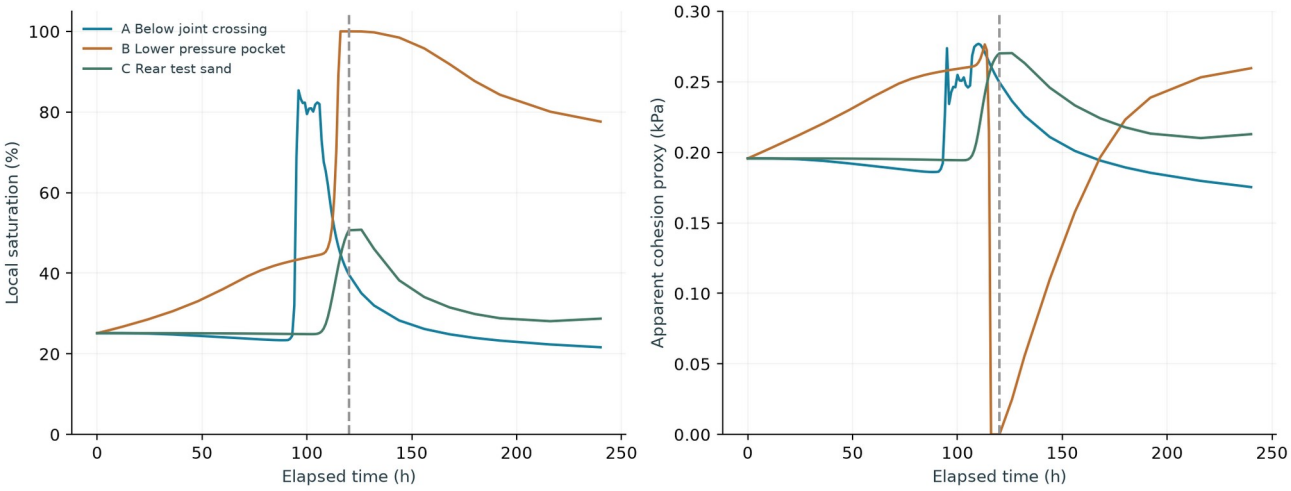


Figure H1. Three fixed nodes followed through the same 240 h record. B lies at the test-sand and restricted-layer interface. The dashed time line is storm end, not the instant all stored water has drained.

Point	Location	x m	y m	z m
A	Below joint crossing	3.053	2.000	3.000
B	Lower pressure pocket	2.955	2.000	0.500
C	Rear test sand	6.531	2.000	1.500

Local saturation Sr is the fraction of pore volume filled with water at one location. It is not the percentage of the whole chamber that is wet. Sr = θ / n, where θ is volumetric water content and n = 0.400749 is the adopted porosity. For example, Sr = 62% corresponds to θ about 0.2485 m³ of water per m³ of soil.

The plot keeps the same node at every time. A is the nearest saved node below the joint crossing, B is the node of highest upper-sand pressure at 120 h, and C samples the rear test sand. They illustrate different local histories; none substitutes for a whole-volume average or a complete sensor grid. Smooth lines connect saved states. [5–9,11]

12B Saturation history and retained water

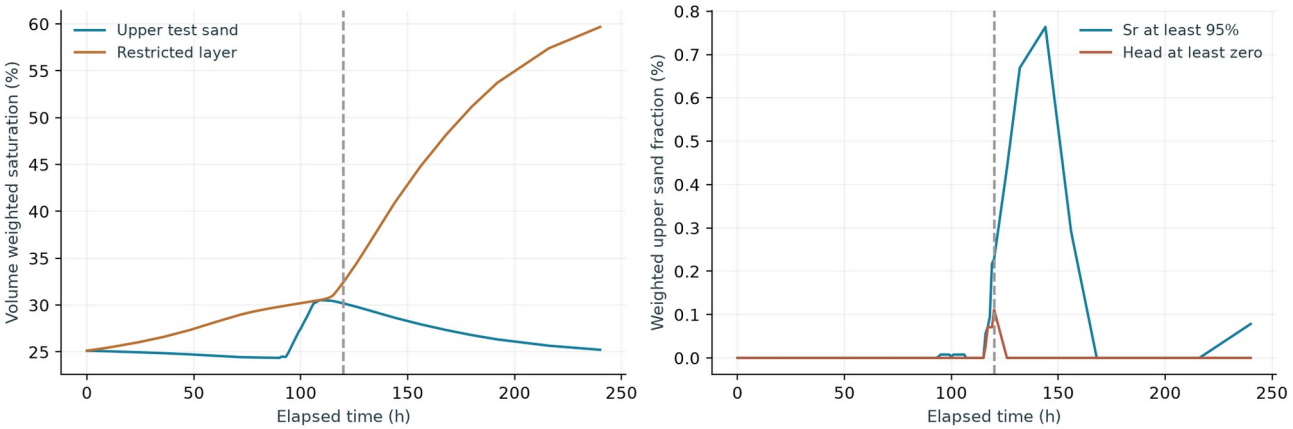


Figure H2. Volume-weighted saturation and upper-sand wet fractions. The 95% band and nonnegative-head criterion are different; near-full saturation may occur while pressure is still slightly negative.

Time h	Mean sand %	Mean lower %	Sr at least 95% volume %	Head at least zero volume %
0	25.13	25.13	0.000	0.000
72	24.44	28.99	0.000	0.000
106	30.18	30.43	0.008	0.000
120	30.18	32.45	0.228	0.111
168	27.34	48.18	0.000	0.000
240	25.23	59.68	0.078	0.000

At 106 h the local maximum reaches 99.996% saturation, yet the maximum upper-sand pressure remains slightly negative. At 120 h approximately 0.111% of the weighted upper sand has nonnegative head. These are nodal volume indicators on the retained mesh, not measured pocket volumes or a converged sharp-front boundary.

By 240 h the upper sand average is close to its initial value, but the restricted layer average has risen to 59.68%. Added storage remains about 31.38 L in the upper sand and 1,964.01 L below it. A recovered upper average therefore does not mean the chamber has dried. The equal-duration drainage window ends at 240 h; continued drainage is not calculated here.

12C Reading local fields and saved maxima

All local saturation, suction and pressure illustrations are post-processing of the retained six-metre solution. Their displayed numerical precision is useful for reproducing that solution, but does not establish measured accuracy. The original figures and plotted coordinates have been preserved.

Interpretation	Required reading of the retained figures
Local saturation Sr	Water volume divided by pore volume. A high local value and a low whole-block mean can coexist; mean saturation cannot specify a local pressure.
Effective saturation Se	The normalized water-content variable in the retention and suction-strength law. It is not interchangeable with Sr.
Pressure and front discharge	The maximum +0.0427 kPa is an upper-sand saved-state result, not necessarily pressure at a drain boundary. Front discharge requires positive pressure at that boundary.
Lower wetting band	The 25 cm band is a reporting region. It is not a mechanically identified slip plane or proof of a continuous failed soil layer.
Stress and reference wedge	The 32 degree wedge is geometric. The vertical stress indicator is not the outward grid pressure or a complete soil stress tensor.
Spatial and temporal limits	Hydraulic mesh convergence is not established. The 30 versus 60 minute maximum-step comparison does not establish spatial accuracy or an exact continuous-time peak.

Saved sampling used for reported extrema

The retained primary record has 53 saved times in hours: 0, 6, 12, 24, 36, 48, 60, 72, 78, 84, 87, 88; every integer hour from 89 through 120; then 126, 132, 144, 156, 168, 180, 192, 216 and 240. Adaptive internal integration steps are distinct from these output times.

In this report, the 106 h facing maximum and the 120 h maximum upper-sand pressure are maxima among the saved states used for reporting. Front collection of 0 L is an output of the adopted inactive seepage boundary; it does not measure drain-mat capacity. A spatial refinement and an independent wetting/drainage benchmark remain needed before treating precise wet-pocket sizes and local extrema as resolved predictions. [7,11,30,31]

13 Suction and apparent cohesion

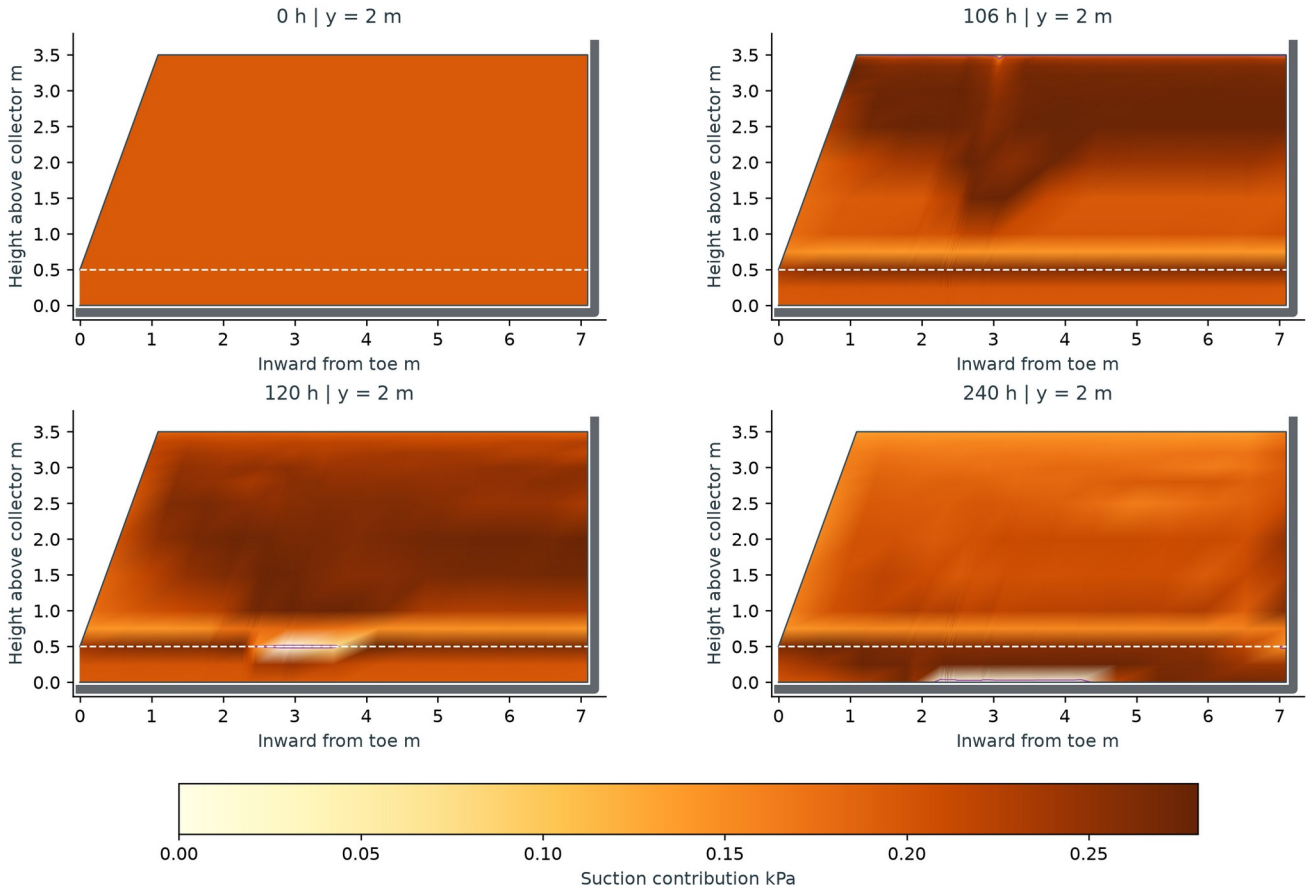


Figure 8. Spatial suction contribution using the assumed Se × suction relation. Zero in a saturated region means loss of this contribution, not negative cement-like bonding.

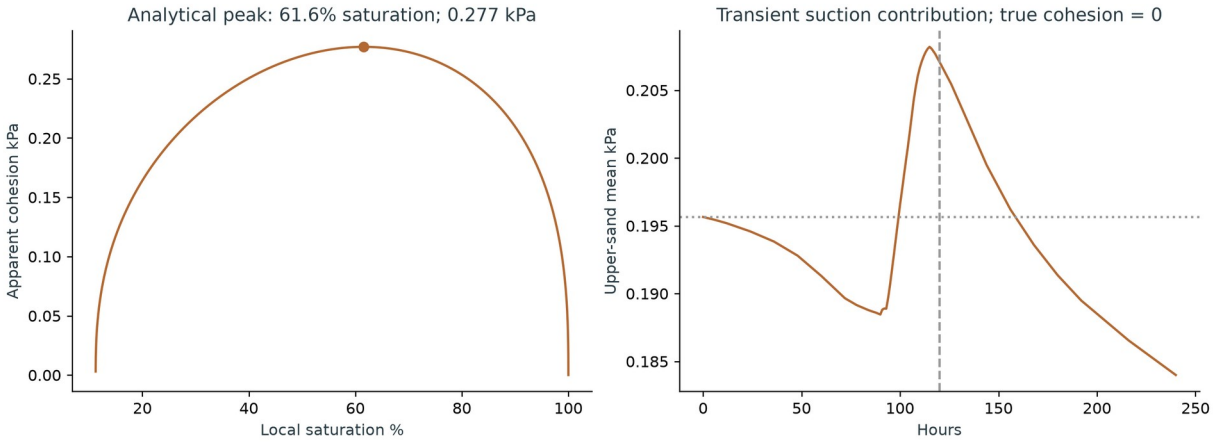


Figure 9. Recalculated analytical maximum: 61.6% saturation and 0.277 kPa. The transient history is unchanged. This small, reversible contribution is not intrinsic cohesion.

The benefit can increase on wetting an initially dry part and disappear on further saturation. It cannot be maximized everywhere by selecting a global saturation percentage. No permanent cohesion is created. The model uses the water state produced by the imposed rain and drainage; it does not tune saturation for a favorable result. [10,12,26]

13A Meaning of suction and apparent cohesion

Definitions used in this assessment

Pore water pressure is u = 9.81h kPa, where h is pressure head in metres. With atmospheric pore-air pressure as zero, matric suction is max(−u, 0). Effective saturation is Se = (θ − θr) / (n − θr), with θr = 0.045. Se and the pore-volume saturation Sr are not interchangeable.

The adopted strength indicator is c_app = Se × max(−u, 0) × tan(32°). True effective sand cohesion c′ remains zero. This is a reversible capillary contribution, not cementation, bonding created by rainfall or an independently measured material strength. Suction-stress literature supports the mechanism; the particular Se weighting and retention parameters require calibration for this sand. [5,8–10,26]

Stage h	Mean c_app kPa	Near 62% volume %	Volume above initial c_app %
0	0.1957	0.00	0.00
72	0.1897	0.00	20.67
106	0.2032	4.41	49.14
120	0.2071	0.96	57.83
168	0.1936	0.45	47.53
240	0.1840	0.42	32.92

Near 62% means the reporting interval 57% to 67%, not a stability threshold. The unchanged analytical relation peaks at approximately 61.6% saturation and 0.277 kPa. A positive contribution exists over a broader unsaturated range. Wetting can first increase this term and then reduce it as pressure approaches zero; saturation removes the suction term.

Corrected maximum calculation: let s = -h > 0, a = 14.5/m, n_v = 2.68 and m = 1 - 1/n_v. Then c_app = 9.81 s tan(32°) [1 + (a s)^n_v]^(-m). Setting its derivative to zero gives (a s)^n_v = 1/(n_v - 2), so s = 0.0796395 m, Se = 0.56724 and Sr = 61.58346%; c_app = 0.276920 kPa. Scalar numerical maximization independently confirms this point. The transient calculation already used the same law; its local fields and time history do not change.

An increase in the average can coexist with a loss of strength at a particular wet pocket. For example, the mean rises from 0.1957 kPa initially to 0.2071 kPa at 120 h while the saturated pocket loses its suction contribution. At 240 h the mean is 0.1840 kPa. No favorable global saturation percentage or natural stable angle is imposed. [10,12,26]

13B Where suction benefit increases and decreases

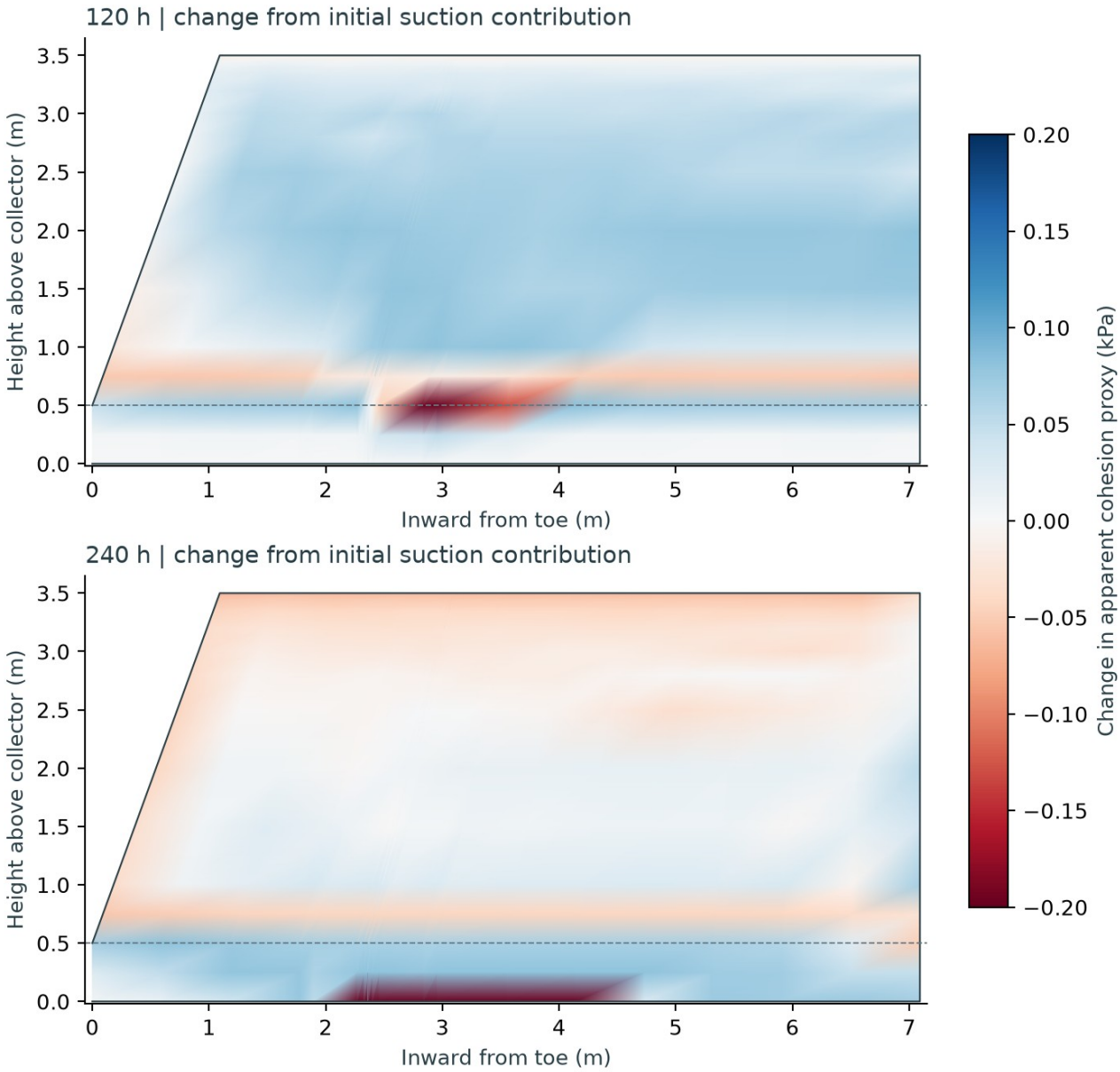


Figure H3. Change in the apparent-cohesion proxy from the initial −2 kPa state at the same locations. Blue is a gain; red is a loss. The dashed line separates the upper sand from the restricted layer.

These sections complement the absolute suction maps already retained. A red region can still have positive apparent cohesion: red means lower than its own initial 0.1957 kPa value. Zero apparent cohesion occurs where suction disappears; a negative difference is not negative intrinsic cohesion.

At 120 h, 57.83% of the weighted upper sand has a contribution above the initial value. At 240 h that fraction is 32.92%, and the upper mean is below its starting value. Redistribution and drainage change both wet and relatively dry regions, so adding or removing water is not uniformly beneficial.

The 62% contour, the largest suction contribution and the mechanically critical region are different concepts. These maps alone do not establish a factor of safety, a slip surface or the amount of unstable soil. Spatial convergence and measured retention remain outstanding. [10–12,26]

14 Water pressure and lower wetting zone

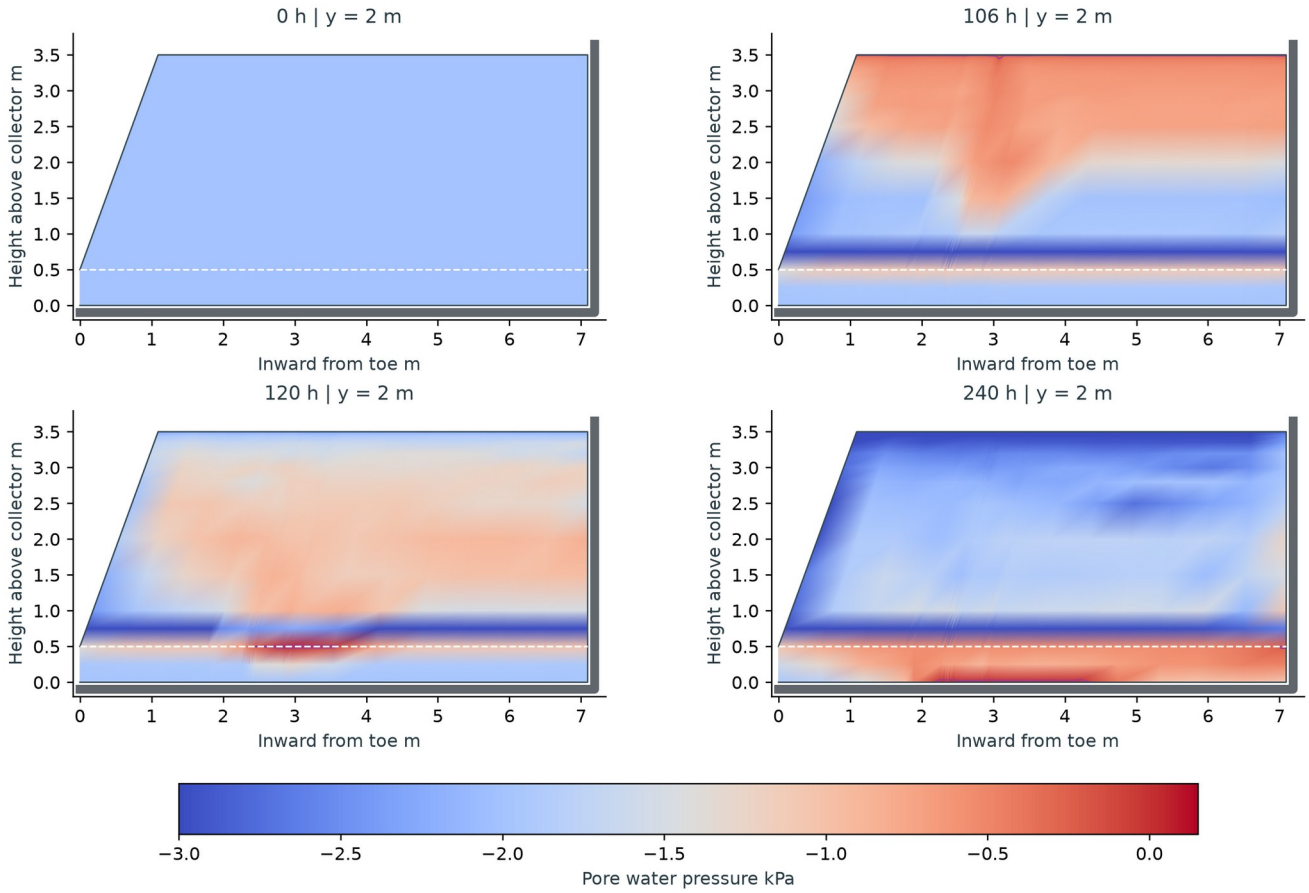


Figure 10. Positive and negative water pressure in the same sections. Colour saturation clips the negative range for readability; exact nodal values are in the supplement.

The lower-permeability layer delays downward drainage. Local gravity flow is controlled by conductivity and hydraulic head, so it need not be uniform over the bottom. A model with a constant bottom flow or a forced equality between rear supply and local bottom discharge would be a different boundary condition. [11]

The earlier 25 cm wet-slip illustration came from a different trial case and cannot be transferred as a fixed failure plane into this revised chamber. Here the lowest 25 cm is marked only as a region to inspect. A wetting contour is not itself a mechanical slip surface.

The outside toe foundation is not part of this seepage mesh. Therefore the prescribed zero toe uplift remains independent of the internal pore-pressure result. Front and bottom outlets must discharge clear of the toe in the proposed apparatus.

14A Lower wetting zone and pressure response

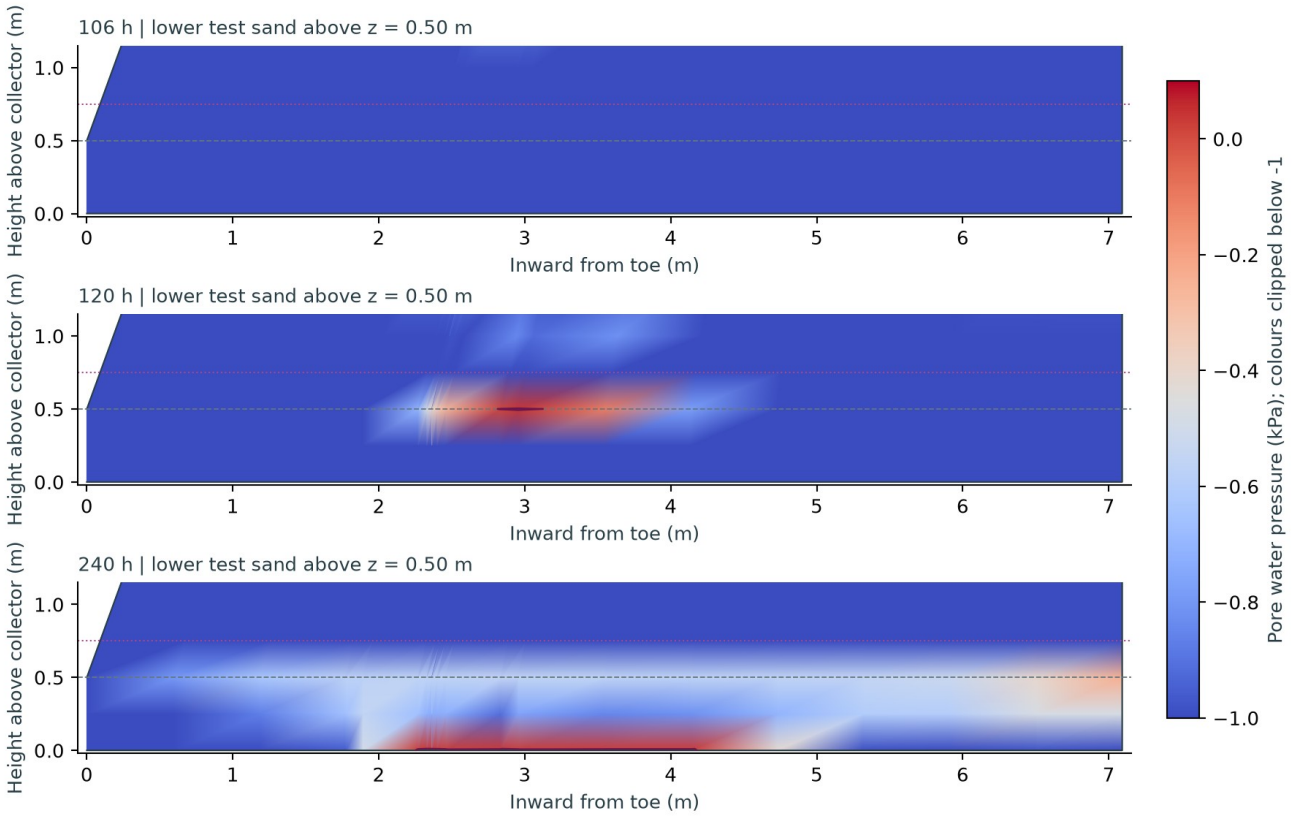


Figure H4. Close cross-sections of the bottom region. Dashed grey marks z = 0.50 m; dotted purple marks z = 0.75 m, the top of the 25 cm review band. A dark zero-pressure contour appears only where present.

Time h	Maximum u in review band kPa	Maximum Sr in review band %
106	-1.0982	45.044
120	0.0427	100.000
240	-0.2459	96.496

The restricted layer is 0.50 m thick with saturated conductivity 8.25×10^{-7} m/s, one hundredth of the upper sand value. It uses the same assumed retention relation. This delays transfer to the base collector; it does not prescribe a uniform discharge or guarantee a permanent saturated layer. [5–9,11]

The front boundary discharges only where positive head reaches it. No front discharge is activated in this saved case, so the 192 L/min index cap is not tested. The internal positive-pressure pocket at 120 h is away from the face. The 25 cm band is an inspection region, not the old trial failure plane. No pore-pressure result here verifies the separately imposed zero uplift under the external toe.

15 Across width variability and pond equivalence

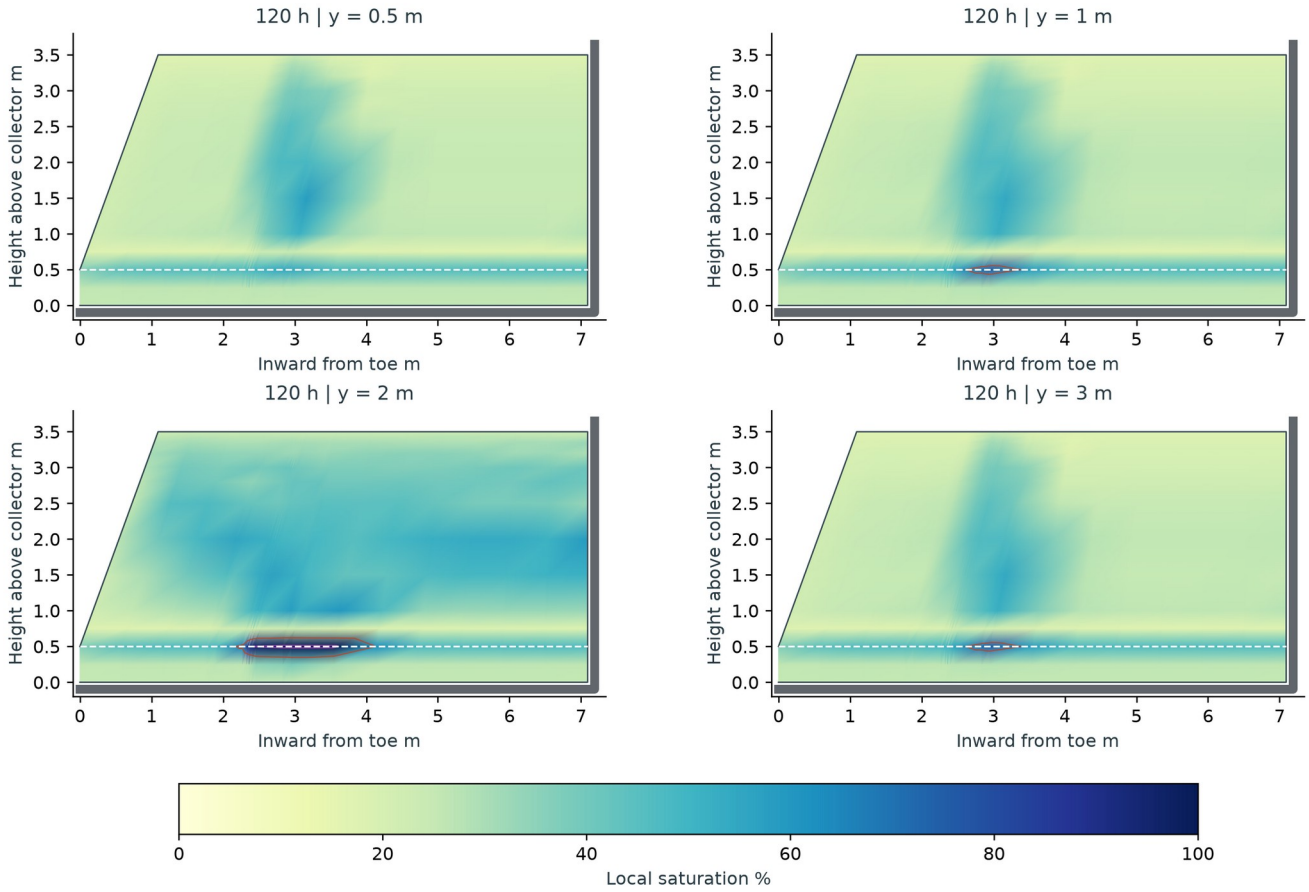


Figure 11. Four sections across the chamber at 120 h. The inward joint follows y = 2 m; other sections are progressively farther from it.

The primary run records a cumulative absolute spatial difference of 368.31 L between natural-joint and common-pond entry distributions. This is a sum of absolute nodal differences, not missing water. The total intake is matched while the distribution can differ.

The original desired pattern—less at the leading edge, more near the crossing and moderate inward—is a qualitative boundary concept. This rerun represents it through routed rainfall and actual joint locations, rather than prescribing a favorable moisture field. The common-pond approximation and unmeasured crack conductance remain consequential limitations.

For physical confirmation, record admitted volume separately along the transverse and inward lines during a preliminary bench-only calibration. A total-flow match alone is insufficient to demonstrate the same suction map.

15A Across width variability and point comparison

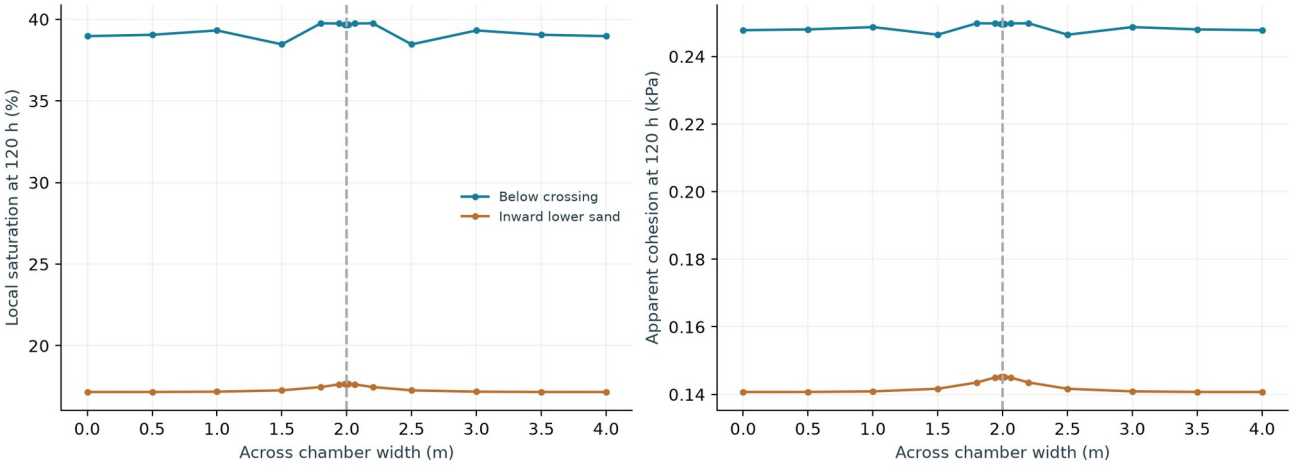


Figure H5. Fixed x and z sampling lines across the full chamber at 120 h. Points are saved mesh nodes; the same colour identifies each line in both plots. Dashed vertical marks the inward joint at y = 2 m.

Sampling line	x from toe m	z above collector m	Sr range across width %
Below crossing	3.053	3.000	38.46 to 39.75
Inward lower sand	5.342	0.750	17.16 to 17.66

The centre section intersects the inward joint, while other sections sample soil farther from that entry line. Widthwise differences arise from joint locations, the transverse surface grade and hydraulic spreading. The earlier four section saturation map is retained alongside this point comparison.

Equal saturation at two points means equal water-filled pore fraction. For unsaturated points, this model’s single retention law maps it to the same pressure and suction proxy. Fully saturated points can have different positive pressures. Equal saturation does not imply equal total stress, confinement or stability. Real soil hysteresis and material variation can change that relation. A mean saturation cannot replace these local values. [5,8–12]

The retained mesh has 5,355 nodes and 8,960 six-node prisms across 4 m. Its fine joint resolution does not establish spatial convergence of the wetting pockets. Monitoring should include points under the crossing, away from the inward joint and above the restricted layer; all point coordinates and histories are supplied.

15B Rainfall intake and ponding equivalence

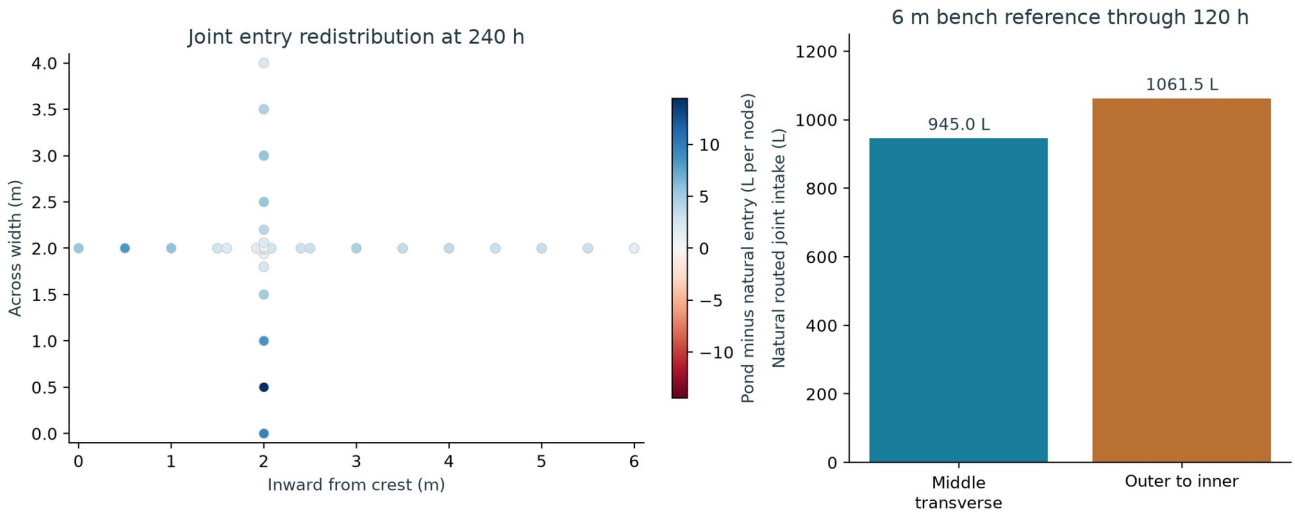


Figure H6. Natural routed entry by joint and cumulative nodal redistribution under common ponding. The left colours are litres assigned to nodes, not flux per unit area; node spacing is unequal.

The six-metre natural reference admits 945.04 L through the middle transverse joint and 1,061.49 L through the outer-to-inner joint. The middle share is 47.10%. These current routed results replace the earlier prescribed 70/30 split and four-metre percentages; the leakage pattern is not tuned to increase suction.

At each step the common pond matches total natural-reference joint intake, Qpond = Qnatural. It has only one water level and cannot independently set all segment fluxes. The cumulative sum of absolute nodal differences is 368.31 L, with effectively zero net difference. Half that sum, 184.16 L, is the redistributed volume counted once, about 9.18% of total joint entry.

Reference surface routing uses 2% inward and 2% transverse grades, Manning roughness 0.015, and entry limited by weir, orifice and Darcy-contact expressions. Provisional factors are 1.4, 0.6 and capture factor 1.0; equivalent contact length is 0.0001 m. It is a resistance parameter, not physical screed thickness. A 2 mm crack requires measured conductance. [13,24]

A common pond can reproduce aggregate entry without reproducing every local saturation history. For closer spatial equivalence, calibrate independently supplied joint zones and measure actual intake, pond storage and withdrawal. Submillimetre model head is not a stand-alone field setpoint. The retained report states this limitation rather than asserting point-by-point equivalence.

15C Physical replay of the calculated intake

The target is the retained rainfall-derived joint intake history. The common water level is a means of supplying that history; it is not an independent requirement to keep the whole bench continuously ponded. The audit identifies two operating regimes within the same retained calculation. [24,31]

Regime	Retained numerical result	Physical control meaning
Supply-limited wetting at zero head	1,555.54 L, or 77.52% of total joint entry, occurs at computed zero common head; these inflow intervals total 54 h.	Meter water to the calibrated joint zones or wet only the area needed to admit the target rate. Do not impose a continuous positive pond in these intervals.
Positive-head ponding	The remaining 450.99 L, or 22.48%, is admitted in positive-head intervals. Maximum calculated common head is 0.584 mm.	Use measured makeup and controlled removal to track the target intake. Calibrate the relationship between level and admission before the test.
Spatial equivalence	184.16 L is redistributed between nodes, counted once: 9.18% of total joint intake.	One common level matches aggregate inflow, not each segment. Independently fed zones are needed if matching the local flux history is required.

At positive-head steps the inverse calculation selects the level required by the conductance law. When that solution would require a negative level, the model uses zero head and scales the potential admission to the available supply. This second regime represents supply-limited wetting; it is not a continuously flooded boundary with an arbitrarily small positive depth.

For the physical replay, separately measure water delivered, pond storage change, surface overflow or withdrawal, and actual joint admission. The admission balance is delivered water minus storage increase and surface removal, with any measurable evaporation accounted for. A fixed positive depth alone cannot guarantee the retained inflow. The submillimetre head is a model result, not a robust uncalibrated field setpoint.

Keep the delayed rear supply during post-storm drainage as recorded. Front and lower collectors remain separate. The retained model gives 0 L front collection at 120 h and 0 L additional by 240 h; approximately 1,995.39 L of additional water remains stored at 240 h. Equal storm and drainage durations do not mean complete drying.

16 Soil wedge stress and weak wet pockets

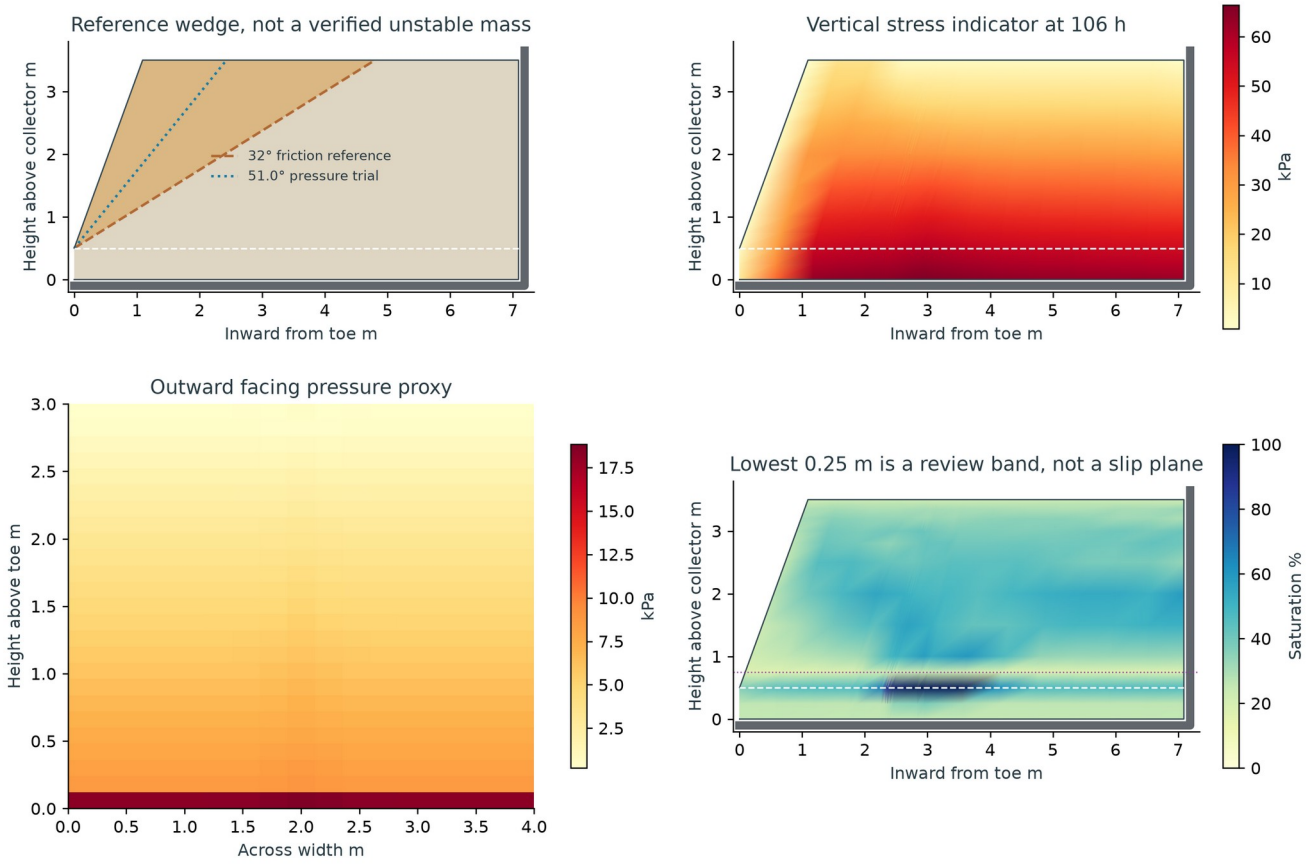


Figure 12. Separate geometric reference, vertical stress indicator, facing pressure proxy and lower wetting map. Stress plots use 106 h; the wetting panel uses 120 h.

The 32° line is the adopted friction-angle reference. Its geometric wedge against the 70° face has 5.564 m² of section per metre width. It is not a calculated unstable mass or a rainfall-dependent natural stable angle. The additional rear bench does not automatically join this wedge.

The 51.0° pressure-trial line maximizes the adopted coefficient in section 8C; it is not a solved slip surface. The derived vertical-stress indicator reaches approximately 58.25 kPa in the test sand. It integrates moisture-dependent column weight and an elastic strip-load influence. The separate facing-pressure field drives the membrane. Neither is a full soil stress tensor or an elastoplastic failure solution.

High applied stress and low available resistance are different quantities. A saturated pocket can lose suction contribution without being the location of maximum total stress. This assessment does not substantiate the earlier 34–37° global-angle estimates for the revised chamber. [12,26]

16A Stress indicators and reference wedge quantities

Quantity	Retained value	Meaning
Face angle	70 degrees	Constructed test geometry
Reference inclination	32 degrees	Adopted effective friction angle
Reference reach from toe	4.801 m	Horizontal reach of the reference line at crest elevation
Reference width behind crest	3.709 m	Difference between the two geometric lines
Section wedge area	5.564 m² per m width	Geometric section only
Full width wedge volume	22.255 m³	Section area multiplied by 4 m
Maximum vertical indicator	58.25 kPa	Upper test sand at 106 h

For height H = 3 m, the reference area is $A = 0.5H^2[\cot(32°) - \cot(70°)]$. It describes the soil between two straight lines. It is not a solved unstable mass, and multiplying it by a bulk unit weight would not establish the force that must be carried by the grid or toe.

The vertical-stress indicator integrates moisture-dependent column self-weight and adds an elastic strip-load influence for the 10 kPa surcharge and 3 kPa screed self-weight. It is highest near the lower part of the retained sand under the loaded region. It does not include a solved stress tensor, plastic redistribution, principal directions or shear-strain localization.

The outward pressure proxy that loads the facing is a different field. It uses water conditions sampled behind the face and the chosen pressure-mobilization law. Neither a vertical-stress maximum nor a wet pocket is automatically the largest outward grid load. The existing stress, pressure and wedge panels remain for comparison. [12,14,24,26]

The 6 m rear extent does not automatically add the entire bench to the reference wedge. The older 34 to 37 degree apparent global-angle estimates and the old 25 cm wet-slip illustration are not validated results for this revised chamber. A separate stability analysis is required to identify a mechanical failure surface and its available resistance.

16B Relating stress to the wet pocket

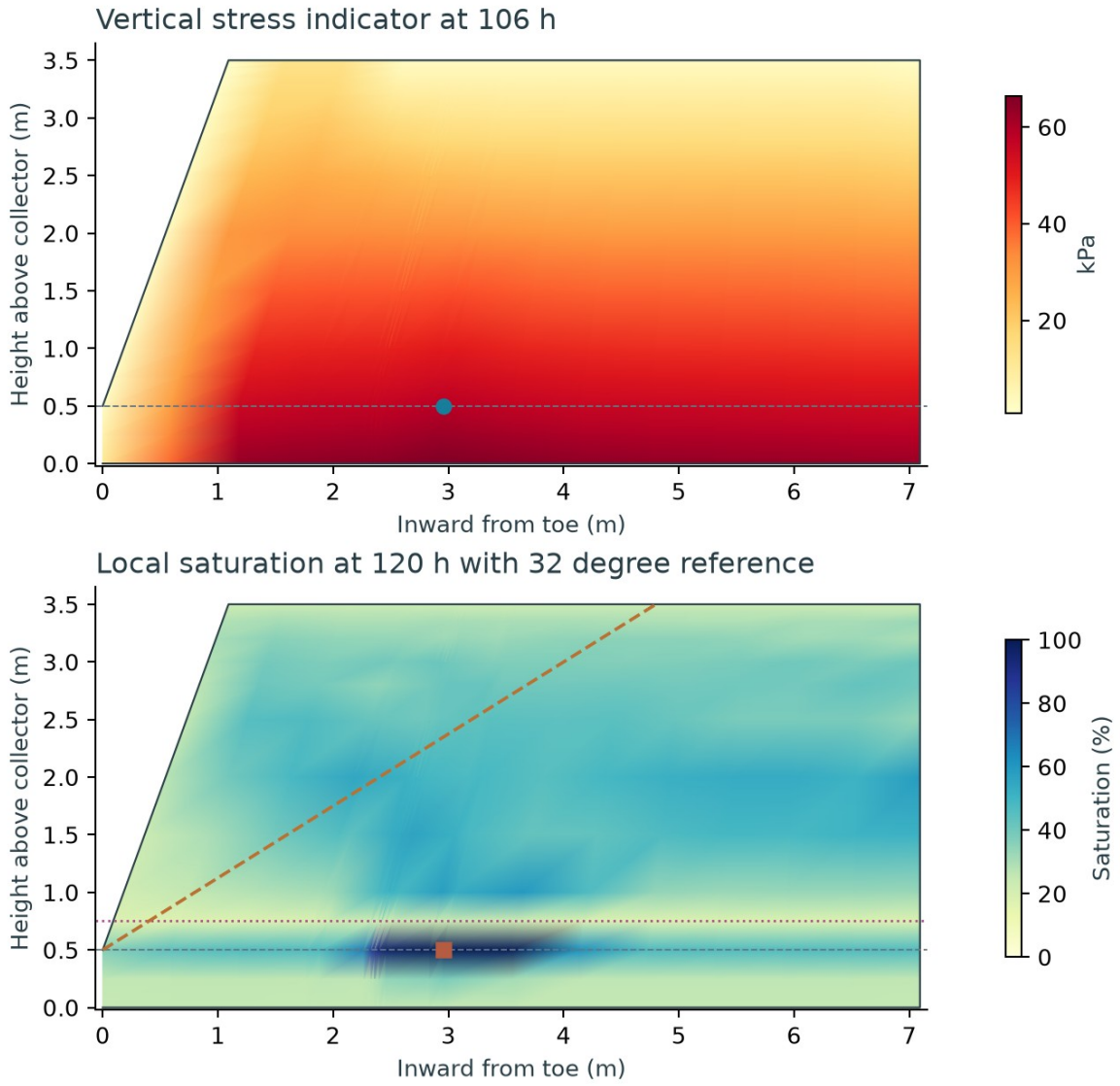


Figure H7. Blue circle marks the maximum vertical-stress indicator in the upper test sand at 106 h. Red square marks the highest centre-section water pressure at 120 h. The orange line is the geometric 32 degree reference, not a calculated failure boundary.

In this saved mesh both marked maxima occur at the same interface node: x = 2.955 m inward from the toe, y = 2.000 m across the width, z = 0.500 m above the collector. The quantities are evaluated at different times. Their co-location does not establish that the node or surrounding pocket has failed.

The vertical indicator is 58.25 kPa at 106 h; the maximum upper-sand water pressure is +0.0427 kPa at 120 h. At a saturated point the assumed suction contribution is zero. Available resistance still depends on effective normal stress, friction, stress direction and facing restraint; subtracting a small pore-pressure value from a vertical indicator is not a full slope-stability calculation.

The lower wetting zone, the reference wedge and the facing bulge band are therefore retained as separate overlays. This preserves where the soil is wet, where load is high and where the facing moves, without treating those three maps as the same mechanism. The full-face and bench deformation sections that follow remain at their original calculated scale.

17 Facing bulge before during and after

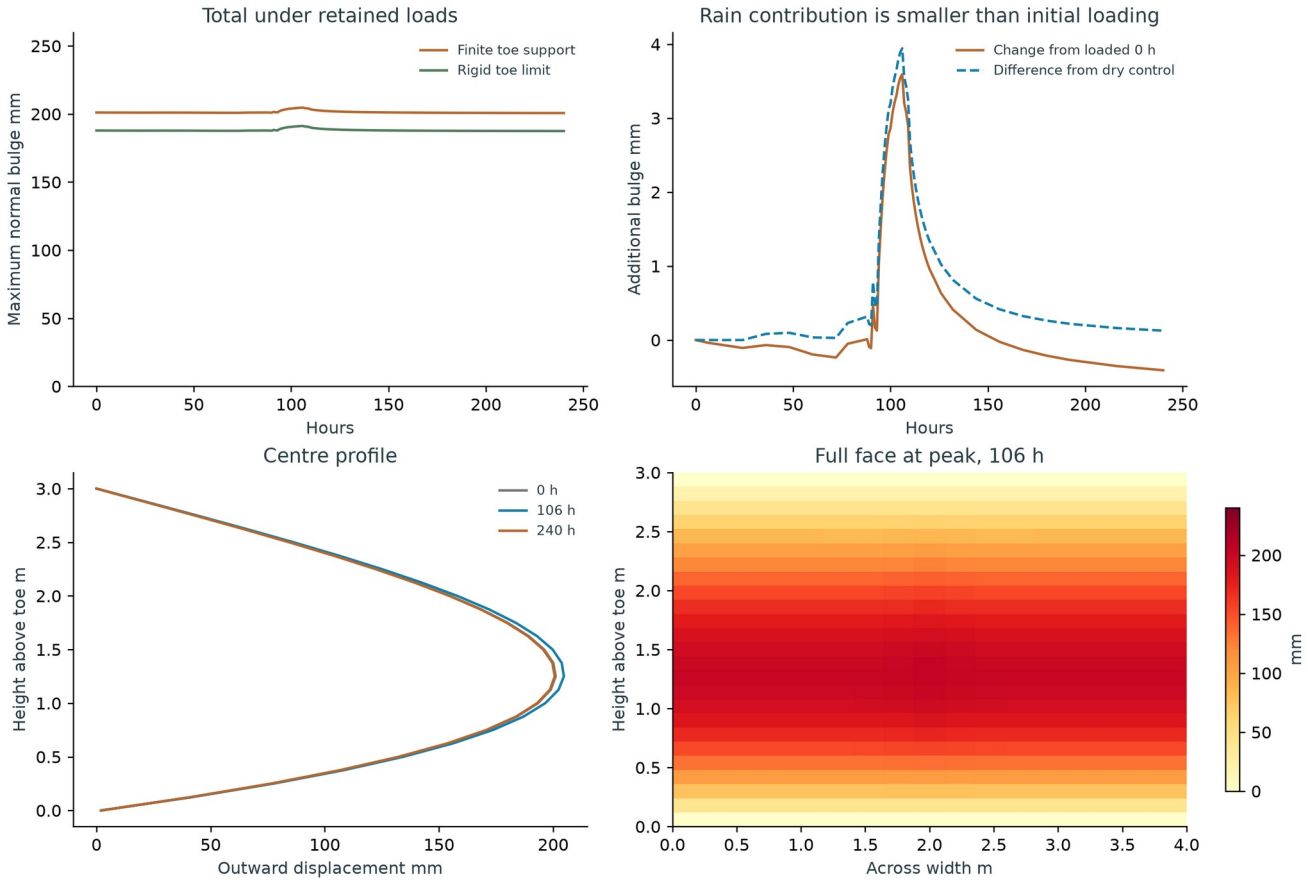


Figure 13. Full-load response, rainfall increment, centre profile and full-face bulge map. Displacements are normal to the original slope plane.

State	Bulge	MD strain	Nominal strength ratio
Loaded before rain	201.09 mm	0.888%	6.62
Saved maximum 106 h	204.69 mm	0.918%	6.41
Storm end 120 h	202.05 mm	0.896%	6.56
After 240 h	200.68 mm	0.885%	6.65

The unbulged shape is an as-installed geometric reference. After applying retained soil and the 10 kPa strip load, the model already predicts substantial deflection before rain. It would be incorrect to portray the entire final bulge as caused by the storm. The dry control distinguishes rainfall effects from redistribution of the initially uniform suction.

17A Pressure and suction sensitivity results

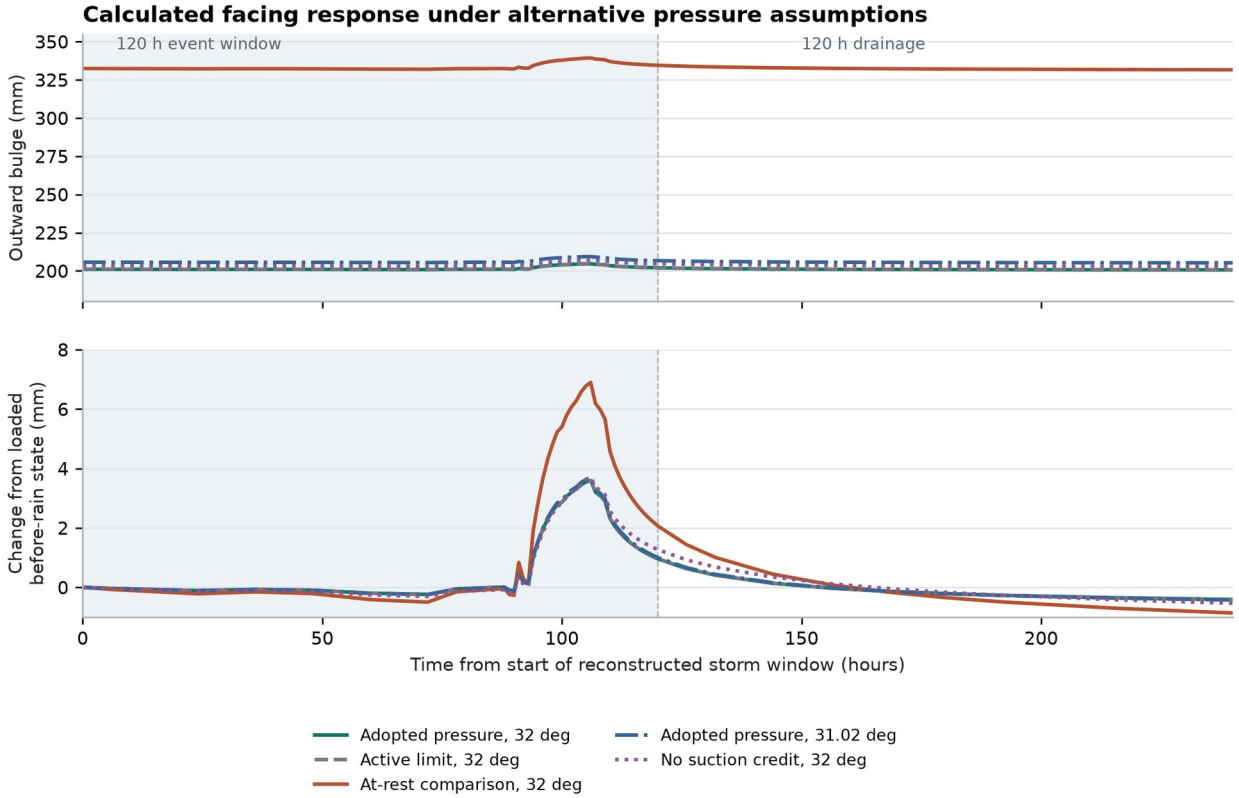


Figure S1. Fresh mechanical replays of the same hydraulic states. Upper graph is total bulge; lower graph is change from each loaded initial state. The at-rest case is a sustained-pressure comparison, not a predicted physical loading path.

Case	Before mm	Maximum mm	After mm	Max grid kN/m
Adopted law 32°	201.09	204.69	200.68	31.20
Active limit 32°	201.02	204.61	200.61	31.20
At-rest limit 32°	332.44	339.34	331.58	62.97
Adopted law 31.02°	205.70	209.39	205.28	32.61
No suction credit 32°	203.43	207.15	202.90	31.95

All five sampled maxima occur at 106 h. The adopted replay reproduces 204.686 mm exactly; the sustained at-rest result is 339.337 mm and its minimum nominal grid ratio is 3.176. Although it remains below the provisional 400 mm facing screen, its current toe fails contact and bearing checks (section 35C). [33]

Removing suction credit increases the saved maximum from 204.69 to 207.15 mm, or 2.46 mm. Suction is included and modestly beneficial in this model. The 31.02 degree comparison gives 209.39 mm. Small modeled rainfall increments do not establish the sensitivity of a physical chamber test. These cases are not a statistical confidence interval.

18 Whole chamber cross section and bulge location

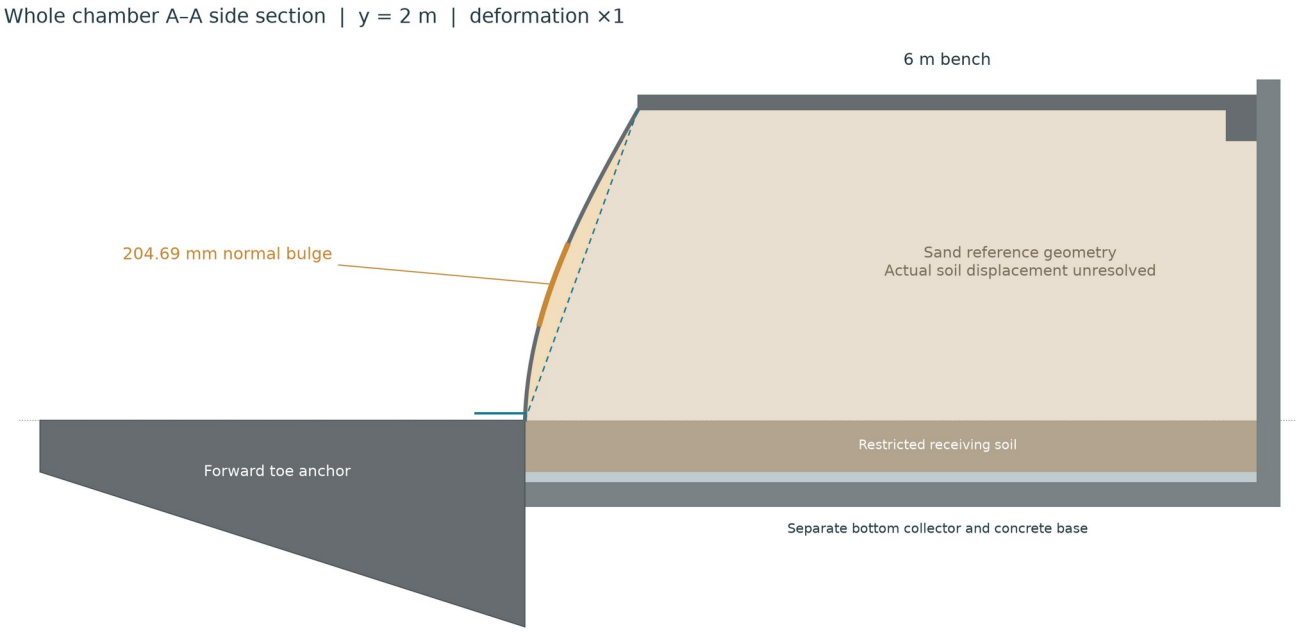


Figure 14. The calculated peak facing in the six-metre chamber, shown in a side section through y = 2 m. The orange segment marks high outward displacement. Both geometric axes use the same scale; displacement multiplier is one.

At 106 h the maximum normal bulge is 204.69 mm at reference height 1.25 m above the toe and y = 2.00 m across the chamber. The display band includes locations with at least 90% of this peak, or 184.22 mm. At the centreline its reference heights are approximately 0.85 to 1.74 m.

The facing shape is drawn at calculated geometric scale. Soil and bench surfaces in this view remain reference geometry; they do not assert zero physical soil or berm movement. Conditional berm bending appears in its own section. The orange band is a display threshold, not a slip surface, detached patch or crack boundary.

The toe remains entirely forward of the original slope foot. Grid entry begins at that foot and turns into the anchor, as detailed in the anchorage section. This side view replaces the deformed 3D projection; the full-face maps retain the location information across the four-metre width.

19 Matching cross section through the peak

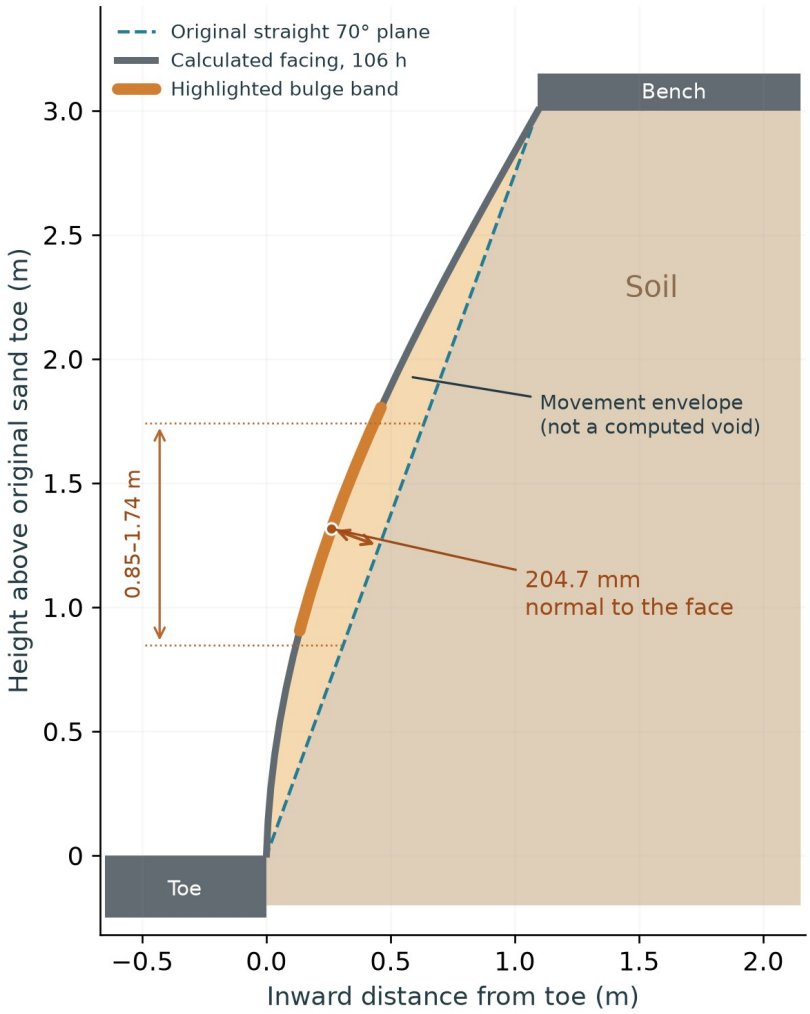


Figure 15. A-A through y = 2 m. The dashed original line, calculated facing and highlighted high-bulge segment use equal geometric scales. Adjacent bench and toe are cropped only in this close view.

The maximum is measured normal to the original slope plane. Its dimension is not the total grid extension and not a horizontal soil displacement. The area between the old and moved facing is a geometric movement envelope. It does not demonstrate an empty space behind the grid.

The 0.85 to 1.74 m band is a convenient location reference for observation. The upper crest and toe restraints also experience deformation demand, even though they are outside the largest-bulge band.

20 Facing appearance before during and after

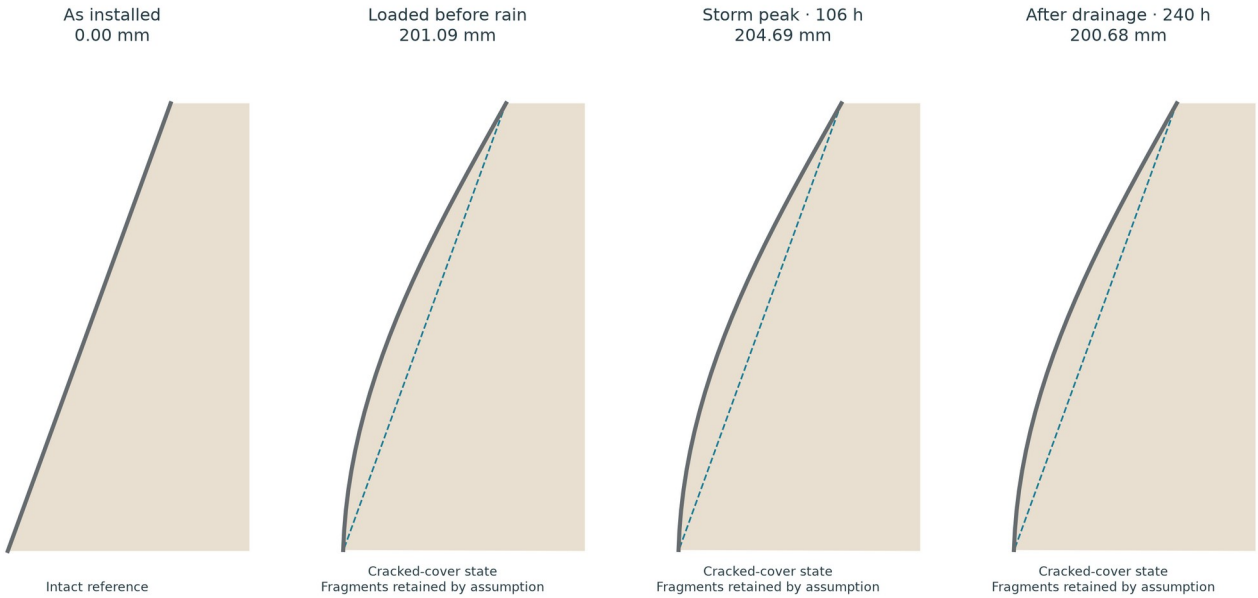


Figure 16. Four centre cross-sections at the same geometric scale. The dashed blue plane is the original profile; the grey line follows the saved facing coordinates. Cover state is labelled without inventing individual crack traces or apertures.

The straight as-installed view is a zero-shape reference, not a solved unsupported sand equilibrium. Once soil pressure and the 10 kPa strip are applied, the model already predicts substantial bulge before rain. It also classifies the cover as cracked in that first loaded state.

The sequence is 0 mm as-installed reference; 201.09 mm loaded before rain; 204.69 mm at the storm peak; and 200.68 mm after drainage. Each solved shape includes the saved tangential and normal displacements. Crack paths and opening widths are unresolved, so the sections do not depict arbitrary cracks growing with time.

Cover fragments remain on the Construck 3D mat by the agreed fixed assumption. Small numerical recovery after the storm does not heal the cover, establish closure of cracks, or calculate permanent soil deformation.

21 Full face displacement maps through time

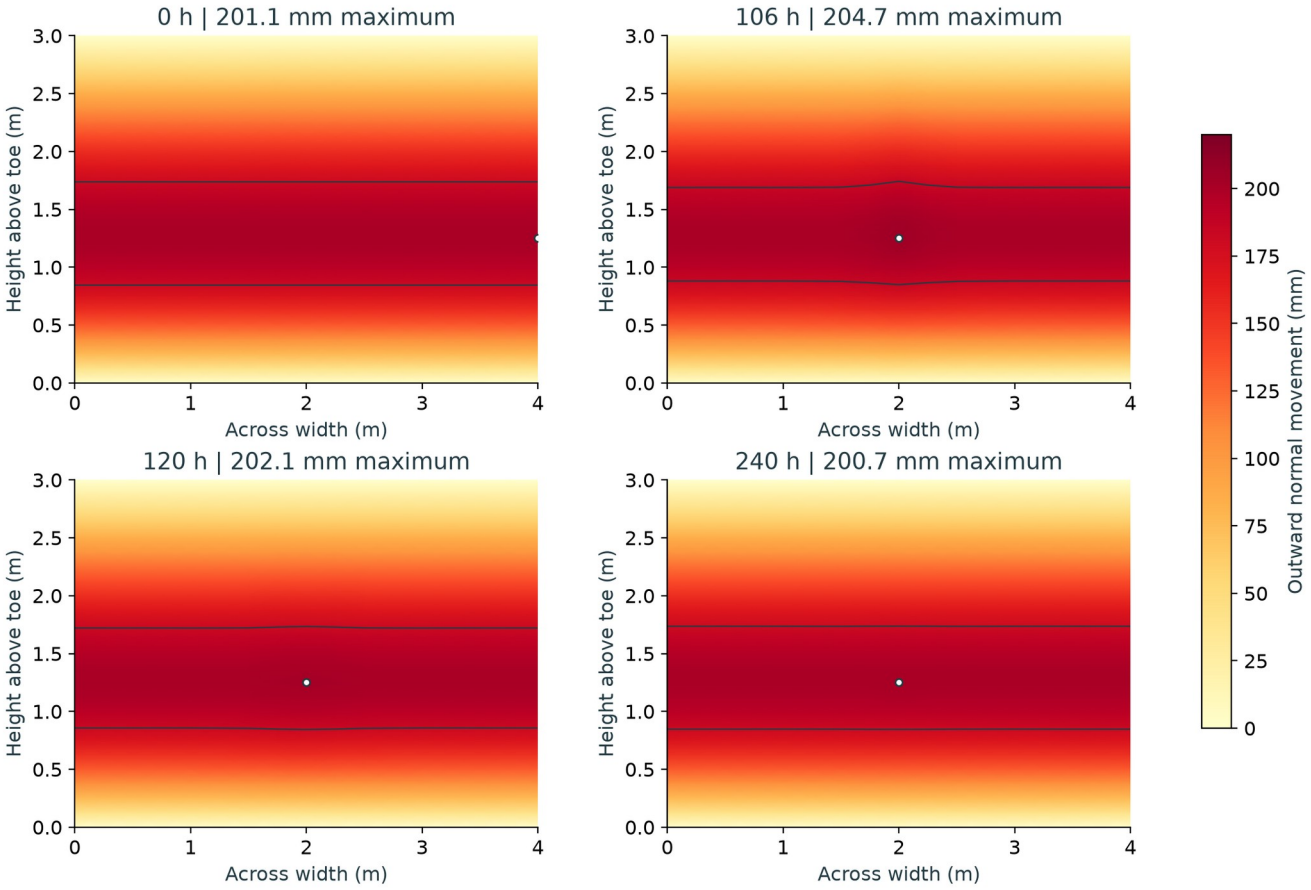


Figure 17. Four saved states on the same 0 to 220 mm scale. Thin contours show 90% of each state maximum; white markers identify numerical maxima.

The bulge occupies a broad lower-middle band. The initial widthwise response is nearly uniform, so a selected boundary node can be the numerical maximum without representing a distinct edge defect. During the storm the largest value is at the centre across the width.

State	Peak bulge	Height above toe	Width coordinate
0 h	201.09 mm	1.25 m	4.00 m
106 h	204.69 mm	1.25 m	2.00 m
120 h	202.05 mm	1.25 m	2.00 m
240 h	200.68 mm	1.25 m	2.00 m

These are saved mesh locations, not precision predictions of a field defect. The primary face has 25 by 17 nodes. Refinement is checked separately; local curvature and the exact position of a maximum remain resolution dependent.

22 Facing profiles and the rainfall increment

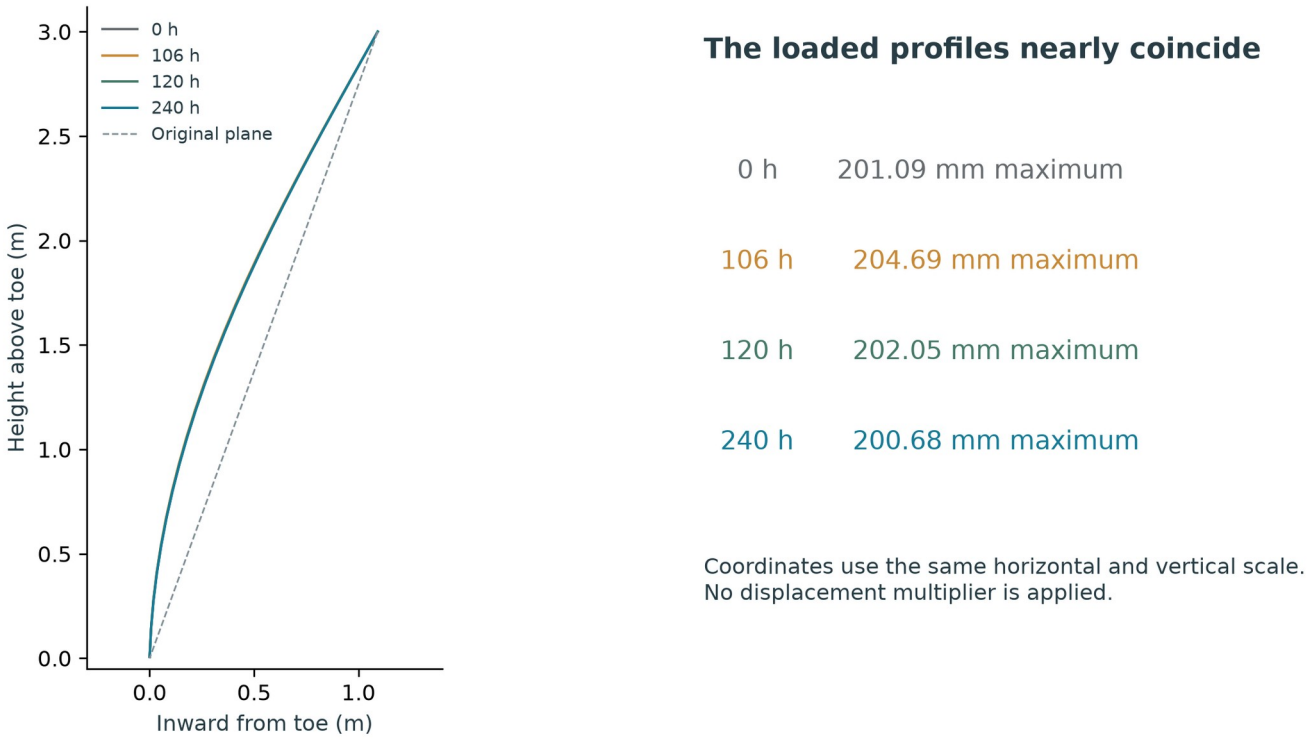


Figure 18. Centre sections use equal horizontal and vertical scales. The loaded curves almost coincide at this scale; exact peak values beside the section distinguish their nonzero differences without enlarging the movement axis.

Time	Maximum bulge	Change from loaded initial	Peak MD tension
0 h	201.09 mm	+0.00 mm	30.20 kN/m
106 h	204.69 mm	+3.59 mm	31.20 kN/m
120 h	202.05 mm	+0.96 mm	30.48 kN/m
240 h	200.68 mm	-0.41 mm	30.10 kN/m

At 106 h the increase from the loaded pre-rain maximum is 3.594 mm. Compared with the same-time dry control it is 3.943 mm. These measures differ because the initially imposed suction also redistributes in the dry control.

Most of the total deflection in this model is associated with loading already present at 0 h. Describing the whole approximately 205 mm bulge as rainfall-induced would be incorrect.

23 When the maximum develops and recovers

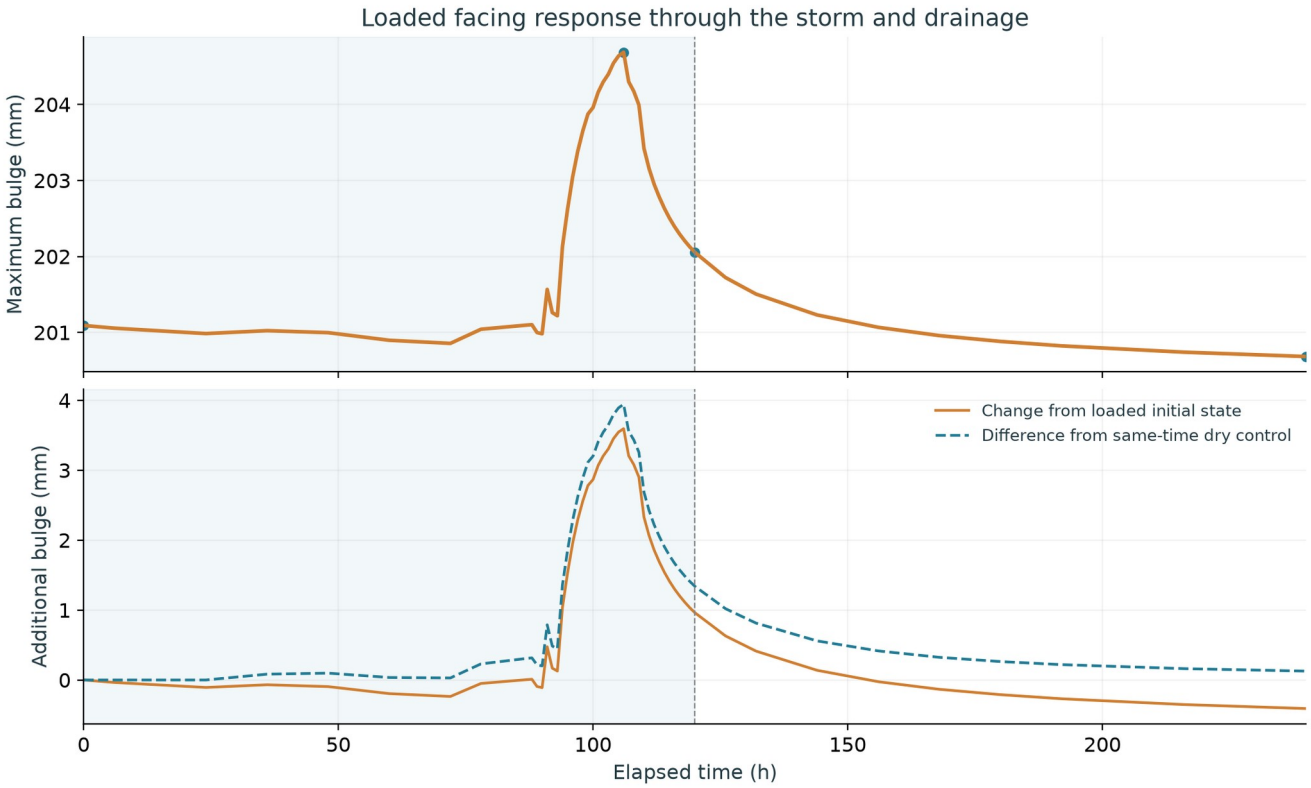


Figure 19. The shaded window is the 120 h storm reconstruction. The following 120 h is drainage, with delayed rear supply allowed by the upstream-flow model. Lines connect the 53 saved states.

The rapid change near the heavy part of the reconstructed event is followed by a declining response. The maximum among saved states occurs before the 120 h event window ends. This is a sequence of equilibrated membrane states, not a dynamic landslide or soil-creep calculation.

The post-storm result remains under the retained 10 kPa surcharge. Recovery represents the selected elastic membrane and pressure framework. Soil plasticity, long-term polymer creep and fracture history are not solved, so permanent movement cannot be inferred from this recovery curve.

24 UV cover cracking and retained layers

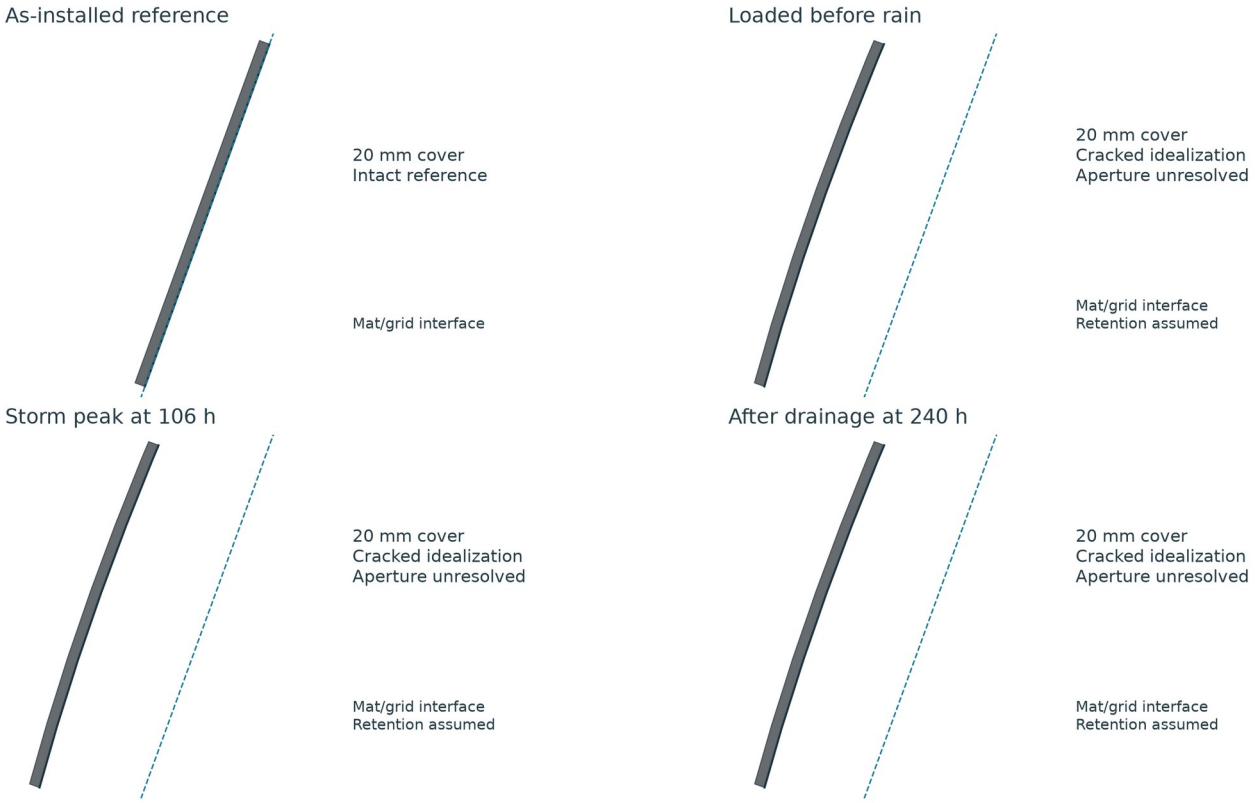


Figure 20. Local physical cross-sections near the bulge. The saved facing profile and a 20 mm cover band use equal geometric scales. Mat and grid are identified at the interface; their unverified physical thicknesses and individual crack apertures are not drawn.

The layer sequence remains cement-plaster UV cover, Construck 3D mat, geogrid, drainage mat and sand. As the flexible facing changes length and curvature, an intact cementitious skin would have to accommodate that demand. The retained intact-cover screen is exceeded, so the model uses a cracked-cover idealization. Retention at the mat is the agreed fixed assumption.

The local sections retain the calculated profile with no exaggerated bends or openings. They show neither intact continuity as a verified outcome nor a particular fractured shape: the cracked state is a material-model classification. Crack number, spacing, width, initiation time and exact trace remain uncalculated.

Retention of fragments is a fixed assumption for this exercise. It is distinct from continuous UV shielding, watertightness and erosion performance through openings. The concrete-pavement literature illustrates why crack width and load transfer matter, but supplies no validated crack width for this proprietary mat-and-cover assembly. [27]

25 Where stretching and bending are greatest

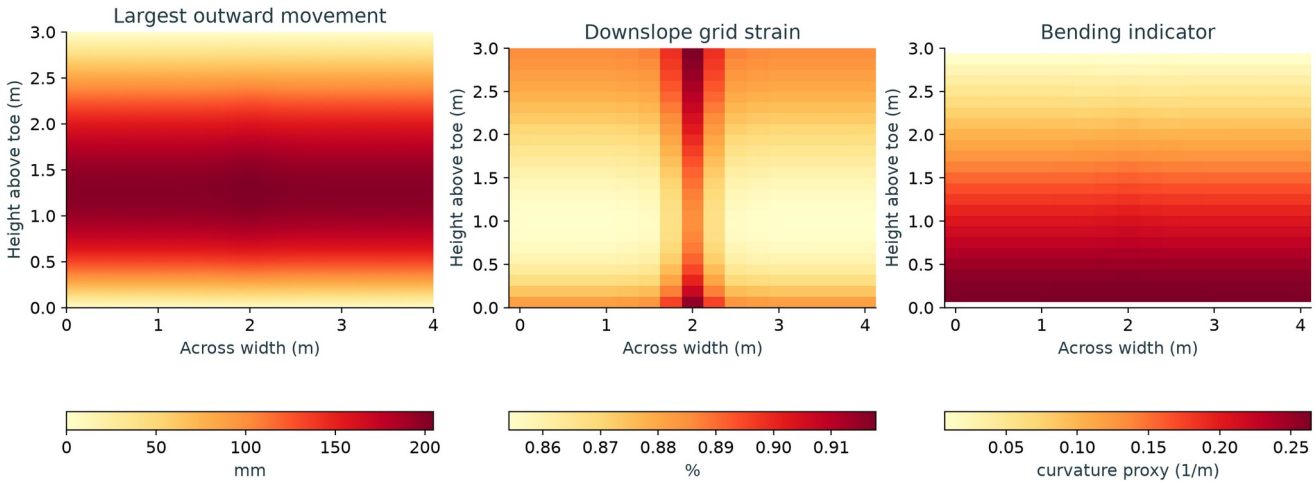


Figure 21. Peak-state displacement, downslope grid strain and curvature proxy. These three indicators describe different aspects of the same deformed facing and do not locate individual cracks.

Indicator at 106 h	Value	Reference height
Outward bulge	204.69 mm	1.250 m
Maximum local MD grid strain	0.918%	2.938 m
Largest downslope curvature proxy	0.264 per m	0.125 m

Largest outward movement is in the lower-middle face. Peak downslope stretching is near the crest, and the largest downslope bending indicator is near the toe. A crack sketch placed only at the bulge maximum would therefore miss other areas of deformation demand.

Downslope stretching can favor cracks transverse to the stretching direction, while changes in curvature create tension on one side of the cover. Existing flaws, bond, shrinkage and restraint affect the actual pattern. No unique crack orientation or fracture location is resolved here. [27]

26 What the cover screen does and does not calculate

Retained cover input or screen	Value
Elastic modulus	5,000 MPa
Assumed tensile strength	0.50 MPa
Assumed flexural strength	1.50 MPa
Thickness	20 mm
Tensile strain screen	0.010%
Curvature screen	0.030 per m

The tensile comparison uses grid extension as the compatible intact-cover strain demand. The bending comparison uses the magnitude of the second difference of normal displacement divided by segment spacing squared. They are screening proxies, not a local cement-plaster damage law.

If either screen is exceeded, the model changes the entire cover to the cracked state. It removes the intact membrane contribution and keeps 0.1% of the original bending stiffness. This residual stiffness is a numerical assumption, not a measured post-crack material property. The cracked flag is already true in the first saved loaded state.

The chamber calculation retains the agreed water-entry law. It does not increase face infiltration when the illustrated UV cover cracks, nor update joint conductance as the berm bends. Thus the combined drawings cannot be read as a fully coupled crack-leakage prediction.

Record crack opening, mat contact, fragment retention and exposed grid area during the physical test. Those observations are needed to determine whether the retained fragments also preserve the intended protective functions; fragment retention alone answers only one part of that question.

27 Grid extension with both end positions fixed

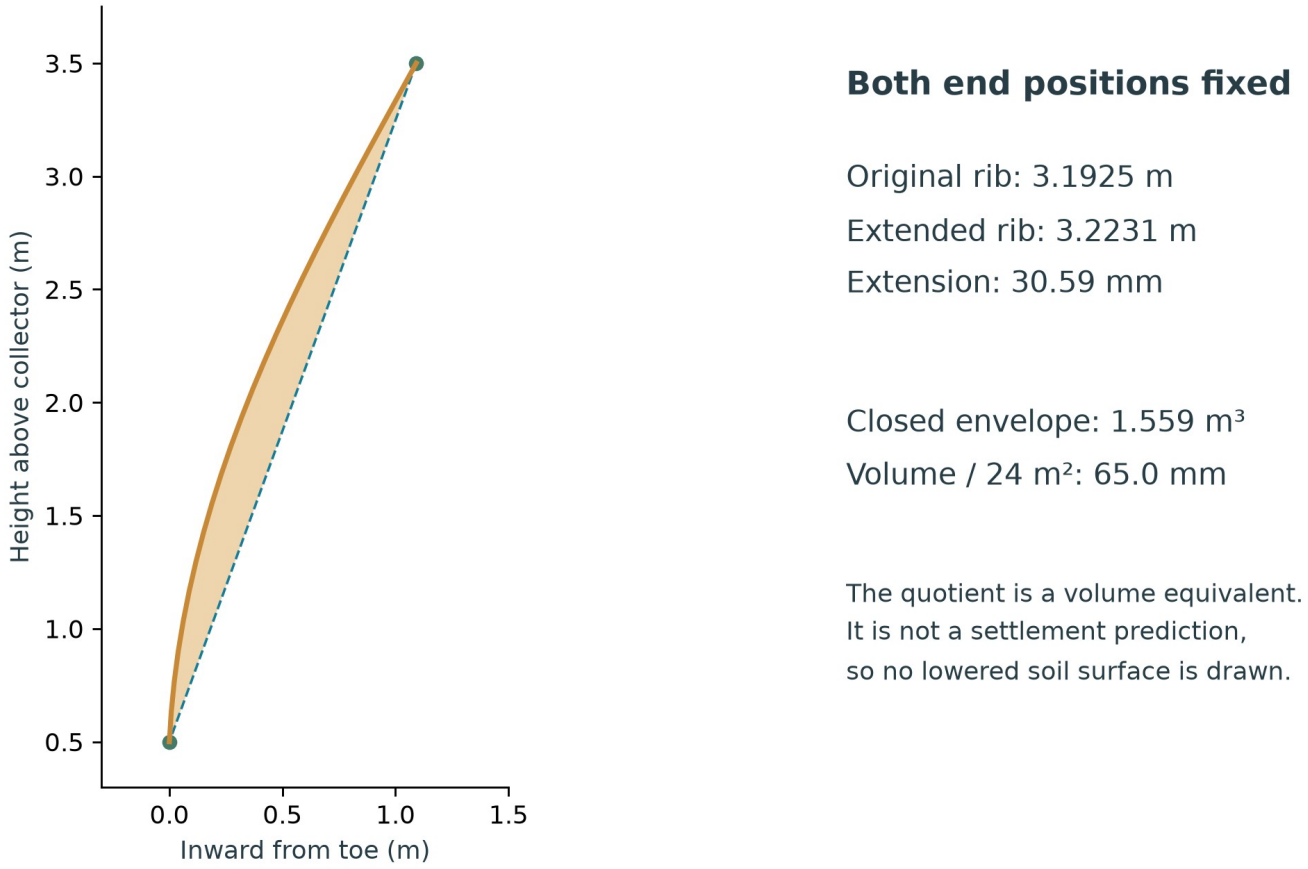


Figure 22. Rigid-toe comparison with both end positions fixed. The left profile uses actual calculated coordinates; the right panel reports geometry values. No volume-equivalent drawdown is drawn as a soil-settlement shape.

The original centre rib is 3.19253 m long. At 106 h it is 3.22312 m, an extension of 30.59 mm or 0.958% on average. The maximum local strain is 0.976%. The 191.21 mm outward bulge is a different geometric quantity from the rib extension.

No grid is pulled through either anchor in this fixed-position comparison. Length is calculated by summing the deformed segment lengths and is checked against the integrated saved MD strains. This confirms the saved grid kinematics; it does not locate the soil feeding the bulge. [28]

The primary case gives 204.69 mm because it allows toe-body movement on its support spring; its largest toe-end movement is 6.32 mm. Fixing that body as well gives 191.21 mm. Both cases assume no local connection slip; they have different foundation restraints.

28 Geometry and soil volume compatibility

Fixed end state	Bulge mm	Rib extension mm	Closed envelope m³
0 h	187.87	29.60	1.558
106 h	191.21	30.59	1.559
120 h	188.76	29.87	1.557
240 h	187.49	29.49	1.554

Peak geometry measure	Primary toe compliance	Both end positions fixed
Closed envelope	1.669 m³	1.559 m³
Equivalent uniform 24 m² drawdown	69.5 mm	65.0 mm

The closed-envelope calculation joins the original and displaced face meshes and caps their boundaries. Reversing the diagonal of every quadrilateral provides an independent triangulation comparison. It includes the saved tangential displacements. The earlier normal-sweep approximation, about 1.666 m³ at peak in the primary case, is close but is a different geometric measure.

For fixed chamber boundaries and no loss of sand, extra face volume must be balanced by motion of other boundaries, changes in soil bulk volume or internal gaps. If the sole source were uniform top drawdown at unchanged bulk density, the equivalent lowering would be the closed envelope divided by 24 m². That division is not a soil-settlement solution.

Local dilation or contraction, distributed shearing and nonuniform drawdown can alter the balance. Water volume alone cannot provide the displaced sand. Published work describes coupling between soil volume change and pore pressure; the present model does not solve that feedback. [29]

28A Bulge and bench volume compatibility

The following quantities reproduce separate retained calculations. They make the scale of possible soil redistribution explicit without assigning an uncalculated settlement pattern or changing the fixed anchorage assumptions. [24,31]

Quantity	Reproduced value	Meaning
Primary face at 106 h	1.66903 m³	Increase in closed facing envelope, including the saved tangential displacement.
Both ends fixed at 106 h	1.55905 m³	Separate rigid-end comparison, not the primary toe-spring response.
Uniform volume equivalent over 24 m²	69.54 mm primary; 64.96 mm rigid-end	Envelope divided by bench area. These are not predicted settlements.
Conditional 4 m support-loss beam	17.87 mm maximum sag	Prescribed support loss, released joint rotation with vertical shear transfer, fixed end levels.
Volume swept by that beam across 4 m width	About 0.17502 m³	About 10.5% of the primary facing-envelope increase; not a coupled mass balance.

The beam sag includes its retained maximum pond-weight allowance of 0.0057269 kPa in addition to screed self-weight and the stated strip loading. Omitting that small allowance gives about 17.85 mm rather than 17.87 mm. The reviewed report value is reproduced when all stated loads are included.

The difference between the 1.66903 m³ face envelope and 0.17502 m³ beam sweep is not a numerical conservation error: these are different model cases that were not solved as one compatible soil/bench system. It shows why the bench example cannot identify the source of all soil needed to fill the bulge.

A physically consistent final shape would require soil redistribution, bulk-volume change, changing support and bench contact to be resolved together, or measured. Grid extension can accommodate outward face movement with fixed connections; it does not identify where the sand originates. Water balance likewise does not supply a soil-solid volume balance.

The retained cross sections and final before/after view remain at deformation x1. Their 17.87 mm berm shape is the labelled imposed-support-loss example, not predicted rainfall settlement. The crack illustrations retain their explanatory role; individual apertures are unresolved.

29 Possible soil movement behind the bulge

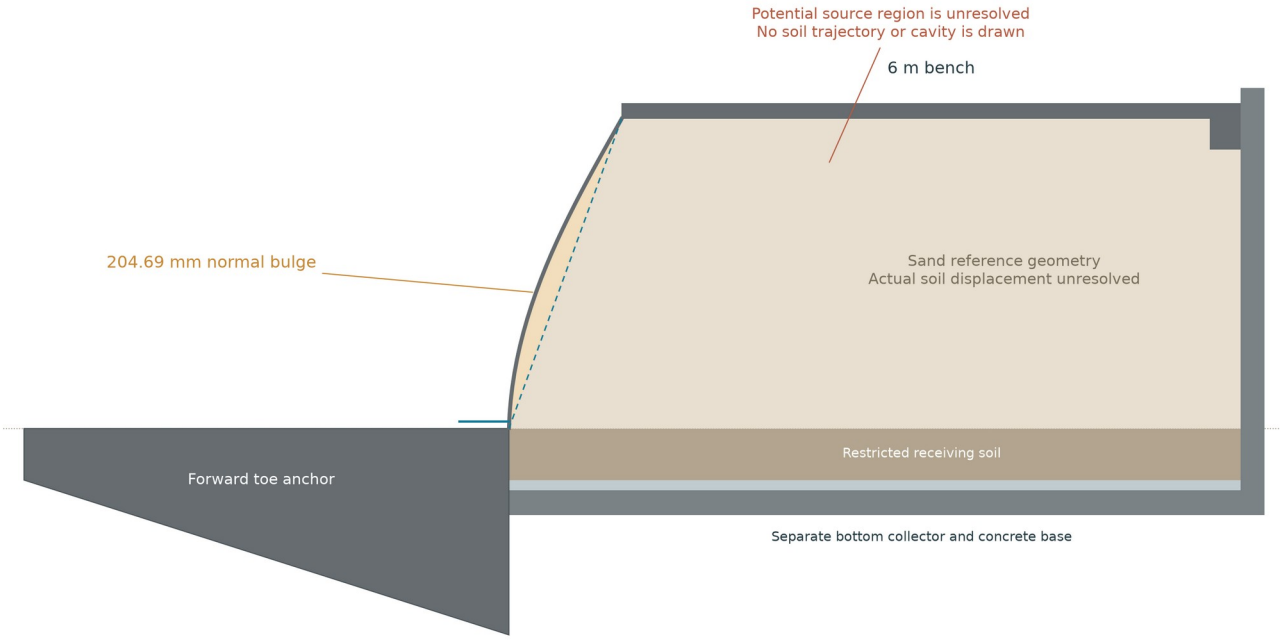


Figure 23. Section through the revised chamber at the saved peak facing state. Soil remains a reference body. No uncalculated upper depression, void or particle-displacement arrows are drawn.

Material immediately behind the moving face and above or behind it could contribute to its changed shape. The model has no solved solid-displacement field, so it does not locate particle trajectories, the support-loss boundary or a verified source wedge. Those unresolved movements are not assigned an arbitrary visible magnitude.

A fixed rear key secures the specified connection but does not keep the supporting sand from deforming. The screed may follow local settlement, bend across it or bridge a separation. Whole-slab sliding is not an automatic consequence of facing bulge.

The 25 cm lower wetting review band and the 32 degree geometric reference wedge in the stress section remain separate concepts. Neither identifies the source of the bulge material or demonstrates that all soil within it has failed.

30 Bench bending and control joint effects



Figure 24. Four full-width bench sections at deformation x1. Dashed blue is the original level. All use the same horizontal and vertical geometric scales. Support-loss length is an imposed input; the peak values are nonzero conditional bending responses.

With an assumed 4.0 m loss of soil support, the released-rotation comparison gives 17.87 mm maximum bending movement at the x = 2 m joint and 0.903° relative rotation. That calculation assumes vertical shear transfer at the joint and fixed vertical positions at the front and rear ends. It is conditional, not the chamber's final settled shape.

The through-crack assumption rules out treating the remaining ligament as uncracked. Reinforcement, bond and joint shear transfer are unspecified. The 5 m support-loss case exceeds the assumed uncracked span capacity: its 81 mm value is an elastic extrapolation, not a valid post-crack prediction. The 1 m beam strip also cannot resolve the joint crossing or full plate action. [25]

A prior elastoplastic soil/contact attempt did not converge. No failed result is used as a prediction or as evidence of physical failure. The report cannot honestly give an actual settlement depth or certify an undisturbed rear sample. A calibrated soil/contact and cracked-slab solution, or direct test measurements, remains required.

31 Berm cross section at calculated scale

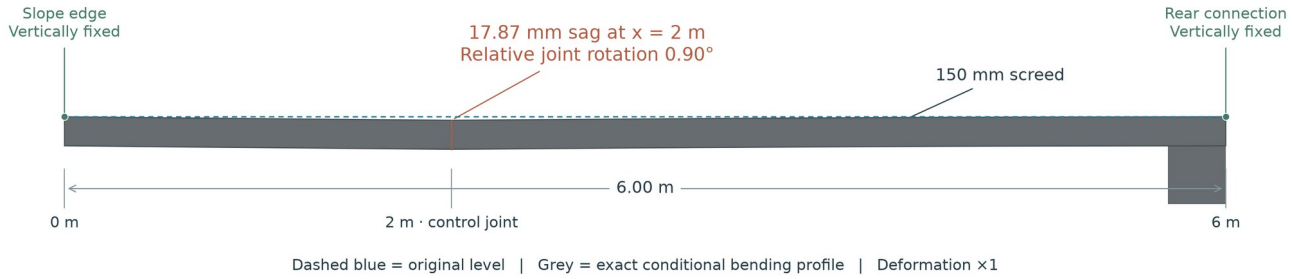


Figure 25. Full 6 m bench cross-section using the exact conditional beam curve. The 150 mm screed thickness and 17.87 mm sag are drawn in the same metre units. Original and moved profiles are both retained; the movement is not set to zero.

The selected 4 m imposed support-loss case gives 17.87 mm downward movement at the control joint 2 m from the slope edge, with 0.903 degrees relative rotation. Vertical positions at the front and rear ends remain fixed in this beam comparison. The complete profile is interpolated with the beam element shape functions, including separate rotations on either side of the joint.

Across a 6 m bench, 17.87 mm is only about 0.30% of the displayed length, so the whole section looks nearly level. This is a consequence of the true geometry, not reduced deformation. The joint detail on the following pages crops the same curve and enlarges both axes equally; its displacement multiplier also remains one.

The support-loss length is a sensitivity input, not a result obtained from rainfall or bulge volume. Actual supporting-soil movement and gaps remain unresolved. No open cavity or artificially lowered soil surface is included in this view.

32 Top view of the berm joints and deformation area

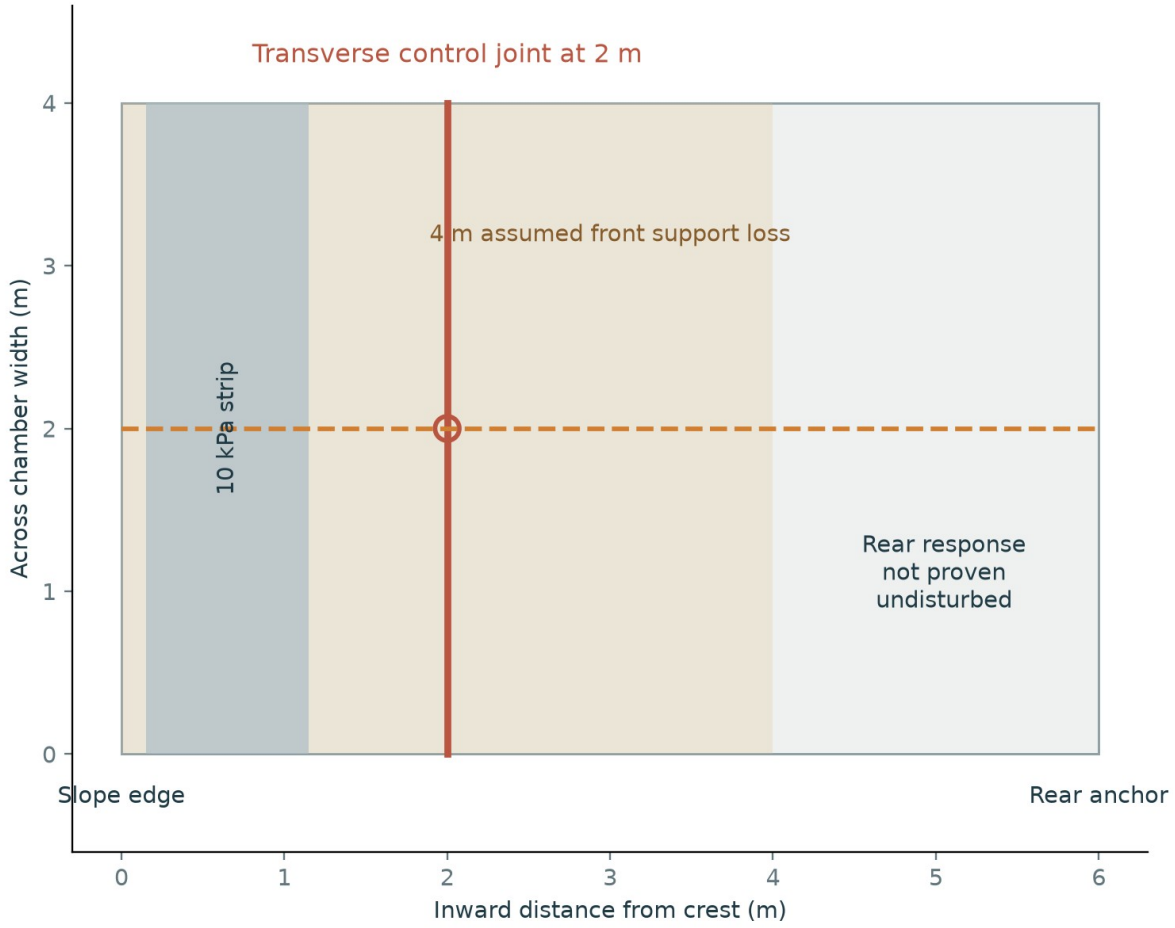


Figure 26. The bench is 6 m inward and 4 m across. The transverse joint remains 2 m from the slope; the longitudinal joint is at mid-width. Shading shows the imposed 4 m support-loss example, not an actual disturbed-soil map.

The red line identifies the joint at the conditional maximum sag. The dashed orange line and circled crossing are observation locations for differential movement; their three-dimensional plate response has not been solved. This plan shows locations only, without a displacement multiplier or an inferred settlement contour over the width.

The original 10 kPa surcharge occupies x = 0.15 to 1.15 m behind the crest across the 4 m width. It has not been spread over the entire six-metre bench. The rear anchor moves to 6 m, while the original joint positions are retained.

The remaining rear area cannot yet be designated an undisturbed sample. That requires observed soil movement or a converged soil-continuum and contact calculation, not simply a longer chamber.

33 Exact cross section at the berm joint

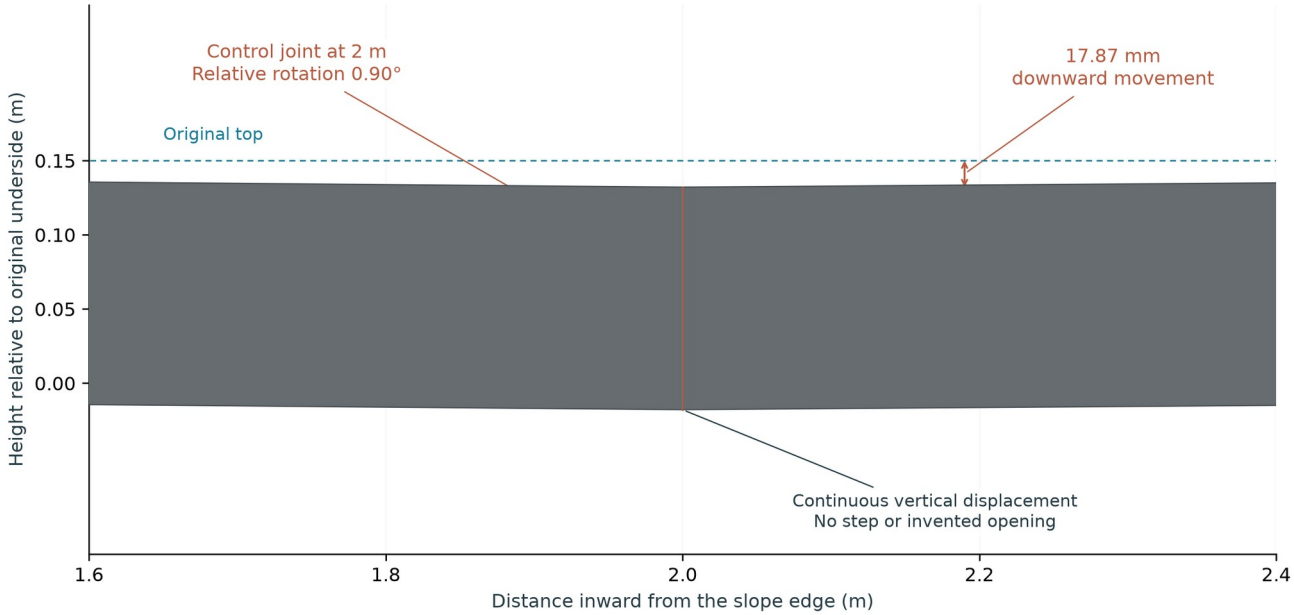


Figure 27. Uniformly enlarged crop of the same calculated beam curve at the 2 m joint. The horizontal and vertical geometric scales are equal. The 17.87 mm dimension and 150 mm screed thickness retain their exact proportion. No crack aperture is invented.

This view makes the nonzero movement visible by showing a smaller physical area, not by increasing sag. The blue dashed original level remains 17.87 mm above the displaced top at the joint. The two adjacent beam segments meet at the same vertical displacement while their rotations differ by 0.903 degrees.

Through-cracks at the partial control cuts remain the hydraulic assumption. The structural model releases joint rotation while retaining vertical force transfer, so there is no calculated vertical step. It cannot determine aperture or a post-crack wedge shape without a joint and reinforcement law; only the joint location is marked.

Assumed front support-loss length	Calculated maximum sag	Interpretation
0 m	0.59 mm	Conditional beam response
1 m	0.65 mm	Conditional beam response
2 m	1.33 mm	Conditional beam response
3 m	5.66 mm	Conditional beam response
4 m	17.87 mm	Conditional beam response

The 5 m example is not included as an accepted shape: its calculated elastic moment exceeds the assumed first-crack capacity of the remaining spans. The numerical extrapolation cannot describe the post-crack response.

34 Toe equilibrium and selected dimensions

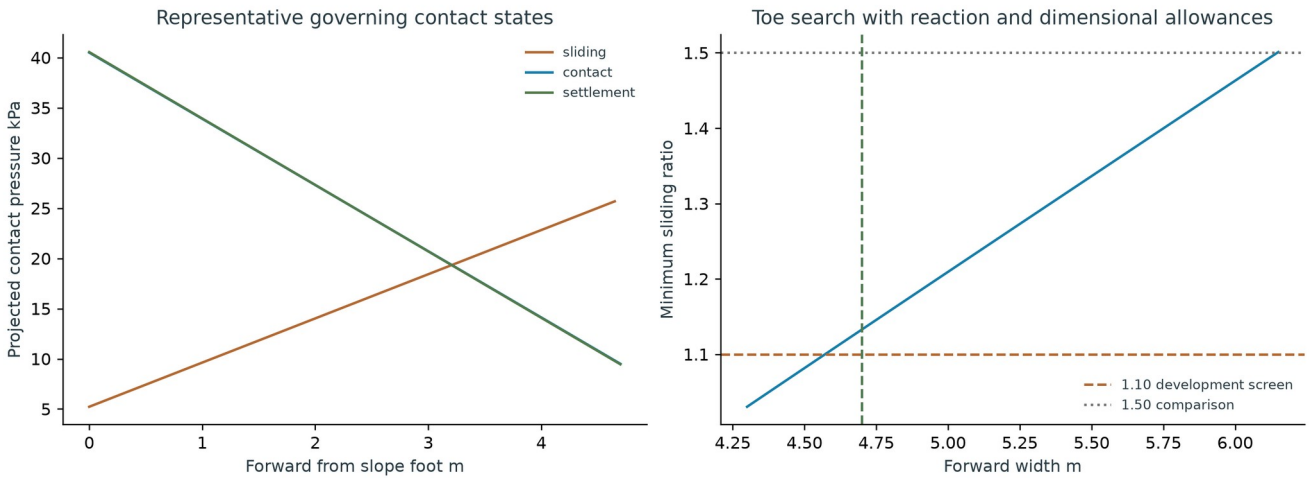


Figure 28. Updated toe screen with exact slope-foot entry. Pressure is the projected foundation contact pressure; the toe body is assumed rigid.

Check	Governing result	Retained criterion
Forward width / depth	4.70 m / 2.00 → 0.50 m	Entirely in front
Volume / gross weight	23.50 m³ / 117.50 kN/m	Full 4 m width
Sliding	1.133	≥ 1.10
Bearing factor	11.59	≥ 3.0
Weight / uplift force	2.81	≥ 1.10
Minimum contact fraction	100.0%	Compression-only equilibrium
Peak contact pressure	40.55 kPa	Below model allowance
Maximum elastic edge compression	7.17 mm	≤ 10 mm provisional

The search first meets the retained screen at 4.60 m, in 50 mm width increments. The selected width is 4.70 m. A 1.50 sliding comparison requires approximately 6.15 m in the same simplified screen. These are adopted-case development results, not a universal margin. The toe does not pass the at-rest pressure comparison in section 35C. [14,24,33]

35 Toe methodology and limits

The retained toe envelope includes horizontal extremes and maximum upward grid reaction from the original S6-1 facing scenarios, plus zero-load bounds. New S6-7 comparisons are reported separately in sections 35B-C. It checks combinations rather than only the single moment of maximum bulge. Reaction factors of 1.00 and 1.10 and 50 mm dimensional reductions are included.

For the trapezoid, gross weight per metre is $\gamma_c B(a+d)/2$. The centroid is $B(a+2d)/[3(a+d)]$ from the deep side. Force and moment balance are resolved on the inclined underside. Full contact is linear; loss of contact is treated as triangular compression where equilibrium permits. No tensile contact, passive resistance or chamber support is credited.

The bearing estimate applies an effective-width shallow-foundation framework with a 4 m finite run and an inclined-base correction. Settlement is an elastic support approximation using $E = 25$ MPa and $\nu = 0.30$. The model does not constitute a calibrated nonlinear foundation analysis. [14]

The toe reaction application is at the surface-level slope foot. The internal L-shaped grid path does not by itself shift that external force to an advantageous point. Full transfer into the toe is assumed; internal bending, bar development, concrete splitting and local breakout are not checked.

Gross weight is retained because the user imposed no hydraulic uplift under the toe. The chamber seepage calculation does not prove that condition. The narrow margin above 1.10 is model-specific. The new at-rest pressure comparison fails toe contact despite unchanged gross-weight and fixed-transfer assumptions (section 35C). Actual foundation bearing and settlement also depend on density, stiffness and drainage measurements.

35A Bearing convention and support compatibility

The original conditional toe result is retained

The selected toe remains 4.70 m entirely forward of the slope, with 2.00 m depth beside the slope and 0.50 m at the outer edge. Its 23.50 m³ total volume, 117.50 kN/m gross weight and 1.880 m centroid from the deep side reproduce. The geogrid enters exactly at the slope foot before forming the assumed fixed L-shaped route. [24,31]

The reproduced governing sliding case includes the 50 mm dimensional reductions and 1.10 reaction multiplier. Normal force is approximately 67.95 kN/m and tangential demand 23.43 kN/m; resistance/demand is 1.13282. This exceeds the retained 1.10 development criterion by a small reserve. It is not a generally applicable field-design safety margin.

Explicit bearing shape-factor convention

The implementation uses effective plan dimensions for its bearing shape factor. FHWA GEC 6 section 5.2.4 recommends full dimensions for that factor while noting an alternative AASHTO effective-dimension convention. The report retains its implemented convention and does not imply exact conformity with every FHWA detail. [14]

Same governing bearing case	Implemented	Full-plan comparison
Shape factor	0.62743	0.65957
Bearing resistance/demand	11.59	12.18

The comparison changes only that case’s shape factor using the full 4.70 m by 4 m plan. It is conservative here, but 12.18 is not a newly searched minimum or a replacement for the retained 11.59 envelope. Separate sliding and bearing treatment is permitted in the cited FHWA guidance; omission of an extra load-inclination factor is not automatically an error.

Movement compatibility remains a separate task

The 5000 kN/m² facing support and the separate rigid-toe foundation calculation are not iterated to one common motion. The 7.17 mm maximum elastic edge compression cannot be substituted for the facing toe endpoint displacement. A stronger assembled-deformation claim requires reactions, translation and rotation compared at the same state and reference point, followed by compatible iteration. None is newly claimed here; fixed loop transfer, crest restraint and zero hydraulic uplift remain unchanged.

35B Reproducing toe sliding and friction sensitivity

The retained original reaction envelope is U = 36.13039 kN/m, H_min = -1.30397 kN/m and H_max = +1.11087 kN/m, with zero-load bounds. U is upward grid force, not water buoyancy. Positive H points forward. The original envelope includes multiple stiffness, mesh and restraint cases; it is broader than the primary replays in section 17A. [24,33]

At the governing combination, the 1.10 reaction multiplier gives U = 39.74343 and H = -1.43437 kN/m. Dimensional reductions give B = 4.65 m, rear depth 1.95 m and outer depth 0.45 m. With gamma_c = 20 kN/m³, W = 111.60 kN/m and underside angle alpha = atan(1.50/4.65).

Resolving the resultant onto the underside gives N = H sin(alpha) + (W-U) cos(alpha) = 67.94616 kN/m and T = -H cos(alpha) + (W-U) sin(alpha) = 23.42527 kN/m. Interface delta = (2/3)phi = 21.33333 degrees; mu = tan(delta) = 0.390554. Sliding ratio = mu N / |T| = 1.132822. This is 2.98% above the adopted 1.10 ratio, after the stated reaction and dimensional allowances.

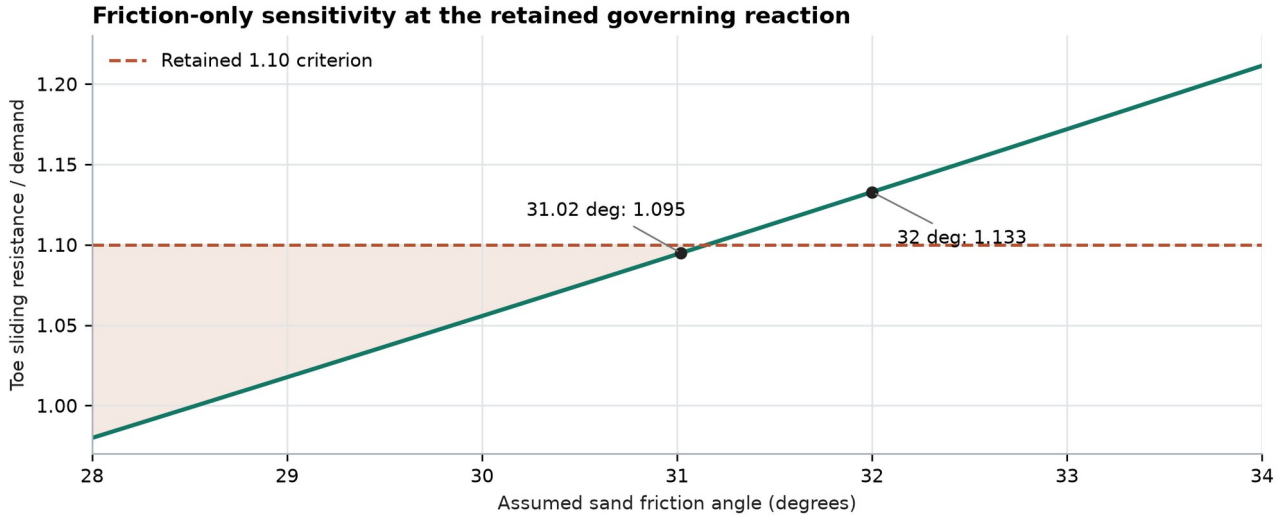


Figure S2. Only interface friction changes; the retained governing forces and dimensions remain fixed. This is an isolated sensitivity, not a full lower-friction chamber rerun.

The literature analogue gives 32 degrees at 1,620 kg/m³ and 27.1 degrees at 1,520 kg/m³ for unreinforced sand [19]. Linear interpolation to 1,600 kg/m³ gives 31.02 degrees, not a measured material value. Holding the original reaction fixed gives 1.09487, below 1.10. The fresh 31.02 degree primary replay gives a separate 1.15652 toe ratio; it does not rerun the broader original envelope or replace the 1.133 result.

Retain 20 kN/m³ as the stated concrete input. A higher measured density would increase toe weight and bench loading together; it is not uniformly conservative for the whole assembly. No buoyancy or new design criterion is introduced in this revision.

35C Toe contact under the upper pressure comparison

The sustained at-rest pressure comparison retains the same toe, soil support, no-hydraulic-uplift condition and perfect embedded load transfer. It is a deliberately different pressure bound, not a calibrated expectation that at-rest pressure persists during large outward movement. It tests whether the existing pass survives uncertainty in the selected law. [33]

Same location and same time

At 106 h on the centreline y = 2 m, the spring support transmits U = 63.43819 kN/m and H = +9.90903 kN/m. These are paired forces from one location, not independent extremes assembled from different times. Force application remains exactly at the original slope foot and toe top.

Geometry and load	Required resultant s	Base length L	Contact result
Nominal; 1.00 reactions	4.41561 m	4.93356 m	31.5% contact
Nominal; 1.10 reactions	4.97611 m	4.93356 m	Outside base
50 mm reductions; 1.00	4.59789 m	4.88595 m	17.7% contact
50 mm reductions; 1.10	5.25367 m	4.88595 m	Outside base

Here s = [W x_c + a H] / N, measured along the inclined base from its deep end; a is the rear depth. Compression-only contact requires 0 < s < L. An s beyond the outer end cannot be balanced by compressive soil support within this model, irrespective of the total toe weight exceeding U.

Even the nominal unfactored case gives a bearing ratio of 2.54 versus the retained 3.0 criterion and approximately 12.91 mm elastic edge compression versus the provisional 10 mm limit. With 1.10 reactions there is no admissible contact equilibrium. No settlement number is reported for that no-equilibrium state; numerical near-edge divergences are not physical displacement predictions.

Effect on the report conclusion

The adopted original envelope still meets its selected criteria, including sliding 1.133. The current 4.70 m toe does not pass across the pressure alternatives. A pressure-independent conditional system pass is therefore not established even with fixed loops and crest. The at-rest comparison also does not prove that this failure will occur in the physical chamber.

The toe is intentionally not enlarged here. Selecting new dimensions would require deciding which pressure model and uncertainty allowances govern, followed by compatible foundation/facing movement checks. This technical submission retains the agreed geometry and reports the failed sensitivity openly.

35D Pressure relief during facing movement

The additional checks support pressure relief while the current toe remains stable along the sampled gradual-loading paths. The conclusion remains a conditional containment pass under the adopted assumptions. These checks extend the mechanical evidence; they do not replace the adverse sustained at-rest comparison in section 35C or establish physical-test safety. [36]

Unchanged assumptions and scope

The 6 m bench, 4 m width, 3 m retained height, 70 degree face, 10 kPa strip surcharge and 4.70 m forward trapezoidal toe are unchanged. Perfect embedded transfer, the fixed crest, retention of cracked cover by the 3D mat, rigid toe and zero hydraulic uplift beneath the toe remain assumed. Original hydraulic states, soil properties, grid stiffness and the primary finite toe spring are retained.

Three pressure release laws

The adopted proxy remains $p = p_a + (p_0 - p_a) \exp[-\max(w, w_{history})/d_m]$ from section 8C. Two deliberately slower sensitivities set $d_m = 30/\ln(20)$ mm and $100/\ln(20)$ mm, respectively. Thus 95% of the LOCAL excess above active pressure is released at 30 mm or 100 mm local movement. These are comparison laws, not measured sand properties. Active pressure remains after relief.

Gradual loading and the toe checks

Step	Calculation performed
Initial loading	33 diagnostic soil-pressure levels from zero to full load at the initial hydraulic state; no surcharge.
Surcharge	Nine intermediate levels from 1 to 9 kPa; 10 kPa at the first full-load hydraulic state.
Storm and drainage	53 original hydraulic states covering the 120 h storm reconstruction and 120 h drainage at 10 kPa.
Total	95 states per law; 285 sampled states across the three laws.

At each state, paired horizontal and upward reactions at the same width location are checked at all 17 toe nodes. Both nominal and 50 mm reduced dimensions and reaction factors 1.00 and 1.10 are used. Retained criteria cover compressive base contact, sliding, bearing, allowable peak pressure, weight-to-uplift ratio and provisional elastic edge compression.

The initial pressure ramp is numerical continuation, not the actual construction or formwork-removal sequence and not elapsed storm time. The paths are quasistatic: inertia, sudden release and crack-triggered dynamic overshoot are not resolved.

35E Pressure relief and toe stability results

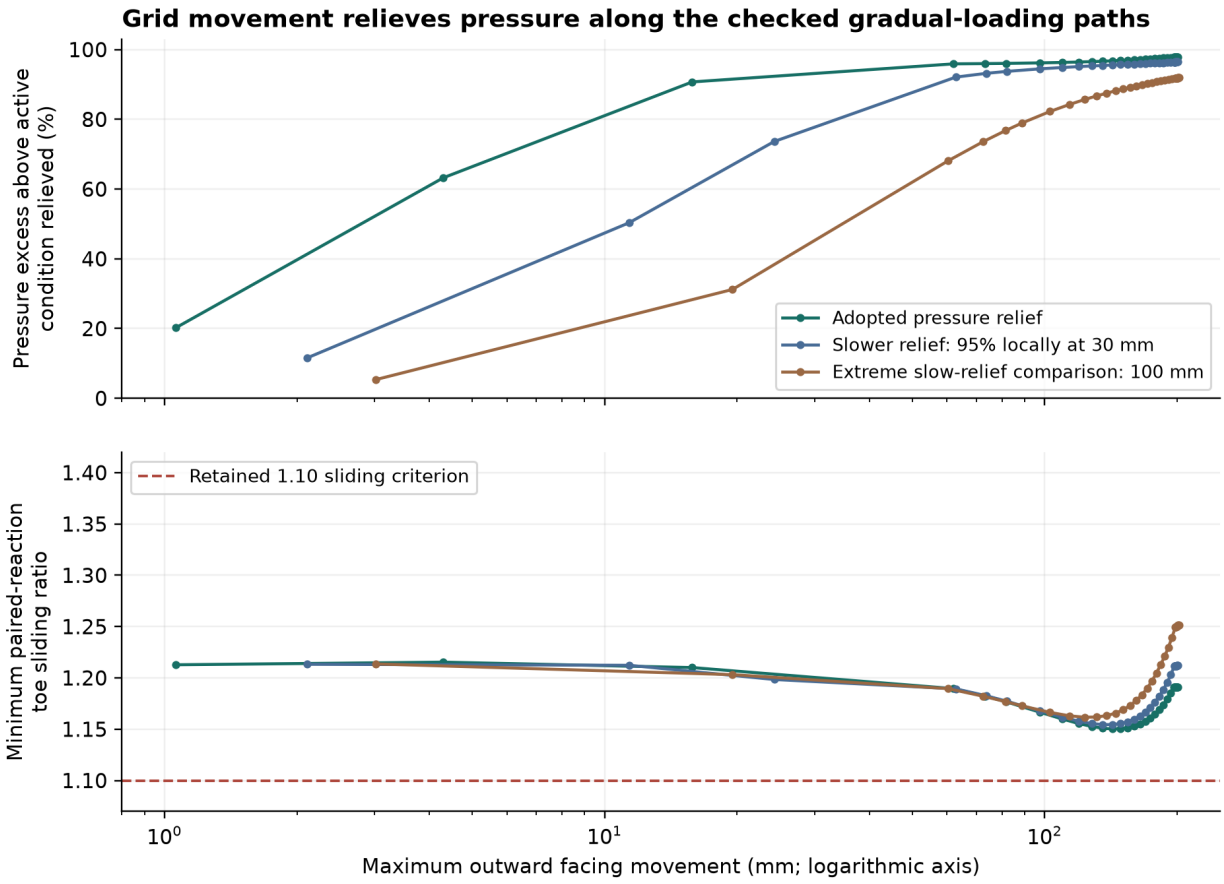


Figure S3. Diagnostic initial pressure ramp and surcharge loading for three assumed release laws. The horizontal axis is logarithmic and uses the maximum face movement; the upper axis shows area-weighted relief of the excess above active pressure. Storm and drainage states are checked but are not drawn on these curves. [36]

Pressure law	Peak bulge mm	Minimum sliding	Minimum contact	Toe checks
Adopted law	204.69	1.150	100%	Pass
Slower relief at 30 mm	204.74	1.154	100%	Pass
Slower relief at 100 mm	205.76	1.162	100%	Pass

All 285 sampled states retain full toe contact and meet the retained toe criteria, including the 1.10 reaction factor. All three maximum bulges occur at the saved 106 h state. These narrower paired-path ratios do not supersede the broader original envelope sliding ratio of 1.133 in sections 34-35B.

The highest pressure-relief percentages refer only to the excess above active pressure, not to removal of all soil load. The pressure and lower-support reaction can redistribute as the face changes shape; a larger relief percentage is not itself a toe-stability criterion.

35F Interpretation and chamber verification

Physical interpretation and published context

Pressure relief during gradual outward movement is more plausible than sustained at-rest pressure across a freely bulging face. Caltrans research reports conventional sand-wall movements to mobilize active pressure of approximately 0.001H to 0.004H, or 3-12 mm at H = 3 m. Those translating or tilting walls are an analogy, not a calibration for this restrained flexible facing. [34]

FHWA guidance explains that a flexible anchored wall can relieve pressure between restraints while transferring load toward its supports. The present calculation does not independently solve this soil arching or redistribution. Consequently, the approximately 205-206 mm global bulge does not demonstrate low pressure at the lower connection or prove actual toe stability. [35]

Retained higher pressure comparison

The sustained at-rest comparison in sections 17A and 35C remains unchanged: maximum bulge 339.34 mm, and no admissible toe contact equilibrium under the amplified paired reactions. It remains an adverse sensitivity to the pressure assumption. The new passing paths neither remove this result nor establish a pressure-independent pass.

Numerical checks and remaining uncertainty

All final optimizer terminations succeeded. Across the three paths, the largest free-force residual is 0.000253 kN and the largest global force imbalance is 0.000463 kN. These support numerical equilibrium of the selected approximation, not physical validation. [36]

The release law is imposed. Coupled elastoplastic soil movement, compatible toe/facing displacement, compaction stresses, dynamic loading and abrupt cracking effects remain unresolved. The construction sequence has not been prescribed. The saved-state checks do not prove that no unsampled transient peak can occur; all earlier report limitations remain applicable.

Measurements that test the prediction

Record facing displacement, earth pressure near the middle and lower restraint, lower-connection force where practicable, and toe tilt or lift on a common time base during loading, wetting and drainage. These observations can distinguish pressure relief in the free face from concentration near the toe. This evaluates the remaining load-distribution mechanism while the connection capacities remain fixed assumptions in the model.

Reporting conclusion

The additional loading-path checks support the expectation that gradual facing deformation can relieve soil pressure while maintaining toe stability under the adopted assumptions. The report retains a conditional containment pass and the higher-pressure failure comparison. Chamber measurements are required to verify this predicted response; no actual-test probability or unconditional system validation is established.

36 Verification and parameter sensitivity

Check	New evidence / limitation
Geometry	24 m² catchment; 0.019996 m² joint path; 78.551 m³ upper soil
Surface operator	Finite-difference Jacobian relative errors below 0.000011
Water storage balance	Maximum absolute error 0.00128 L
Pond conservation	Below 0.000001 L numerically
Facing force balance	Maximum imbalance 0.000454 kN
Optimizer termination status	Successful termination; equilibrium checked separately
Imposed crest endpoint	Zero by imposed restraint
Hydraulic mesh convergence	Not established; local pockets remain resolution-dependent
Physical validation	No final chamber measurements available

Hydraulic scenario	Joint entry L	Peak L/min	Max pond mm
30 min maximum step	2,006.54	2.519	0.605
Primary; 60 min maximum step	2,006.53	2.517	0.584
70% capture; 1 mm contact path	1,423.94	1.681	0.818

These rows separate bookkeeping, force equilibrium and imposed conditions; none is physical validation. Facing refinement from 24 × 16 to 48 × 32 changes reported bulge by at most 0.497 mm. With grid stiffness at 75%, 100% and 125%, the largest checked bulge is 228.04 mm and the minimum nominal strength ratio is 5.60. These comparisons meet the retained 400 mm / 1.10 screens but do not quantify total uncertainty.

The 1800 s maximum-step case checks temporal sensitivity. The longer contact path and reduced capture case test leakage assumptions. Neither is a confidence interval. Conservation and equilibrium establish execution of selected equations, not physical accuracy. The beam formulation was checked against an analytical beam and a refined mesh. [7,11,24]

36A Independent reproduction and remaining checks

The retained arithmetic, water, geometry, toe and beam checks reproduce. The corrected suction curve remains unchanged. S6-7 adds 265 full-load mechanical states across five replays (53 per case), plus loading steps and fresh toe screens. The adopted replay exactly reproduces the original maximum. New sensitivities are separate from the original envelope. No hydraulic reintegration or physical validation is claimed. [31,33]

Check	Reproduced result	Scope
Water accounting	2,006.53 L joints; 190.43 L rear; 2,196.96 L total admission	Matches retained integration
Maximum saved water closure error	0.001282 L	Conservation, not spatial validation
Facing at 0 / 106 / 120 / 240 h	201.09 / 204.69 / 202.05 / 200.68 mm	Matches saved displacement
MD grid strain at primary maximum	0.91775%	Matches deformed segment lengths
Rigid-end centre-rib extension	30.59 mm at 106 h	Matches separate fixed-end geometry
Conditional bench sag and rotation	17.87 mm; 0.90293 degrees	Imposed 4 m support loss
Toe screen	Sliding 1.13282; bearing 11.58777; maximum contact pressure 40.55 kPa	Matches adopted formulas
Analytical suction peak	Sr approximately 61.6%; c_app 0.277 kPa	Recalculated maximum and corrected graph

Verification not completed by this revision

Hydraulic spatial refinement and an independent infiltration/drainage benchmark remain outstanding. Conservation, a hydrostatic patch check and time-step sensitivity are useful but do not establish wetting-front or local-pocket accuracy. The printed local fields must continue to be read with that limitation.

Compatible facing/foundation displacement and a converged soil/bench/contact response are also unresolved. Those omissions do not revoke the declared fixed assumptions; they restrict the interpretation of the derived results. The original nonconverged soil/contact attempt is not evidence of either physical failure or final settlement.

Extra digits are retained in reproducibility records and selected audit rows to show agreement. They do not indicate the accuracy of a real chamber prediction. The supported claim is an adopted-case numerical containment/toe screen. The new pressure comparison does not pass toe contact. Actual settlement, erosion performance and field behavior require separate evidence; neither scenario is a validated physical prediction.

36B Evidence limits and completion requirements

The fixed assumptions remain those in section 5. Numerical verification checks implementation of a selected model; physical validation checks whether it represents the chamber. A converged optimizer, a zero imposed crest displacement and a closing water account have different meanings and cannot together certify the product.

Evidence	Completed in this edition	What it does not establish
Mechanical replay	265 full-load states; all solvers terminate successfully; free-force residual < 0.000251 kN	Correct sand pressure or plastic redistribution
Global force balance	Largest replay imbalance < 0.000524 kN	Material or boundary calibration
Pressure alternatives	Active, adopted and sustained at-rest histories	An experimentally justified pressure law
Friction and suction	31.02 degree and zero-suction comparisons; retained inputs unchanged	Measured phi or calibrated suction strength
Toe check	Fresh envelopes plus paired at-rest reaction check	A compatible nonlinear foundation/membrane displacement
Existing water and beam checks	Retained water balance, step comparison, hydrostatic patch and beam benchmark	Hydraulic spatial convergence or actual bench settlement

Items that require additional evidence

Resolve hydraulic spatial convergence and independent wetting/drainage benchmarks before treating local pockets and extrema as accurate. Refine saved hydraulic and mechanical times around the rapid storm period; interpolated plotting lines do not supply missed extrema. The uniform initial -2 kPa suction is an imposed placement state; the existing dry control captures gravity redistribution, not proof of initial hydrostatic equilibrium.

The 17.87 mm beam result assumes a 4 m support loss and shear transfer across a rotation-released joint. A wet through-crack can transfer shear through reinforcement, but that reinforcement law is unspecified. Soil movement, gap formation, plate action at the crossing and bench contact must be resolved together or measured before giving an actual settled shape.

The nominal grid ratio is not a long-term design factor. Product-specific creep, installation and durability data and transverse stiffness are needed for a field claim [15,17]. The 400 mm movement limit, 10 mm toe movement limit and 1.10 ratio are provisional research criteria. Adding these comparisons does not convert them into prescribed acceptance standards.

37 Scientific support and claim boundaries

Mechanism	Supporting evidence	What remains unverified
Rainfall input	HKO event totals and plot [1–4]	Exact hourly raw record; local-site return period
Unsaturated flow	Richards/retention/conductivity [5–9,11]	Actual soil parameters; spatial convergence
Joint ingress	Surface hydraulics [13]	2 mm crack law and conductance; moving aperture
Suction contribution	Suction stress literature [10,12,26]	Se coefficient for this sand; hysteresis [32]
Grid containment	Tensile reinforcement principles [15,17]	Pressure sensitivity quantified; pressure law and physical response uncalibrated
Toe support	Shallow-foundation methods [14]	Inclined contact and stiffness calibration
Bench response	Joint function and load transfer [25]	Soil redistribution, cracked plate/contact solution
Cover retention	User fixed assumption [24]	Cracked-cover bond and erosion/particle retention

An externally anchored geosynthetic cover has a plausible containment load path. Existing studies do not need to duplicate every accessory to support that concept. However, analogy cannot supply an unmeasured connection capacity or validate a new assembled product. Patent status is separate from performance evidence.

The report supports a conditional research hypothesis and a test protocol; the new pressure comparison limits the adopted-case toe pass. It does not establish a single natural stable slope angle, global slope safety, a complete system pass, or a measured final bench deformation. Erosion loss is not calculated by the seepage/membrane exercise; relevant rainfall-erosion testing remains separate. [18]

38 Physical test replay and measurements

Measurement / control	Implementation purpose
Bench admission	Replay ponding-and-outlet-replay.csv; measure joint intake separately from pump flow and pond storage
Pond head	Multiple level sensors; regulate makeup and removal, including near-zero supply-limited periods
Joint zoning	Calibrate the two lines and the crossing before filling the main chamber
Rear admission	Three measured supply zones with the saved delayed upstream-flow schedule
Front collector A	Dedicated pipe and calibrated tank; readings at 120 h and 240 h
Lower collector B	Independent collection below restricted soil; never mix with A
Moisture and pressure	Probe grid beneath each joint, off-joint, near face and above restricted soil
Facing and grid	Photogrammetry/displacement survey plus grid strain and loop-slip measurements
Bench and joints	Settlement grid, joint rotation/opening, underside support/contact observations
Toe	Translation, edge settlement, tilt and foundation contact pressure

Use the saved time-dependent schedule, not a constant 3.3 or 1 L/min supply and not the peak rainfall intensity throughout the test. During post-storm drainage, the rear reference cell may still release stored water. Ending all rear supply at 120 h would change the retained scenario.

Record sediment in the front collection as well as water. Document retained cover fragments and any local detachment. The chamber isolation, surcharge support, safe construction sequence and deep external toe excavation require engineered apparatus details before a physical test. These measurements are directly needed to test the fixed assumptions, not additional numerical claims.

39 Reproducibility and reporting statement

This consolidated revision uses the completed six-metre hydraulic domain, surface routing, inverse pond control, facing histories and toe screen. Additional post-processing supplies the expanded deformation views and geometry audit. It preserves the old reports separately. The figures and tables use the new outputs, except the explicitly labelled conditional bench formulation and literature/source records retained for context.

Supplied item	Contents
PDF / DOCX; prior HTML archive	PDF and editable source are S6-7; archived HTML is an earlier edition
Figures	Revised chamber, anchorage, water, stress, bulge and summary drawings
Numerical data	Pond replay, inlet/outlet volumes, saturation/storage summaries, stress indicator, facing fields and toe search
Model source and input files	Executable source with fixed assumptions recorded; run commands in the data guide
Reference register	Linked bibliography, evidence scope and retained public HKO source files
Bench sensitivity	Assumed support-loss comparisons; not a measured or calculated actual support-loss map

Suggested reporting statement: “A custom six-metre Plus 200 chamber model met the selected facing/toe screens under its adopted pressure law and fixed anchorage/retention assumptions. A sustained at-rest pressure sensitivity failed toe contact; the pass is model-specific. Soil redistribution and actual bench settlement remain unresolved. These are numerical research estimates for test planning, pending material and chamber validation.”

Prepared with AI assistance. No external institution has endorsed the assembly or these predictions. Responsible authorship, independent technical review and a publication venue should be established before scientific submission. Standards are cited for relevant test scope; no compliance is asserted without performing the specified tests.

39A Revision provenance and retained files

Edition S6 7, dated 13 October 2026, preserves the S6-6 report and all 49 illustrations. Five fresh mechanical histories reuse the S6-1 hydraulic fields and fixed assumptions. New pressure/friction graphs, toe calculations and corrected conclusions are integrated. No new storm, geometry selection, material fit or coupled soil-displacement simulation is substituted. [24,31,33]

Retained S6 4 supplement path	Purpose
numerical-run/reference/rain_hourly.npy	120-hour reconstructed storm; also printed in section 9B.
ponding-and-outlet-replay.csv	Time-dependent bench admission, pond control and separate outlets.
numerical-run/model/simulate3d.py and pond.py	Hydraulic mesh, storage, boundary laws, inverse pond control and saved times.
numerical-run/model/facing.py	Pressure sampling, membrane scenarios and support treatment.
assessment.json and expanded-hydraulic-detail.json	Consolidated results, locations and hydraulic interpretation.
facing-stage-metrics.csv and selected-facing-fields.npz	Saved deformation states and figure provenance.
conditional-bench-model.py and conditional-cracked-bench.csv	Separate imposed-support-loss beam response.

The S6-4 numerical supplement remains the hydraulic archive; S6-6 retains the suction correction. The S6-7 supplement adds sensitivity.py, five histories/results, same-location toe checks and graph data. It preserves original inputs and writes separately. Tables and figures in sections 17A and 35B-C supersede no original hydraulic field; they extend the mechanical evidence.

Audit source: ConstruckSlope-Plus-200-Independent-Technical-Review.pdf, 13 October 2026, supported by independent-checks.json and targeted-checks.json. This is an internal AI-assisted computational review, not laboratory evidence, peer review or endorsement by an external institution.

Reviewed S6 4 PDF SHA-256:
65514c333f291b169cbef15e1910ab5d5fa387bc194728d9aaa195849c2cdcdd

Preservation checks retain every original section and all 49 S6-6 image assets byte for byte; two calculated graphs are added. Fixed-assumption entries and original deformation scales remain intact. Conclusions and affected explanations are corrected in place. New pressure sensitivities do not change the labels or values of the adopted-case plots.

References 1 to 5

1 Hong Kong Observatory

Report on Severe Typhoon Haikui 2311. Tropical Cyclones in 2023. Event rainfall attribution and dates.

Evidence scope: 641.1 mm Haikui rainfall event. No chamber leakage fraction supplied.

https://www.hko.gov.hk/en/publica/tc/tc2023/section3_4rpt.html

2 Hong Kong Observatory

Monthly Weather Summary September 2023. Table 2.3.1 and Figure 2.3.5, including printed page 60.

Evidence scope: Daily event rainfall and hourly plot used for digitization.

https://www.hko.gov.hk/en/publica/mws/files/mws202309.pdf

3 Hong Kong Observatory

The Year's Weather 2023. Record rainfall accumulation intervals.

Evidence scope: Published 1 to 24 hour totals constrain reconstruction.

https://www.hko.gov.hk/en/wxinfo/pastwx/2023/ywx2023.htm

4 Hong Kong Observatory

Daily rainfall at Hong Kong Observatory in 2023. Official machine readable dataset.

Evidence scope: Exact daily totals, with trace treated as zero.

https://data.weather.gov.hk/weatherAPI/cis/csvfile/HKO/2023/daily_HKO_RF_2023.csv

5 van Genuchten M Th

1980. A closed form equation for predicting the hydraulic conductivity of unsaturated soils. Soil Science Society of America Journal 44:892–898. DOI 10.2136/sssaj1980.03615995004400050002x.

Evidence scope: Retention curve formulation; parameters still require calibration.

https://acsess.onlinelibrary.wiley.com/doi/10.2136/sssaj1980.03615995004400050002x

References 6 to 10

6 Mualem Y

1976. A new model for predicting the hydraulic conductivity of unsaturated porous media. Water Resources Research 12:513–522. DOI 10.1029/WR012i003p00513.

Evidence scope: Unsaturated conductivity framework; no product endorsement.

https://agupubs.onlinelibrary.wiley.com/doi/10.1029/WR012i003p00513

7 Celia M A Bouloutas E T and Zarba R L

1990. A general mass conservative numerical solution for the unsaturated flow equation. Water Resources Research 26:1483–1496. DOI 10.1029/WR026i007p01483.

Evidence scope: Mixed form and mass conservation; mass closure alone does not establish spatial accuracy.

https://agupubs.onlinelibrary.wiley.com/doi/10.1029/WR026i007p01483

8 Carsel R F and Parrish R S

1988. Developing joint probability distributions of soil water retention characteristics. Water Resources Research 24:755–769. DOI 10.1029/WR024i005p00755.

Evidence scope: Statistical hydraulic parameter background; class averages are not site measurements.

https://agupubs.onlinelibrary.wiley.com/doi/10.1029/WR024i005p00755

9 PC Progress

HYDRUS online help. Water Flow Parameters and soil hydraulic catalog.

Evidence scope: Sand theta r 0.045, alpha 0.145 per cm, n 2.68 and K 712.8 cm/day. Catalog explicitly describes approximate class averages.

https://www.pc-progress.com/en/OnlineHelp/HYDRUS3/WaterFlowParameters.html

10 Lu N and Likos W J

2006. Suction stress characteristic curve for unsaturated soil. Journal of Geotechnical and Geoenvironmental Engineering 132:131–142. DOI 10.1061/(ASCE)1090-0241(2006)132:2(131).

Evidence scope: Physical basis for suction related strength. Does not validate chi = Se for this sand.

https://doi.org/10.1061/(ASCE)1090-0241(2006)132:2(131)

References 11 to 15

11 Thoms R B Johnson R L and Healy R W

2006. User's guide to the Variably Saturated Flow process to MODFLOW. USGS Techniques and Methods 6 A18. DOI 10.3133/tm6A18.

Evidence scope: Richards flow, surface ponding and seepage face boundary methods; benchmarks required for a new solver.

https://pubs.usgs.gov/publication/tm6A18

12 Iverson R M

2000. Landslide triggering by rain infiltration. Water Resources Research 36:1897–1910. DOI 10.1029/2000WR900090.

Evidence scope: Transient infiltration and pore pressure influence instability; separate stability analysis is needed.

https://pubs.usgs.gov/publication/70022499

13 Federal Highway Administration

2024. Urban Drainage Design. Hydraulic Engineering Circular 22, Fourth Edition. FHWA HIF 24 006.

Evidence scope: Surface conveyance and inlet interception framework. No verified 2 mm screed joint coefficient.

https://www.fhwa.dot.gov/engineering/hydraulics/pubs/hif24006.pdf

14 Federal Highway Administration

2002. Geotechnical Engineering Circular 6 Shallow Foundations. FHWA SA 02 054. Chapters 5 and 6.

Evidence scope: Eccentric loading, bearing capacity and settlement framework; custom inclined toe remains an approximation.

https://www.fhwa.dot.gov/engineering/geotech/pubs/010943.pdf

15 Federal Highway Administration

November 2009. Design and Construction of Mechanically Stabilized Earth Walls and Reinforced Soil Slopes. GEC 11 Volume I. FHWA NHI 10 024.

Evidence scope: Geosynthetic strength reduction and reinforcement design context. Embedded reinforced soil is not the same system as an external facing.

https://highways.fhwa.dot.gov/sites/fhwa.dot.gov/files/FHWA-NHI-10-024.pdf

References 16 to 20

16 ASTM International

2022. ASTM D4716/D4716M 22. Standard test method for determining in plane flow rate per unit width and hydraulic transmissivity of a geosynthetic using a constant head.

Evidence scope: Relevant drainage characterization route; not evidence this assembly has passed.

https://store.astm.org/d4716_d4716m-22.html

17 ASTM International

2023. ASTM D6637/D6637M 15 reapproved 2023. Standard test method for determining tensile properties of geogrids by the single or multi rib tensile method.

Evidence scope: Relevant grid index testing. Index tensile results alone are not long term design strengths.

https://store.astm.org/d6637_d6637m-15r23.html

18 ASTM International

2019. ASTM D6459 19. Standard test method for determination of rolled erosion control product performance in protecting hillslopes from rainfall induced erosion.

Evidence scope: Full scale rainfall erosion comparison framework. The ponded chamber is not an ASTM D6459 compliance test.

https://store.astm.org/d6459-19.html

19 Prasad J and Purohit D G M

2017. A Study on Shear Strength for Dune Sand Reinforced With Nylon Fibres. IJIRSET 6:18664–18668. DOI 10.15680/IJIRSET.2017.0609186.

Evidence scope: Only unreinforced sand data used: Gs 2.67, 32 degrees at 1620 kg/m3 and 27.1 degrees at 1520 kg/m3. Not a project material test.

https://www.ijirset.com/upload/2017/september/186_67_A%20%20Study.pdf

20 Conti S, Splinter K D and Turner I L

2025. Geotechnical Stability Analysis of Dune Face Erosion by Waves. Journal of Geophysical Research Earth Surface 130:e2024JF008160. DOI 10.1029/2024JF008160.

Evidence scope: Experimental and numerical analog for pore pressure and loss of apparent cohesion in sand. Wave forcing differs from this chamber.

https://agupubs.onlinelibrary.wiley.com/doi/10.1029/2024JF008160

References 21 to 25

21 Construck technical source set

CS SPaaP 01 Rev 0 test standard, measurement tables and full scale bench chamber drawings. Internal development documents.

Evidence scope: Original chamber and measurement basis; later user decisions supersede original dimensions.

22 Construck product data sheets

ConstruckGrid HS 200 100, ConstruckDrain and ConstruckMat. June 2024. ConstruckScreed CSB CS TDS 003. December 2025. Internal manufacturer data.

Evidence scope: Product index properties; not independent proof of assembled chamber performance.

23 Construck internal interlock test

Load Bearing Capacity Test of Benches Geogrid Interlock. Four page in house pullout report. Date not specified in reviewed text.

Evidence scope: 6.25 kN single aperture slippage result for a 400 grade specimen; not the present 200 grade rebar loop.

24 ConstruckSlope Plus 200 numerical assessment S6-1

13 October 2026. Fresh six-metre chamber rerun, source files, flow histories, membrane calculations and toe screens.

Evidence scope: Primary numerical evidence for this revision. Not a physical test or independent validation.

25 Federal Highway Administration

2019. Technical Advisory T 5040.30: Concrete Pavement Joints.

Evidence scope: Saw cuts as weakened planes; cracked-joint load transfer depends on detailing. Pavement guidance is an analogy, not a bench design approval.

https://www.fhwa.dot.gov/pavement/ta504030.pdf

References 26 to 29

26 Godt J W, Sener-Kaya B, Lu N and Baum R L

2012. Stability of infinite slopes under transient partially saturated seepage conditions. Water Resources Research 48, W05505. DOI 10.1029/2011WR011408.

Evidence scope: Transient saturation and suction affect stability; a separate failure calculation is required. Does not establish a natural stable angle for this chamber.

https://doi.org/10.1029/2011WR011408

27 Federal Highway Administration

2005. Computer Based Guidelines for Concrete Pavements Volume II. FHWA-HRT-04-122. Chapter 2, Early Age Pavement Behavior.

Evidence scope: General context for concrete tension, restraint, crack width and load transfer. A different concrete application, not a crack model for this cover.

https://www.fhwa.dot.gov/publications/research/infrastructure/pavements/pccp/04122/02.cfm

28 Federal Highway Administration

2013. Composite Behavior of Geosynthetic Reinforced Soil Mass. FHWA-HRT-10-077. Chapter 3, Analytical Model for Calculating Lateral Displacement of a GRS Wall With Modular Block Facing.

Evidence scope: General reinforcement strain and soil displacement compatibility. Different geometry and reinforcement arrangement; does not validate this product.

https://www.fhwa.dot.gov/publications/research/infrastructure/10077/003.cfm

29 Iverson R M

2005. Regulation of landslide motion by dilatancy and pore pressure feedback. Journal of Geophysical Research 110 F02015. DOI 10.1029/2004JF000268.

Evidence scope: Soil volume change and pore pressure can interact during shearing. The present chamber model does not solve this feedback.

https://www.usgs.gov/publications/regulation-landslide-motion-dilatancy-and-pore-pressure-feedback

References 30 and 31

30 Pressure activated drainage boundary

PC-Progress. HYDRUS 5 User Manual. Boundary-condition discussion of seepage faces. Full manual linked below; the review used it to check the meaning of an inactive negative-pressure boundary.

HYDRUS 5 User Manual

Evidence scope: supports the established seepage-face modeling concept. It does not validate this proprietary assembly, the adopted 0.01 m contact resistance, filter behavior or actual drain-mat throughput. The report uses a custom solver, not HYDRUS software.

31 Internal computational review of S6 4

ConstruckSlope Plus 200 Independent Technical Review. 13 October 2026. Eight-page review of the 58-page S6 4 master report, with independent-checks.json and targeted-checks.json as calculation records. Prepared with AI assistance as an external-style audit of the supplied report.

Evidence scope: independent arithmetic and saved-field post-processing; targeted reproduction of the retained beam routine; primary-source checks and visual review. No full new storm integration, completed hydraulic spatial convergence, physical chamber testing or external institutional endorsement is claimed. This is internal evidence, not a published research study.

Reference roles retained

References 1 to 29 are retained; reference 15 uses the document date November 2009. References 32 and 33 add the suction relation and new calculation record. HKO records support the selected event; published hydraulic and soil-mechanics literature supports individual equations and mechanisms; manufacturer information supplies declared index inputs. None independently validates every component of the assembled Plus 200 system.

FHWA GEC 6 [14], sections 5.2.3.7 and 5.2.4, especially printed page 62, supports the clarified bearing-factor discussion in section 35A. The retained full official PDF is in the original numerical package under reference-documents/FHWA-GEC6-Shallow-Foundations.pdf.

References 32 and 33

32 Lu N Godt J W and Wu D T

2010. A closed-form equation for effective stress in unsaturated soil. Water Resources Research 46, W05515. DOI 10.1029/2009WR008646.

Publisher record and paper

Evidence scope: supports the effective-saturation-weighted suction-stress framework used for c_app. It does not identify the retention parameters of the test sand, calibrate the facing pressure law, or validate the proprietary chamber. The current application retains its assumed parameters.

33 S6 7 mechanical replay and toe audit

ConstruckSlope Plus 200 technical revision, 13 October 2026. Internal calculation record: sensitivity.py; adopted32, active32, atrest32, adopted31 and nosuction32 histories/results; atrest-same-location-contact.json; sensitivity-summary.csv; and Figures S1-S2. Each replay uses 53 archived S6-1 target hydraulic states and nominal 24 × 16 facing discretization. No new hydraulic solution or soil-displacement field is claimed.

Evidence scope: reproducible computational sensitivity and equilibrium screening, prepared with AI assistance. This is internal technical evidence, not an external publication, peer review, laboratory result or independent institutional endorsement.

Reference verification and application

HEC-22 fourth edition [13], the cited ASTM editions [16,17], and FHWA report numbers [27,28] were checked against their publisher records. Reference 15 uses November 2009 printed in GEC-11; its report number is FHWA-NHI-10-024. The January 2019 revision of T 5040.30 [25] supersedes its 1990 predecessor. Its pavement-joint scope remains an analogy.

Reference 20 is now cited for the apparent-cohesion mechanism, with wave forcing distinguished from the chamber. Original internal sources [21-24] remain identified as internal; the 400-grade aperture result is not assigned to the Plus 200 loop. Published analogues support individual mechanisms, not the complete assembly.

The report and its supplement retain all earlier technical sections and illustrations. The new graphs quantify pressure and friction uncertainty. The final page continues to show the adopted-case geometry at deformation x1; it is not a visual prediction of the failed upper-pressure comparison.

References 34 to 36 and S6 8 provenance

34 California Department of Transportation research

Development of Improved Guidelines for Analysis and Design of Earth Retaining Structures. Table 2-1, wall movements for mobilization of active earth pressure. Caltrans research report, contract 65A0413, task 2270.

Caltrans published research report

Evidence scope: conventional translating or tilting sand walls can mobilize active pressure with relatively small movements. It does not establish the release distance, force distribution or safety of this fixed-ended geogrid system.

35 Federal Highway Administration

Ground Anchors and Anchored Systems. Geotechnical Engineering Circular No. 4, FHWA-IF-99-015, June 1999. Sections 4.4.3-4.4.4 and 5.2 discuss earth pressure, deformation and support load redistribution.

FHWA GEC 4 published manual

Evidence scope: flexible anchored walls redistribute soil pressure toward supports; at-rest pressure assumes restraint. This is a mechanism analogy and does not prescribe a calibrated pressure law for the Plus 200 chamber.

36 S6 8 pressure relief loading path check

ConstruckSlope Plus 200, 13 October 2026. Internal AI-assisted numerical sensitivity record: check.py, three 95-state histories and results, selected fields, pressure-release-check.csv, technical-record.json, and Figure S3. Issued as ConstruckSlope-Plus-200-Pressure-Release-Check.zip. Original model and hydraulic dependencies remain in the S6-7 technical supplement.

Evidence scope: reproducible equilibrium and sensitivity screening under the fixed assumptions. It is not an external publication, an independent institutional review or a measured chamber result. No new hydraulic integration, toe optimization or coupled soil-displacement analysis is included.

Revision preservation

Edition S6-8 adds sections 35D-F, Figure S3 and references 34-36 to S6-7. All previous technical sections, tables, fixed assumptions, 51 image assets, the higher-pressure comparison and original deformation scales are retained. The original envelope sliding ratio remains 1.133. The adopted-case conclusion remains conditional containment pass.

The source and new records are retained separately. Publication of this additional interpretation does not alter the S6-1 hydraulic archive, the S6-6 suction correction or the five S6-7 mechanical comparisons. The final visual summary continues to depict the adopted-case geometry only.

40 Final before and after visual summary

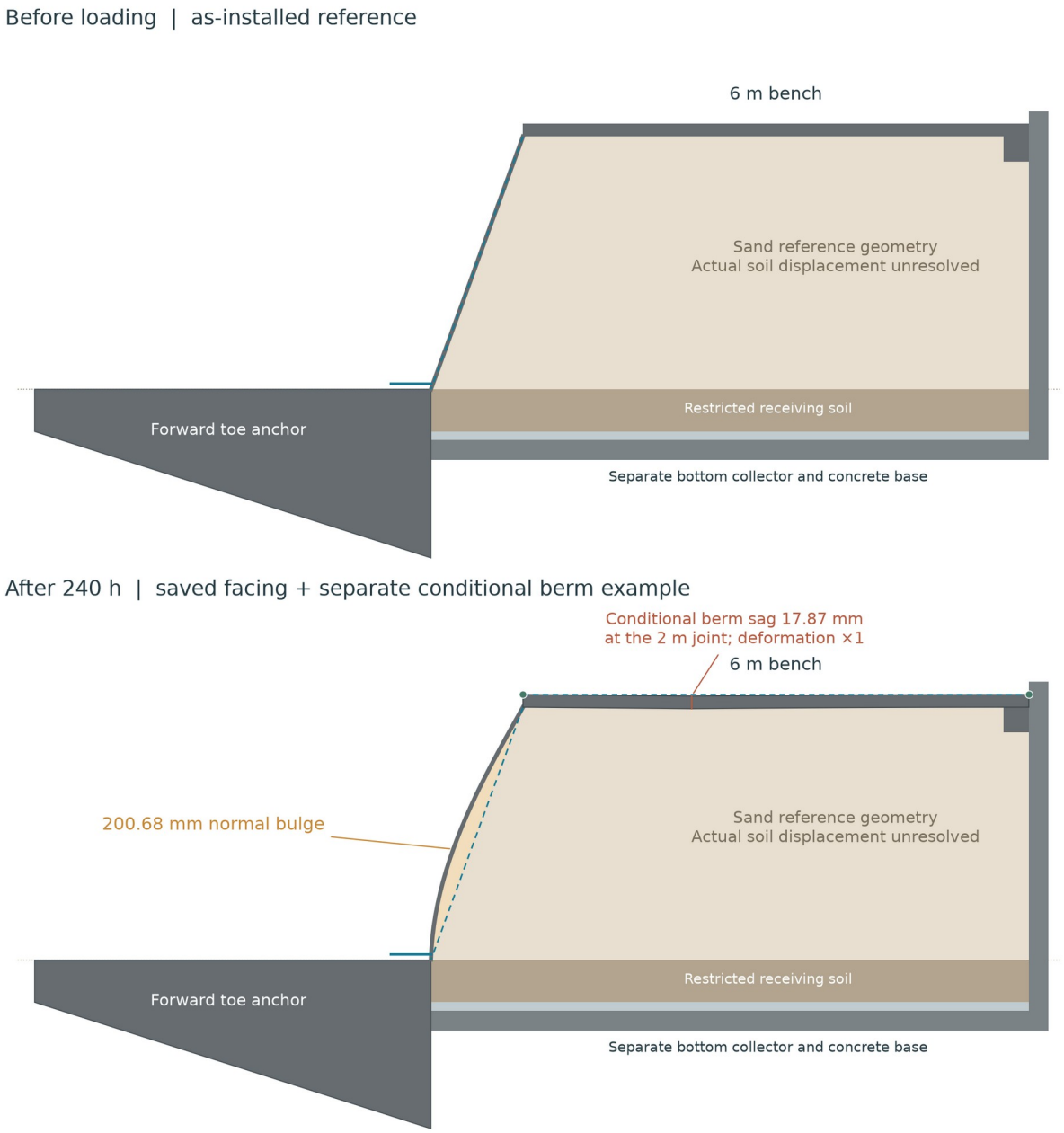


Figure 29. Before and after in side section, both at deformation x1. The lower view combines the saved 240 h facing with the separate conditional 17.87 mm berm case; it is not a coupled prediction of final soil settlement.

In the adopted case, after-drainage bulge is 200.68 mm versus a 204.69 mm saved peak. The separate 17.87 mm berm example assumes 4 m support loss. The 4.70 m toe passes the adopted envelope, but fails the sustained at-rest pressure comparison (339.34 mm peak bulge). This retained drawing shows the adopted case only. Cracked-cover retention remains assumed. The added gradual-loading checks support pressure relief while the toe remains stable under the adopted assumptions (sections 35D-F). The conclusion remains a conditional containment pass; the higher-pressure failure comparison is retained.

Front collection is 0 L by 120 h and 0 L additional by 240 h in the adopted model; the lower collector is separate. Total soil entry is 2,196.96 L. Actual soil settlement and crack apertures remain unresolved.